

POLITECNICO DI TORINO

Department of Mechanical and Aerospace
Engineering

Master Degree in Mechanical Engineering

Master Degree Thesis

Railway structures: thermographic analysis on welded
butt joints



Supervisors:

Prof.ssa Raffaella Sesana
Prof.ssa Francesca Maria Cura'

Candidate:

Andrea Della Sala

Company Tutor:

Ing. Mauro Piombo

Contents

1. Introduction	1
2. Welding: basic characters and definitions in railway market.....	2
3. Types of welding machines	6
4. Welding joint execution: procedures, personnel and parameters	8
4.1 Procedures and personnel qualifications	9
4.2 Characteristic parameters: current, tension, speed, gas flow rate and torch angle	11
5. Welding aluminium alloys	13
6. Welding imperfections and defects in aluminium.....	16
6.1 Hot crack formation	17
6.2 Liquation cracking in HAZ	18
6.3 Hydrogen in welding aluminium	19
7. Quality levels of acceptance	21
8. Non-Destructive Testing (NDT).....	25
8.1 Ultrasonic testing	26
8.2 Radiographic testing.....	30
8.3 Visual testing.....	33
8.4 Penetrant testing	34
9. Thermography: theory outline	37
9.1 Thermography: techniques and acquisition systems.....	39
9.2 Passive thermography	40
9.2.1 Fields of applications of the passive thermography.....	41
9.3 Active thermography.....	43
9.3.1 Heating sources	43
9.3.2 Active thermography techniques	44
9.3.3 Pulse Thermography	44
9.3.4 Pulsed phase thermography	49
9.3.5 Lock-in thermography	50
9.3.6 Step heating.....	54
9.3.7 Vibrothermography.....	55

9.3.8	Thermoelastic analysis of stresses	56
10.	The experimental equipment	58
10.1	Objective and description of the experimental procedure.....	58
10.2	Samples description and identification	58
10.3	Welding machine	60
10.3.1	Welding parameters setting	62
10.3.2	Samples preparation.....	67
10.4	Ultrasonic equipment	69
10.5	Test setup for passive thermography.....	71
10.5.1	Instron 8801	73
10.5.2	Vibrophone	74
10.5.3	IRTech camera.....	75
10.5.4	Passive thermography: data collection and elaboration.....	76
10.6	Fatigue test: joint stress analysis	77
10.6.1	Loading scheme for the 1 st batch	77
10.6.2	Loading scheme for the 2 nd batch	79
10.6.3	Joint static verification.....	81
10.6.4	Joint fatigue life calculation.....	83
10.7	Test setup for active thermography.....	85
10.7.1	FLIR camera	88
10.7.2	Active thermography: data collection and elaboration	88
11.	The experimental results for the 1 st batch samples	92
11.1	Radiographic investigation for defect characterization.....	92
11.2	Fatigue and passive thermographic test results	97
11.3	Active thermographic investigation	104
12.	The experimental results for the 2 nd batch samples	109
12.1	Penetrant testing for surface defects identification	109
12.1.1	Defect-free samples	111
12.1.2	Samples with inclusion	112
12.1.3	Samples with root incomplete penetration.....	113
12.1.4	Samples with porosities	113

12.2	Ultrasonic test.....	114
12.2.1	Defect-free samples	118
12.2.2	Samples with inclusion	120
12.2.3	Samples with incomplete root penetration.....	122
12.2.4	Samples with porosities	123
12.3	Fatigue and passive thermographic test results	125
13.	Conclusions.....	129
14.	Appendix A.....	131
14.1	Defect-free samples.....	131
14.2	Samples set with inclusions	132
14.3	Samples set with incomplete root penetration	134
14.4	Samples set with porosities	135
15.	Bibliography	137

Index of Figures

Fig. 2.1 main parts of a weld seam for definition of filler dilution (from [6]).	2
Fig. 2.2 Dendritic structure of a weld seam (from [21]).	3
Fig. 2.3 Arc welding: different sections of an arc in function of length L and voltage U (from [51]).	4
Fig. 2.4 Force on the arc - induced magnetic field (from [3]).	5
Fig. 2.5 Asymmetric and ferromagnetic workpiece - arc deviation (from [3]).	5
Fig. 4.1 Metal transfer in arc welding (from [51]).	11
Fig. 4.2 Tip to work distance (from [51]).	12
Fig. 4.3 Torch angle from [51]	12
Fig. 6.1 Hydrogen in aluminium welding (from [15]).	19
Fig. 6.2 Escape mechanism of hydrogen (from [51]).	20
Fig. 8.1 clustered non-planar discontinuity according ISO 23279 (from [32]).	29
Fig. 8.2 single non-planar discontinuity according to ISO 23279 (from [32]).	29
Fig. 8.3 Main dimensions for equipment disposal for a butt joint radiographic test (from [30]).	31
Fig. 8.4 Voltage selection in function of materials tested and penetrated thickness in radiographic testing (from [30]).	32
Fig. 9.1 Black body isotherm emission spectrum (from [5]).	37
Fig. 9.2 Design of a thermal image camera (from [17]).	39
Fig. 9.3 BLIP detectivity in function of the sensors used (form [17]).	40
Fig. 9.4 Spatial resolution in function of the distance (from [22]).	42
Fig. 9.5 Contrast decay of a thermal image in function of a defect depth (from [17])	45
Fig. 9.6 Defect depth vs max thermal contrast (from [53]).	46
Fig. 9.7 Test bench example (from [54]).	46
Fig. 9.8 Sketch of a test bench with inductors (from [26]).	47
Fig. 9.9 Temperature difference vs time of a sound (1) and defective (2) parts (from [26]).	49
Fig. 9.10 sinusoidal behaviour of the four captures (from [13]).	51
Fig. 9.11 Lock-in test bench (from [42]).	52
Fig. 9.12 Ultrasound excitation for thermographic investigation (from [14]).	53
Fig. 9.13 Step heating test bench (from [40]).	54
Fig. 9.14 Example of vibrothermography test bench (from [16]).	55
Fig. 10.1 Welding machine used during the experimental tests	60
Fig. 10.2 Flowmeter for gas cylinder. The tap (a) and the flow meter (b)	61
Fig. 10.3 Welding machine interface: summary of the gas parameters selection.	63
Fig. 10.4 Fronius special 4-step mode (from [12]).	64
Fig. 10.5 Penetration stabilizer (from [12]).	64
Fig. 10.6 Stick-out compensation (from [12]).	65

Fig. 10.7 Arc correction during the welding process (from [12]).....	65
Fig. 10.8 Welding machine interface - parameters setting for the 1st run.....	66
Fig. 10.9 Welding machine interface - parameters setting for the 2nd and 3rd run ..	66
Fig. 10.10 Degreasing phase of the samples.....	67
Fig. 10.11 Brushing phase of the samples.	67
Fig. 10.12 Positioning of the sample.	68
Fig. 10.13 Ultrasonic equipment: probe + device.....	69
Fig. 10.14 Detector: main parameters setting	69
Fig. 10.15 test bench and sample in unloaded condition.	71
Fig. 10.16 Test bench for passive thermography investigation at 100Hz.....	72
Fig. 10.17 Instron 8801 (from [18]).....	73
Fig. 10.18 Test bench and sample in loaded condition.....	73
Fig. 10.19 Loading conditions for the tested specimen.	73
Fig. 10.20 Vibrophore used during the tests.	74
Fig. 10.21 Acquisition parameters in Timage Connect	75
Fig. 10.22 Timage Connect: selection of region of interest (ROI).	76
Fig. 10.23 Butt-joint section	77
Fig. 10.24 Schematic representation of the test bench for 1st batch samples.....	77
Fig. 10.25 bending moment on the structure – 1st batch samples.	78
Fig. 10.26 Schematic representation of the test bench for 2nd batch samples.	79
Fig. 10.27 bending moment on the structure - 2nd batch samples.	80
Fig. 10.28 Detail category chosen for the fatigue investigation (from [11]).	84
Fig. 10.29 Test bench for active thermography from [24])	85
Fig. 10.30 Test bench for active thermography	85
Fig. 10.31 MultiDES System - interface for parameters setting (from [24]).....	86
Fig. 10.32 MultiDes system – interface for coordinates setting (from [24]).	87
Fig. 10.33 Laser head, infrared camera and sample under investigation.....	87
Fig. 10.34 Research IR software.....	88
Fig. 10.35 Centre of laser for investigation with active thermography.	90
Fig. 10.36 Box object of a frame in Research IR.	90
Fig. 10.37- 3D image of the subsequent frames.	91
Fig. 11.1 Rhythm software to view radiographic images	92
Fig. 11.2 Rhythm software parameters.	92
Fig. 11.3 Radiographic image of defect free sample 1 of 3.....	93
Fig. 11.4 Radiographic image of defect free sample 2 of 3.....	93
Fig. 11.5 Radiographic image of defect free sample 3 of 3.....	93
Fig. 11.6 - 2% of porosities according to ISO 10042 (from [47]).	94
Fig. 11.7 Radiographic image of samples with inclusion 1 of 3	94
Fig. 11.8 Radiographic image of samples with inclusion 2 of 3	94
Fig. 11.9 Radiographic image of samples with inclusion 3 of 3	94
Fig. 11.10 Radiographic image of samples with incomplete root penetration 1 of 3	95

Fig. 11.11 Radiographic image of samples with incomplete root penetration 2 of 3	95
Fig. 11.12 Radiographic image of samples with incomplete root penetration 3 of 3	95
Fig. 11.13 Radiographic image of samples with porosities 1 of 3.....	96
Fig. 11.14 Radiographic image of samples with porosities 2 of 3.....	96
Fig. 11.15 Radiographic image of samples with porosities 3 of 3.....	96
Fig. 11.16 - 10% of porosities reference sample according to ISO 10042 (from [47]).	96
Fig. 11.17 Fatigue test results of 1st batch samples: cycles to failure.....	97
Fig. 11.18 S-N curves in presence of pores (from [41]).	98
Fig. 11.19 Cycles to failure in presence of porosities and incomplete root penetration (from [35]).	98
Fig. 11.20 S-N curves for defect free samples (from [39]).....	99
Fig. 11.21 crack in weld toe.....	101
Fig. 11.22 Crack in a sample with inclusion.....	101
Fig. 11.23 Area of investigation in passive thermographic test.....	101
Fig. 11.24 Temperature increment and displacement for a sample with inclusion sampled at 0.008Hz.....	102
Fig. 11.25 Temperature increment and displacement for a sample with inclusion sampled at 1Hz.....	102
Fig. 11.26 Active thermographic testing of the sample without defects – OK3L1.	104
Fig. 11.27 - OK3L1 weld seam after the fatigue test.....	105
Fig. 11.28 Active thermographic testing of the sample with an inclusion – IN1L2.	105
Fig. 11.29 IN1L2 weld seam after the fatigue test.....	106
Fig. 11.30 Active thermographic testing of the sample with incomplete root penetration – MP3L1	106
Fig. 11.31 MP3L1 weld seam after the fatigue test.	107
Fig. 11.32 Active thermographic testing of the sample with porosities – PO2L2...	107
Fig. 11.33 Sample with porosities – PO2L2: crack at the surface.....	107
Fig. 12.1 Samples after the cleaning procedure.....	109
Fig. 12.2 Samples after the application of red penetrant.	110
Fig. 12.3 Samples after the application of white developer.....	111
Fig. 12.4 Penetrant testing results for defect-free samples 1 of 3.....	111
Fig. 12.5 Penetrant testing results for defect-free samples 2 of 3.....	111
Fig. 12.6 Penetrant testing results for defect-free samples 3 of 3.....	112
Fig. 12.7 Penetrant testing results for samples with inclusion 1 of 3.	112
Fig. 12.8 Penetrant testing results for samples with inclusion 2 of 3	112
Fig. 12.9 Penetrant testing results for samples with inclusion 3 of 3	112
Fig. 12.10 Penetrant testing results for samples with incomplete root penetration 1 of 3	113
Fig. 12.11 Penetrant testing results for samples with incomplete root penetration 2 of 3	113

Fig. 12.12 Penetrant testing results for samples with incomplete root penetration 3 of 3	113
Fig. 12.13 Penetrant testing results for samples with porosities 1 of 3	113
Fig. 12.14 Penetrant testing results for samples with porosities 2 of 3.	114
Fig. 12.15 Penetrant testing results for samples with porosities 3 of 3.	114
Fig. 12.16 V1 block for probe and detector calibration.....	115
Fig. 12.17 V1 block - probe angle calibration.	115
Fig. 12.18 V2 probe - angle and 0-scale calibration.	116
Fig. 12.19 Ultrasound testing: max and min positions of probe to cover the entire joint volume.	116
Fig. 12.20 Ultrasonic testing results for defect-free samples 1 of 3.	118
Fig. 12.21 Ultrasonic testing results for defect-free samples 2 of 3.	119
Fig. 12.22 Ultrasonic testing results for defect-free samples 3 of 3.	119
Fig. 12.23 Ultrasonic testing results for samples with inclusion 1 of 3.....	120
Fig. 12.24 Ultrasonic testing results for samples with inclusion 2 of 3.....	120
Fig. 12.25 Ultrasonic testing results for samples with inclusion 3 of 3.....	121
Fig. 12.26 Ultrasonic testing results for samples with incomplete root penetration 1 of 3.	122
Fig. 12.27 Ultrasonic testing results for samples with incomplete root penetration 2 of 3.	122
Fig. 12.28 Ultrasonic testing results for samples with incomplete root penetration 3 of 3	123
Fig. 12.29 Ultrasonic testing results for samples with porosities 1 of 3.....	123
Fig. 12.30 Ultrasonic testing results for samples with porosities 2 of 3.....	124
Fig. 12.31 Ultrasonic testing results for samples with porosities 3 of 3.....	124
Fig. 12.32 Fatigue test results of 2nd batch samples: cycles to failure.....	125
Fig. 12.33 Crack after the fatigue test on the specimen with porosity.	126
Fig. 12.34 Passive thermographic investigation on IN03L2 sample.	127
Fig. 12.35 Passive thermographic test on OK5L1 sample.....	127
Fig. 12.36 Passive thermographic investigation on MP02L2 sample.....	128
Fig. 12.37 Passive thermographic investigation on PO4L2 sample.	128
Fig. 14.1 Passive thermography results for defect-free samples 1 of 3. Temperature increment and displacement vs elapsed cycles.	131
Fig. 14.2 Passive thermography results for defect-free samples 2 of 3. Temperature increment and displacement vs elapsed cycles.	131
Fig. 14.3 Passive thermography results for defect-free samples 3 of 3. Temperature increment and displacement vs elapsed cycles.	132
Fig. 14.4 Passive thermography results for samples with inclusion 1 of 3. Temperature increment and displacement vs elapsed cycles.....	132
Fig. 14.5 Passive thermography results for samples with inclusion 3 of 3. Temperature increment and displacement vs elapsed cycles.....	133

Fig. 14.6 Passive thermography results for samples with inclusion 2 of 3. Temperature increment and displacement vs elapsed cycles.....	133
Fig. 14.7 Passive thermography results for samples with incomplete root penetration 1 of 3. Temperature increment and displacement vs elapsed cycles.	134
Fig. 14.8 Passive thermography results for samples with incomplete root penetration 2 of 3. Temperature increment and displacement vs elapsed cycles.	134
Fig. 14.9 Passive thermography results for samples with incomplete root penetration 3 of 3. Temperature increment and displacement vs elapsed cycles.	135
Fig. 14.10 Passive thermography results for samples with porosities 1 of 3. Temperature increment and displacement vs elapsed cycles.....	135
Fig. 14.11 Passive thermography results for samples with porosities 2 of 3. Temperature increment and displacement vs elapsed cycles.....	136
Fig. 14.12 Passive thermography results for samples with porosities 3 of 3. Temperature increment and displacement vs elapsed cycles.....	136

Index of Tables

Tab. 1 Grades of automation in arc welding (from [3]).	6
Tab. 2 Designation of welding processes according to ISO 4063 (from [49]).	8
Tab. 3 Requirements for a butt-joint WPQR according to ISO15624-2.	10
Tab. 4 Argon and helium properties (from [37]).	14
Tab. 5 Imperfections designation according to ISO 6520-1	16
Tab. 6 Imperfections designation according to ISO 6520-1	17
Tab. 7 Reference values of stress factors according to ISO 15085-2.	21
Tab. 8 - Weld performance classes (from [36]).	22
Tab. 9 Inspection classes (from [36]).	22
<i>Tab. 10 Acceptance levels for quality imperfections according to ISO 10042.</i>	24
Tab. 11 Non-destructive tests according to ISO 9712 (from [28]).	25
Tab. 12 Reference sensitivity setting for ultrasonic testing according to ISO 17640.28	
Tab. 13 Penetrant testing: methods classification according to ISO 3452-1 (from [27]).	34
Tab. 14 Heat sources for active thermographic investigations (from [17]).	43
Tab. 15 Main electrical characteristics of the welding machine generator.	60
Tab. 16 First part of the Welding Procedure Specification used during the experimental tests.	62
Tab. 17 Second part of the Welding Procedure Specification used during the experimental tests.	62
Tab. 18 Main geometrical parameters for the 1st batch loading condition.	78
Tab. 19 Main geometrical parameters for the 2nd batch loading condition.	80
Tab. 20 Values of Rp02, Rm and hardness as declared by the manufacturer on the samples under test.	82
Tab. 21 Reference (minimum) values proposed by Eurocode 9.	82
Tab. 22 Values of forces and stresses used in the experimental investigation	83
Tab. 23 Constant parameters for all the investigations with active thermography.	89
Tab. 24 Parameters measured before testing the samples with active thermography before the fatigue assessment.	89
Tab. 25 Parameters measured before testing the samples with active thermography after the fatigue assessment.	89
Tab. 26 Eurocode 9 vs real values: estimation of safety factors for the 1st batch samples.	100
Tab. 27 Eurocode 9 vs real values: estimation of safety factors for the 2nd batch samples.	126

1. Introduction

In the railway sector, aluminium is becoming the preferred alloy for the car-body shell construction. Welding aluminium alloys for structural applications has to comply to specific Standards that allow to guarantee the proper design, the manufacturing and the in-service reliability. In the railway market, welding is often defined as Special Process. Indeed, even if the process parameters are controlled, the conformance of the resultant weld can be checked only with destructive tests. Although some destructive tests can be done in the welding validation phase, in the past years, the non-destructive evaluation of these structures has assumed a crucial role both at a manufacturing and at in-service levels.

In this work, a preliminary examination of the most used Standards for aluminium welding in railway constructions has been done in terms of:

- arc welding process description;
- principal defects that can be generated during the arc welding process;
- acceptance quality levels for the aluminium structures;

The second part of this work focuses the attention on the most used non-destructive techniques applied to the welds.

A general description of ultrasonic, radiographic, visual and penetrant testing is given with their reference Standards.

The thermographic investigation is the emerging technique that can be used to assess the structure conformity of a welded component. Due to a lack of ISO standardization on thermography applied to the welds, the theory of both the active and the passive thermographic investigations is presented, with the main fields of application found in literature.

Regarding the third part, an experimental procedure has been carried out with the goal of comparing the material response in a passive and active thermographic investigation. In this context some plates with a butt-joint in the middle have been prepared. In these samples the most occurrent defects that can be found in welding have been reproduced: inclusions, incomplete root penetration and porosities. A temperature-based post-processing technique has been elaborated to evaluate the temperature trend during the fatigue test with the passive thermographic investigation and the temperature trend before and after the fatigue test with active thermographic investigation.

This thesis work has been conducted with the collaboration of Alstom Ferroviaria Spa.

2. Welding: basic characters and definitions in railway market

In the welding processes the basic concept is to bond two equal materials in a shape described on a drawing. In railway this process is often used to manufacture both the car body shell and the train bogies.

A general classification of welding is related to autogenous welding and heterogenous welding. In the latter case the base material does not participate to the welding process and the filler material has a fusion temperature below the base material one. It is even divided into:

- Soldering, if the filler fusion temperature is below 400 °C;
- Brazing, if the filler fusion temperature is above 400 °C but below the fusion temperature of the base material;

In this work only autogenous welding will be considered because it is the most used for structural assemblies. In such a case the base material directly participates to the welding process. The chemical composition of the filler material is in general different from the base material, thus creating a heterogeneous structure when solidified. In addition, fillers have compounds that deoxidate or depurate the pool. In this second case, the compound reacts with the impurities obtaining a final compound with a less specific weight that can be eliminated with superficial slag. The gaseous compounds inside the pool tend to rise to the surface but when the solidification speed is too fast or the gaseous compounds too high, it is possible to have porosities or blowholes embedded in the welding.

The filler dilution is a parameter to identify the mix between the base material and the filler material in square butt joints. As Coniglio et al. [6] have reported in their work, it is defined as:

$$filler\ dilution = \frac{B + C}{A + B + C} \cdot 100 (\%)$$

Where A, B and C are reported in Fig. 2.1:

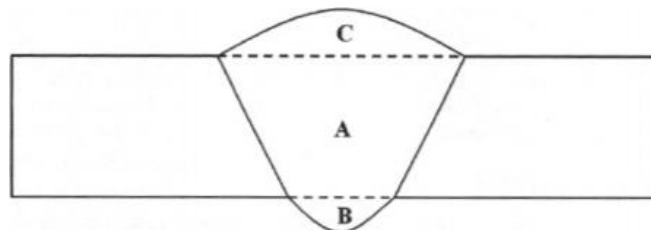


Fig. 2.1 main parts of a weld seam for definition of filler dilution (from [6]).

In MIG or MAG welding this value ranges between 5% and 40%.

During the solidification, the weld bead assumes a dendritic structure. In fact, when the weld pool starts its solidification at the solid liquid interface, the first crystal germs form and they continue to grow up in the maximum cooling preferential direction, generating the dendrites. In materials not subjected to allotropic transformations, such as aluminium alloys, where the multi-pass welding is used, the grains, which solidify in subsequent runs, follows the dendritic behaviour of the previous run. As reported in [21], in the final structure of the fused zone, the dendrites, are inclined as the welding proceeds.

In addition to this, the dendritic formation depends upon welding speed and, near the weld centre, there is the formation of equiaxed dendrites as showed in the below Fig. 2.2:

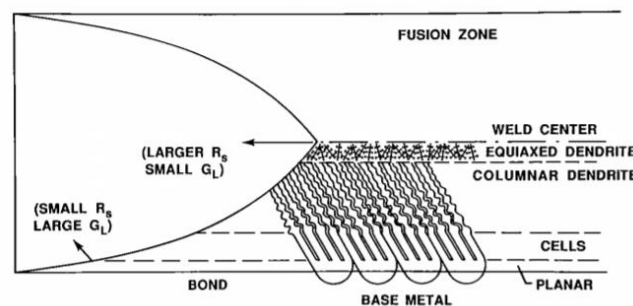


Fig. 2.2 Dendritic structure of a weld seam (from [21]).

Among the welding processes, arc welding constitutes the most used technique to weld steels or aluminium alloys. The arc welding is included into autogenous fusion welding processes and it is divided into:

- 1- Metal arc welding:
 - Manual metal arc welding;
 - Submerged arc welding;
- 2- Gas Shielded arc welding:
 - Gas metal arc welding (MIG/MAG)
 - Gas tungsten arc welding (TIG)
 - Plasma welding

The electric arc can be:

- *indirect* when the arc is between two electrodes and the base material is not a part of the electric circuit;
- *direct* when the arc is between the electrode and the base metal which constitute the other electrode:

- *with fusible electrode* when the electrode is composed by the filler material;
- *with non-fusible electrode* when a refractory electrode is used and the filler material is added where foreseen.

Finally, the electric arc power supply can be:

- in direct current with electrode negative (DCEN) where the negative pole is the electrode and the positive pole is the workpiece;
- in direct current with electrode positive (DCEP) where the positive pole is the electrode and the negative one is the workpiece;
- in alternating current.

The basic principle is that when between two electrodes, one positive and one negative a voltage drop is measured, an electric field is generated in the mean in which the electrodes are positioned. If the voltage drop is incremented the electrons emitted by the negative pole are accelerated through the positive one. At this stage it is possible that the voltage drop is so high that the electrons bump the gas molecules and the valence electrons are excited. Thus, a new bidirectional flow of charges is generated: positive ions flow to the cathode and negative ions flow to the anode. In this way there is a current flow. Then the thermal effect is evident when the bumps between the electrons from the cathode and the positive ions from anode become more frequent due to the higher voltage.

The arc can be divided into three regions that are reported in the below Fig. 2.3 [51]:

- the anode region with a crater form, from which the positive charges are emitted.
- the arc column that acts as a connection between the anode and the cathode regions and in which electrons and positive ions present;
- the cathode region, from which the negative charges are emitted;

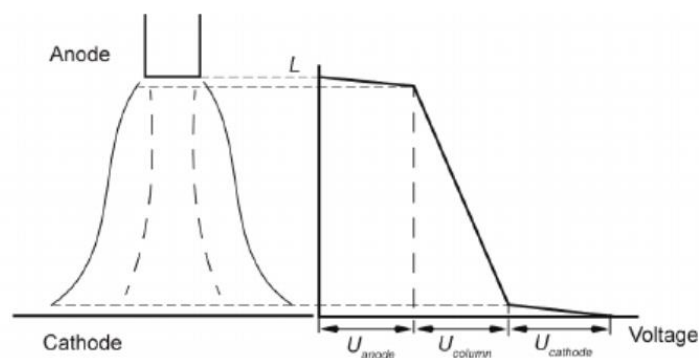


Fig. 2.3 Arc welding: different sections of an arc in function of length L and voltage U (from [51]).

As the Fig. 2.3 shows, the three regions have different slopes. The potential loss at anode and at cathode depends on the material used and represents the major losses with respect to the whole potential drop. Instead, the voltage drop inside the fused zone is less steep and its effective value depends on environment in which the arc burns. The more this environment is ionizable, the less is the voltage drop.

As seen a positive and negative sides have to be present in order to start welding. Often the workpiece can be ferromagnetic and the magnetic field, induced by previous treatments or by welding, can influence the welding arc which is deflected. This deflection starts from electrode up to the base material and when it overcome a certain value, the magnetic force will deform the arc so much that the welding is unacceptable. As stated in [3], in two cases the welding action influences the arc stability in steels:

- 1- If the operator starts to weld away from the workpiece lead: in this case the current has to change direction as approaching to the workpiece and the flux lines of the magnetic field are concentrated in the curve as reported in the Fig. 2.4;
- 2- If the workpiece is asymmetric and ferromagnetic as reported in the below Fig. 2.5;

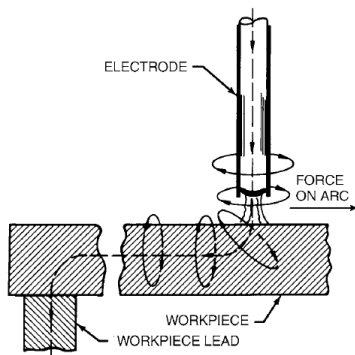


Fig. 2.4 Force on the arc - induced magnetic field (from [3])

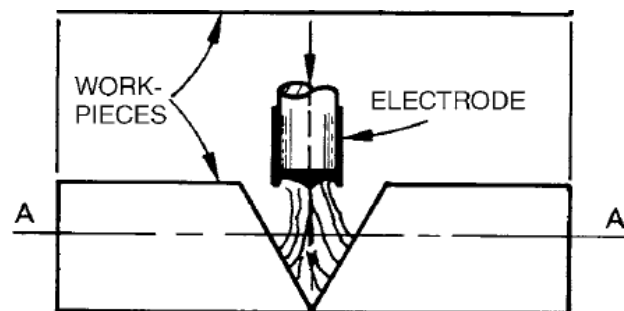


Fig. 2.5 Asymmetric and ferromagnetic workpiece - arc deviation (from [3]).

This phenomenon can be reduced by using one or more of the following techniques:

- If allowed by the welding process, to use of alternate current: the asymmetry of the alternated magnetic field can be compensated by eddy currents induced in the workpiece.
- To reduce the arch length and the welding current in order to minimize the arc deviation and to reduce the magnetic phenomenon respectively.

- To use the welding beads in order to limit to them the start and the end of the welding, critic points for arc blow.
- To position the mass socket in the middle of the joint, having the mass both at the start and at the end of the joint.

In railway market, welding is often defined as Special Process. Indeed, even if the process parameters are controlled, the conformance of the resultant weld can be checked only with destructive tests.

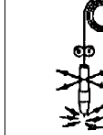
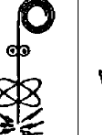
In railway industry an emerging material is aluminium that, thanks to the high performances of its 6xxx alloys in terms of both mechanical resistance and lightweight, is becoming the preferred material to be used for structural design. However, it is quite common to use also steels especially for bogies design where a compromise between lightweight, safety and mechanical performances has not yet found in in-service applications.

Among the arc welding processes, the most used in railway for both aluminium alloys and steels are TIG and MIG processes used to weld butt, fillet weld and lap joints in various shape and dimensions.

3. Types of welding machines

It is relevant to classify the welding operations based on the automation grade that they have. Thus, as reported in [3], six different categories can be found, as shown in the scheme of Tab.1.

Tab. 1 Grades of automation in arc welding (from [3]).

Method of Application	Manual	Semiautomatic	Mechanized	Automatic	Robotic	Adaptive Control
Arc Welding Elements/Function						
Starts and maintains the arc	Person	Machine	Machine	Machine	Machine (with sensor)	Machine (robot)
Feeds the electrode into the arc	Person	Machine	Machine	Machine	Machine	Machine
Controls the heat for proper penetration	Person	Person	Machine	Machine	Machine (with sensor)	Machine (robot) (only with sensor)
Moves the arc along the joint (travels)	Person	Person	Machine	Machine	Machine (with sensor)	Machine (robot)
Guides the arc along the joint	Person	Person	Person	Machine via prearranged path	Machine (with sensor)	Machine (robot) (only with sensor)
Manipulates the torch to direct the arc	Person	Person	Person	Machine	Machine (with sensor)	Machine (robot)
Corrects the arc to overcome deviations	Person	Person	Person	Does not correct; hence, potential weld imperfections	Machine (with sensor)	Machine (robot) (only with sensor)

As showed in the above Table, the main characteristic that allows to automatize the welding process is the automatic feeding of the electrode that also constitutes the filler material. A further step is the mechanization of the process in which, to reduce the operator errors and to avoid production stops due to bad parts produced, microprocessors are implemented in welding machines, helping the operator in parameters setting. The consistent improvement of the recent years technology has led to a development of new strategies to reduce manufacturing costs and to improve the product quality. In this sense automatic, robotic and adaptative machines have created a great opportunity for developing manufacturing plants. For example, a robot can be used when dealing with very long components and multiple welds per time. Indeed, equipping a movable gantry with robots holding welding torches, it is possible to reduce manufacturing time welding simultaneously different parts of a single component.

4. Welding joint execution: procedures, personnel and parameters

As seen, one of the possibilities to execute a welding joint is with the continuous arc welding method. Between the welding wire, that acts both as electrode and filler, and the piece an electric arc is produced. A mechanism allows to obtain the continuity in feeding the torch with the wire. In general, a gas is used to protect the welding pool from external contamination. However, in particular cases, as the one of the welding processes where a cored wire is adopted, the wiring gas protection is not used.

A classification of welding processes is given by UNI EN ISO 4063 [49] that depicts the nomenclature of the various welding processes. A resume of the arc welding processes is reported in the following Tab. 2:

Tab. 2 Designation of welding processes according to ISO 4063 (from [49]).

ISO 4063 designation	Description
11	Manual metal arc welding without gas protection
12	Submerged arc welding
14	Gas-shielded arc welding with non-consumable tungsten electrode
15	Plasma arc welding
114	Self-shielded tubular cored arc welding
131	MIG welding with solid wire electrode
135	MAG welding with solid wire electrode
136	MAG welding with flux cored electrode
137	Tubular cored metal arc welding with inert gas shield

In this work all the experimental tests are referred to process n. 131, the most used to weld aluminium alloys.

4.1 Procedures and personnel qualifications

When dealing with welding of aluminium alloys, care has to be taken by the personnel in joint execution. This is obtained with a mechanism of welder qualification as reported in UNI EN ISO 14732 [50] and UNI EN ISO 9606-2 on a welding procedure specification (WPS). For arc welding, the requirements for a welding specification are reported in UNI EN ISO 15609-1 [44] as a list of parameters that can be used as a guide for WPS preparation. The ones used for the joint execution for the experimental investigation are:

- Parent material used;
- Material dimensions;
- Welding process;
- Sketch of the joint;
- Joint position for execution according to ISO6947;
- Joint preparation;
- Welding technique;
- Welding consumables;
- Electrical parameters: voltage and current.

The welding specification can be validated by using one of the following techniques, as stated in UNI EN ISO 15607 [43]:

- a) Welding procedure test: a standardized part is used.
- b) Tested welding consumables: used to qualify a specific WPS since some materials do not deteriorate significantly in HAZ.
- c) Previous welding experience based on the manufacturer proven experience that have resulted in a successful weld execution on the same material and joint.
- d) Standard welding procedures according to ISO 15614.
- e) Pre-production welding test: used in all the cases in which the designed joint does not represent the actual one.

The use of standard welding procedure is quite common and includes also the welds realized for the experimental investigation.

In UNI EN ISO 15614-2 [45] the principal tests to carry out and to record into the welding procedure qualification report form (WPQR) are given.

In particular, the ones for a butt joint with full penetration are reported in the below Tab. 3:

Tab. 3 Requirements for a butt-joint WPQR according to ISO15624-2.

Test piece	Type of test	Extent of test
Butt joint with full penetration	Visual	100%
	Radiographic or ultrasonic	100%
	Penetrant testing	100%
	Transverse tensile test	2 test specimens
	Transverse bend test or fracture test for cast materials or wrought/cast combination	2 root and 2 face specimens
	Macroscopic examination	1 test specimen
	Microscopic examination	1 test specimen

The welding specification is valid indefinitely.

Regarding the personnel, UNI EN ISO 14732 [50], describes four methods to qualify the welding operators:

- a) Qualification on a standard WPS as reported in ISO 15614
- b) Qualification based on pre-production welding test ISO 15613
- c) Qualification on a test piece as per ISO 9606
- d) Qualification on a production sample test

The qualification mechanism consists in an initial qualification performing some welding tests on a specific component and finishes with a certificate with an expire date. Each 6 month the renewal shall be done and the responsible for welding activities confirms that the welder has applied the qualification in its work.

However, every two years two components welded on the production line not earlier than six months before, have to be tested with radiographic or ultrasonic examination in order to verify that the joint execution reaches the expected quality level. If this is not verified, the qualification can be revoked.

4.2 Characteristic parameters: current, tension, speed, gas flow rate and torch angle

During the welding process, some characteristic parameters are used. Among all it's important to consider that the combination of these parameters depends upon the gas used, the filler metal adopted and the base metal.

During the filler metal transfer two limit behaviour of the filler can be identified [51]: spray arc and short arc transfer. In the first case, after having overcome a certain value of the current called "critic", there is the detachment of small filler droplets at high frequency. This process is governed by electrodynamic forces.

In the case of short arc, the metal filler has a low dripping frequency. With low tension values, the droplets enter in contact with the pool, resulting in an instantaneous short circuit. This process is governed by electromagnetic forces that allows for droplet detachment.

For intermediate values of current and tension, the metal transferring is particularly irregular and governed by gravity force: this is typical of globular transferring where the droplets have high dimensions.

The representation of the three types of transfer in function of current and voltage is reported in the Fig. 4.1 below:

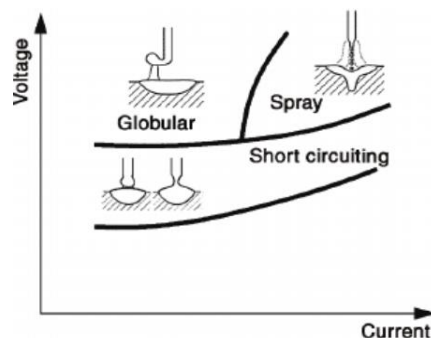


Fig. 4.1 Metal transfer in arc welding (from [51]).

The correlation of current, tension, speed, gas flow rate and torch angle will influence the final weld [51]:

- the current has an influence on the penetration depth. In fact, the Joule dissipated power increases increasing the current, having a deeper penetration and an increase of deposited metal. Indeed, the current influences the velocity of the charges involved in arc formation and consequently the thermic energy of the arc increases.
- the voltage value influences the deposition width. In this case too, the arc has a fundamental role because the voltage influences the number of charges

involved in the arc. For this reason, greater is the voltage, wider the arc until a certain limit value of voltage for which the arc is unstable.

- the welding speed is a key factor if related to the penetration. With speeds higher than 60 mm/min the welding seam will result significantly tighter and with low penetration.
- The gas protection has the double effect of protecting the pool during the welding process and at the same time creates the proper atmosphere for the arc generation. The gas flow rate is adjusted in function of the gas density, of the nozzle diameter and the current intensity.
- The contact tip to work distance influences the welding penetration. In this case lack of fusion defect can be generated. The distance (1) in the following Fig. 4.2 represents the contact tip to work that should remain constant during the welding process:

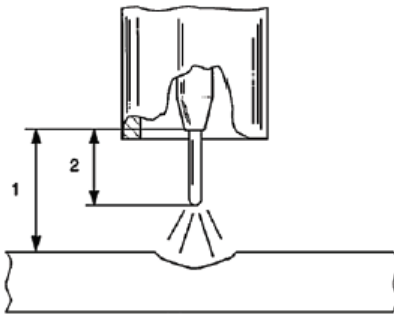


Fig. 4.2 Tip to work distance (from [51]).

- The torch angle is another important parameter to be defined. Two methods are commonly used: backhand welding and forehand welding, reported in Fig. 4.3. In the first case the torch is positioned in the opposite direction with respect to the wire advance. The arc energy is concentrated upon the pool and produces a greater penetration even if the pool visibility is difficult. In the second case the torch orientation is in the push direction, with a concave pool and less penetration.

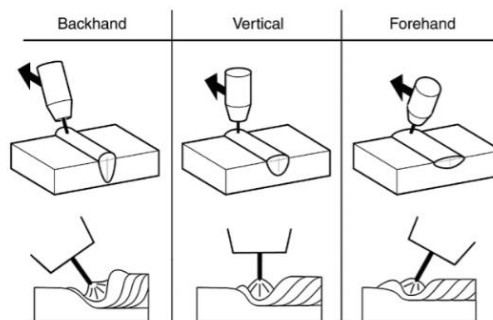


Fig. 4.3 Torch angle from [51]

5. Welding aluminium alloys

The aluminium alloys are highly used in airplane manufacturing as well as in trains manufacturing.

The common characteristics of all the alloys are:

- Low fusion temperature: $510 \div 650 \text{ } ^\circ\text{C}$.
- Low specific weight: $2,66 \div 2,85 \text{ g/cm}^3$.
- High thermal and electric conductivity.
- Al content greater than 95%

Adding some elements to the base metal, allows to obtain an enhancement of properties and in particular:

- Si reduces the thermal dilatation coefficient;
- Mg increases the corrosion resistance in alkaline environment and in sea;
- Mn increases the mechanical strength and the corrosion properties;
- Cu increases the mechanical resistance in hot conditions
- Zn associated with Mg enhances the mechanical strength.

In general, the aluminium alloys can be divided into two categories:

- Work hardened alloys: mechanical properties are enhanced with plastic deformation of the material;
- Thermal treatment alloys: mechanical properties are enhanced with a thermal treatment. The complete designation of tempers is reported in UNI EN 515 [1]. The thermal treatment is described with a letter followed by one or more numbers, indicating the sequence of the heat treatments applied. In this work the material AW6082-T6 will be used.

This is an Al-Mg-Si alloy solubilized and artificial aged as reported by the applicable Standard:

- The first thermal treatment is adopted to heat up the alloy above the solubilization curve and to have the second phase solubilized in the first one. At this point the temperature is maintained until the solid solution is homogeneous and the alloy is tempered at a below temperature to obtain a supersaturated solution.
- The second heat treatment is based on maintaining at a certain temperature the alloy in order to obtain better mechanical properties. In [25] it's reported the influence of time and temperature of aging on mechanical properties of this alloy. Both the yield and tensile strength increase with increasing aging time up to 10 hours at $160 \text{ } ^\circ\text{C}$. At higher temperature ($190 \text{ } ^\circ\text{C}$) the alloy shows an increase of mechanical properties up to 6 hours but after this time an overaged condition is

detected. In this case both the strength and the fracture toughness diminish.

One of the main problems of welding an alloy is the effect that the welding produces on the heat affected zone. Indeed, the welding process can be seen as a thermal treatment in which solubilization or recrystallization occurs.

Two aspects should be considered:

- 1- Aluminium alloys have a greater thermal conductivity than the steel alloys. For this reason, it is difficult to obtain a localized material fusion. Moreover, the material deformations due to the heat exchange are great and they are difficult to control.
- 2- The formation of a compound called alumina (Al_2O_3). This oxide is particularly dangerous during the welding process because its fusion temperature is around 2050 °C, temperature which is much higher if compared to the fusion temperature range of aluminium (600÷650 °C). This can lead to incomplete fusion of the base material resulting in oxide inclusions or lack of penetration.

For this reason, the thermal source required should be of high power and concentrated in the point of fusion to avoid metal deformations.

In addition, the alumina content is not easy to be removed by chemical attack. Thus, when the welding process where inert gas protection is adopted, the current polarity inversion allows to obtain the oxide removal from the pool. In this process there is a flux of the ions and electrons from the electrode to the pool.

In MIG (Metal Inert Gas) process it's common the input with direct current and the electrode (wire) connected to the positive pole. A mechanism allows to heat up the wire obtaining a faster filler deposition

Regarding to the gas protection it is possible to have, in MIG, a combination between Ar and He in different percentages. The most common percentages are 30% of Ar and 70% of He mixture. In the work [37] Ar and He effects have been deeply evaluated. In Tab 4 the properties of the two gases have been reported:

Tab. 4 Argon and helium properties (from [37]).

	Argon	Helium
Ionization potential	15.8 eV	24.6 eV
Arc initiation	Good	Poor
Arc stability	Good	Poor
Thermal conductivity (cal/sq. cm/cm/°C/s)	0.406×10^{-4}	3.32×10^{-4}
Density (relative to air)	1.38	0.137
Cleaning action	Good	Poor

The most important parameters are ionization potential and thermal conductivity. Ionization potential is the potential required to form an ion. Therefore, higher values of this parameter mean a relative difficult arc formation and stability. The thermal conductivity is higher in He than in Ar. This will help in a more efficient heat transfer to the workpiece when adding helium. In addition, with different combinations of Ar and He, a different penetration depth occurs: in general, higher content of Ar will result in a deeper penetration.

6. Welding imperfections and defects in aluminium

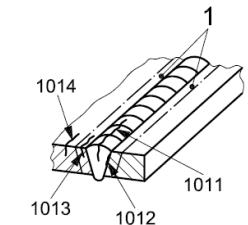
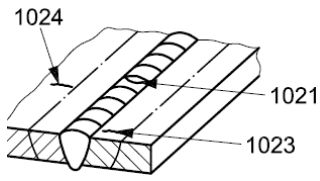
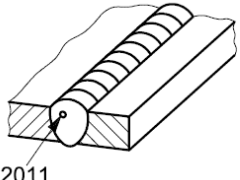
The first distinction between defect and imperfection is given in UNI EN ISO 6520-1 [48]. An imperfection is a discontinuity or a deviation from a foreseen geometry while a defect is an unacceptable imperfection around or inside the welding.

The Standard classifies into 6 categories the imperfections that can be found when dealing with welding:

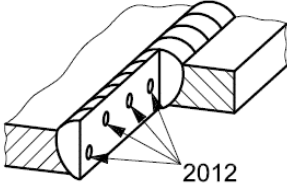
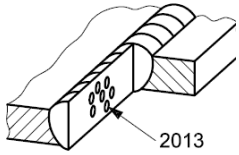
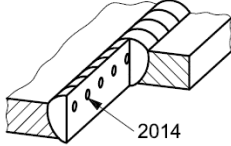
- 1- cracks;
- 2- cavities;
- 3- solid inclusions;
- 4- lack of fusion and penetration;
- 5- imperfect shape and dimension;
- 6- miscellaneous imperfections;

In this work will be reported the most significant ones and, in any case, related to the ones found during the experimental investigation. In the pictures of Tables 5 and 6, the numbers identify the crack location and the relative designation within the standard.

Tab. 5 Imperfections designation according to ISO 6520-1

Type of imperfection	Picture
Longitudinal crack: parallel to the weld axis.	
Transverse crack: transversal with respect to weld axis	
Gas pore	

Tab. 6 Imperfections designation according to ISO 6520-1

Type of imperfection	Picture
Uniformly distributed porosity: pores distribution uniform trough the weld	 <p>2012</p>
Clustered porosity: gas pores with a random geometric distribution	 <p>2013</p>
Linear porosity: gas pores distributed along the weld axis in a row	 <p>2014</p>
Slag inclusion: isolated inclusion. Also metallic with 3043 designation	 <p>3012</p>
Incomplete root penetration: one or both the faces of root not melted	 <p>4021</p>

6.1 Hot crack formation

One of the imperfections that can occur in aluminium is the hot cracking. When the pool is completely in liquid state, any stress is present due to the lack of mechanical continuity between the parts. When the welding is completely solidified, the shrinkage stresses are acting on the whole section of the joint.

An intermediate state, more dangerous, occurs when the two phases, liquid and solid, coexist. Indeed, shrinkage stresses start acting on the solid phase where the resistant section is smaller than the nominal one. This factor is accentuated if some impurities are present in the pool: due to their fusion temperature less than the base material, around the dendrites a certain amount of liquid phase remains. This contributes to reduce the resistant section and to increase the intergranular stresses to which the material has to react with its plastic deformation. If the plastic deformation does not occur, hot cracks, inter-dendrites, are formed.

The factors which influence the formation of hot cracks are:

- 1- High shrinkage effect during the solidification.
- 2- High values of ΔT during the solidification.
- 3- Hot crack weakness in the material.
- 4- High grain dimensions in the fused zone: low grain bonds formation.
- 5- Impurities.

Cross et al. in their work [7] observed that the cracking process is guided by the strain rate in the examined aluminium alloys. When a limit strain rate is exceeded, the crack nucleates. In addition, the grain refinement is a favourable element to be considered when dealing with the weldability of aluminium alloys to obtain a crack free welding.

6.2 Liquefaction cracking in HAZ

A phenomenon like hot cracking is liquefaction cracking and it occurs in HAZ. Heat Affected Zone, often abbreviated with HAZ, is the zone adjacent to the fused zone in which a thermal treatment occurs due to the heat generated by the welding process and the subsequent cooling.

During the cooling in HAZ, microcracks can occur. These cracks are also called hot cracks in the heat affected zone.

Chemical composition, filler metal and the joint design show a significant influence on liquefaction cracking in aluminium alloys. In [20] alloys 6005 T6 and 6082 T6 have been investigated with 4043 and 5036 filler metals. The conclusion of this research is that the result with 4043 filler, with the same welding parameters, is a welding with less cracks with respect to 5036 filler but with poor aesthetic aspect due to the dark welding produced.

Using MIG or TIG technique changes the heat input, resulting higher in TIG of about a factor of four. For this reason, the MIG technique is better than TIG in terms of crack formation: the lower the heating of the surface, the better is the behaviour from the point of view of liquefaction cracking.

Last, the fine grain dimension and low impurities help in reducing stresses produced in the welding.

When dealing with materials which do not show an allotropic transformation, like aluminium alloys, it is important to reduce the variation of chemical and mechanical properties of the base alloy when welded. In general, the following alterations can occur:

- Coalescence;
- Secondary phase precipitation;
- Hardening or ageing

Coalescence and precipitation of grains generate material softening with a decrease in both the yielding and ultimate strength and an increase in ductility.

6.3 Hydrogen in welding aluminium

Hydrogen molecule in nature exists in lots of compounds. For this reason, the most common source in welding is the metal surface where contaminations like oil, grease or humidity are present. However, when welding using protective gases, the protection inefficacy of the welding pool or humidity inside the gas, can be the source of hydrogen. A practical example is related to the ion H^+ that, associated in form of molecule in MIG welding process applied to aluminium alloys can give as result micro porosities, dangerous from structural point of view.

Pre and post heating will favour hydrogen elimination.

The pressure inside the cavities where the hydrogen is trapped, generates the reticular distortion and the reduction of the slipping planes inside the material. The hydrogen pores are important both in microstructural analysis and in impact toughness property of the resulting joint. As demonstrated in [15], it can be distinguished two microstructures, as showed in the following Fig. 6.1:

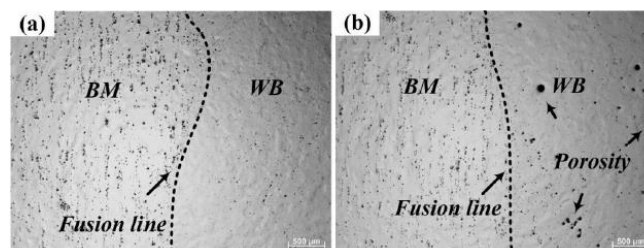


Fig. 6.1 Hydrogen in aluminium welding (from [15]).

In figure a) there is the microstructure of a hydrogen free welding. In this case no porosities are seen both in base metal and pool even if the hydrogen content is low ($0,18 \mu\text{g/g}$). In b) some porosities appear in the pool while the base metal remains as in figure a) with a hydrogen content of $0,38 \mu\text{g/g}$.

The micro cracks inside the material are initiation sites of rupture during the Charpy test, used to measure the impact toughness. For this reason, the higher is the content of hydrogen inside the structure, the lower will be the impact toughness revealed by the test.

The escaping mechanism takes place when the solidification starts and strongly depends upon the solidification velocity: if this parameter is too high, atomic hydrogen cannot escape and it remains trapped in molecular form. A good representation of this aspect is reported in the Fig. 6.2 below:

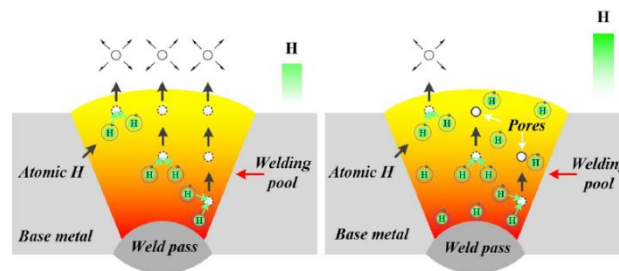


Fig. 6.2 Escape mechanism of hydrogen (from [51]).

As the welding pool solidifies, the hydrogen partial pressure diminishes. The solubility of hydrogen partial pressure (P_{H_2}) is proportional to the square root of the partial pressure multiplied by the balance constant K :

$$S_H = K \sqrt{P_{H_2}}$$

Therefore, during the solidification process, ions H^+ are combined in molecular form, obtaining pores that will tend to escape due to the decreasing solubilisation of hydrogen. In case of high hydrogen content, it is possible that not all the hydrogen has enough time to escape and there is the formation of pores just over the welding surface.

7. Quality levels of acceptance

In examining the imperfection when an aluminium structure is designed the manufacturer have to comply to specific requirements that both Eurocode 9 and UNI EN 15085-3 [36] specifies. UNI EN 15085 is specific for railway applications.

In part 3 of UNI EN 15085 attention is given to the stress category and the weld performance class.

From the stress categories, divided into high, medium and low, the safety categories can be obtained. The safety categories are classified into three levels:

The category *high* means that the weld failure can lead to serious consequences on both people and structure,

The category *medium* means that the weld failure can lead to an important damage on the structure and potential consequences on personal injuries.

The category *low* means that the weld failure does not impact on the structure functionality and the consequences on people are improbable.

The standard gives the stress factor that the designer has to meet in order to comply to the stress category. The stress factor is the ratio between the calculated stress over the fatigue admissible one.

Referencing values are reported in the Tab. 7 below:

Tab. 7 Reference values of stress factors according to ISO 15085-2.

Stress Category	Stress factor (S)
High	$\geq 0,9$
Medium	$0,75 \leq S < 0,9$
Low	$< 0,75$

Furthermore, the weld performance classes can be defined based on safety and stress category as follows in the Tab. 8 below:

Tab. 8 - Weld performance classes (from [36]).

Stress categories	Safety categories		
	High	Medium	Low
High	CP A ^a	CP B ^c	CP C2
Medium	CP B ^b	CP C2	CP C3
Low	CP C1 ^d	CP C3	CP D

^a Weld performance class CP A is a special class which applies only for welds with full penetration and full accessibility for inspection in production and maintenance.

^b Weld performance class CP B:
CP B for safety category „high“: is only valid for welds with full penetration and full accessibility for inspection in production and maintenance.

^c CP B for safety category „medium“: is also valid for welds without the possibility for a volumetric test; in this case a special remark “medium safety category/increase of surface test is required” shall be indicated on the drawing and the tests according to Table 1 of EN15085-5:2007 shall be carried out.

^d Weld performance class CP C1:
CP C 1 is also valid for welds without the possibility for volumetric testing. In this case a special remark “surface test necessary” shall be indicated on the drawing and the tests according to Table 1 of EN 15085-5:2007 shall be carried out.

Based on the weld performance class, the respective inspection class can be found. At this point per each combination of the 9 possibilities in the above-mentioned matrix, a table with the required controls for welding quality assurance can be derived, as showed in Tab. 9:

Tab. 9 Inspection classes (from [36]).

Stress category	Safety category	Weld performance class	Quality levels for imperfections EN ISO 5817 EN ISO 10042	Inspection class	Volumetric tests RT or UT	Surface tests MT or PT	Visual examination VT
High	High	CP A	see Table 5 or Table 6	CT 1	100%	100 %	100 %
High	Medium	CP B	B	CT 2	10%	10 %	100 %
High	Low	CP C2	C	CT 3	Not required	Not required	100 %
Medium	High	CP B	B	CT 2	10%	10 %	100 %
Medium	Medium	CP C2	C	CT 3	Not required	Not required	100 %
Medium	Low	CP C3	C	CT 4	Not required	Not required	100 %
Low	High	CP C1	C	CT 2	10 %	10 %	100 %
Low	Medium	CP C3	C	CT 4	Not required	Not required	100 %
Low	Low	CP D	D	CT 4	Not required	Not required	100 %

Even if for all the tests a visual examination is required, surface or volumetric tests are required only in case of inspection class CT 2 and CT1.

The Quality levels for imperfections are then listed in UNI EN ISO 10042 [47] if dealing with aluminium alloys. These levels are B, C or D depending on the stress and safety category that the designer chooses in UNI EN 15085-3.

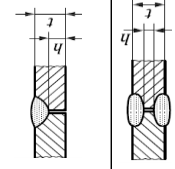
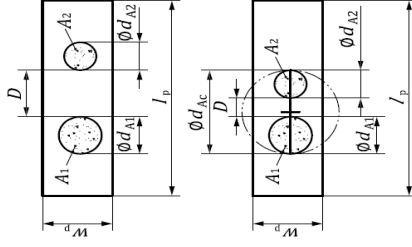
This Standard distinguishes two types of imperfection: surface and internal imperfections. They are linked to ISO 6520-1. The following imperfections, related to butt welds with full penetration, are here reported:

- 1- Porosities.
- 2- Inclusions.
- 3- Lack of penetration.

In Tab 10 acceptance criteria for the above-mentioned imperfections are classified over ISO 10042. These values have to be used in evaluating such imperfection and the welded part should be scrapped or reworked where these values are not respected.

Tab. 10 Acceptance levels for quality imperfections according to ISO 10042

Limit for imperfections for quality levels						
Reference No. in ISO 6520-1	Type	Remarks	t mm	D	C	B
2013 (Clustered (localized) porosity)	Surface imperfection	The total gas pore area within the cluster is represented by a circle of diameter, dA, surrounding all the gas pores. The requirements for a single gas pore shall be met by all the gas pores within this circle. A permitted porous area shall be local. The possibility of the pore cluster masking other imperfections shall be taken into consideration. If D is less than dA1 or dA2, whichever is smaller, then the total gas pore area is represented by a circle of diameter, dAc, where dAc = dA1 + dA2 + D. Systematic clustered porosity is not permitted.	≥0,5	dA ≤ 25 mm or dA,max ≤ wp dA corresponds to dA1, dA2 or dAc whichever is applicable	Not permitted	Not permitted
2013 (Clustered (localized) porosity)	Internal imperfection	The total gas pore area within the cluster is represented by a circle of diameter, dA, surrounding all the gas pores. The requirements for a single gas pore shall be met by all the gas pores within this circle. A permitted porous area shall be local. The possibility of the pore cluster masking other imperfections shall be taken into consideration. If D is less than dA1 or dA2, whichever is smaller, then the total gas pore area is represented by a circle of diameter, dAc, where dAc = dA1 + dA2 + D. Systematic clustered porosity is not permitted.	≥0,5	dA ≤ 25 mm or dA,max ≤ wp	dA ≤ 20 mm or dA,max ≤ wp	dA ≤ 15 mm or dA,max ≤ wp/2
2014 Linear porosity	Surface imperfection	-	≥0,5	Not permitted	Not permitted	Not permitted
2014 Linear porosity	Internal imperfection	-	≥0,5	Short imperfections permitted	Not permitted	Not permitted
2011 Gas pore	Internal imperfection	-	≥0,5	d ≤ 0,4s or 0,4a but max. 6 mm	d ≤ 0,3s or 0,3a but max. 5 mm	d ≤ 0,2s or 0,2a but max. 4 mm
2012 Uniformly distributed porosity	Internal imperfection	-	0,5 to 3 ≥3 to 12 >12 to 30 >30	≤6 % ≤10 % ≤15 % ≤20 %	≤2 % ≤4 % ≤6 % ≤8 %	≤1 % ≤2 % ≤3 % ≤4 %
304 Metallic inclusion	Internal imperfection	if there is more than one inclusion, the total length is the sum of the single ones.	≥0,5	l ≤ 0,4s or 0,4a but max. 6 mm	l ≤ 0,3s or 0,3a but max. 4 mm	l ≤ 0,2s or 0,2a but max. 3 mm
402 Incomplete root penetration	Surface imperfection	-	≥0,5	Short imperfections but no systematic imperfections. h ≤ 0,2t max. 2 mm	Not permitted	Not permitted
402 Lack of penetration (incomplete penetration)	Internal imperfection	-	≥0,5	Short imperfection: h ≤ 0,2t, but max. 2 mm	Not permitted	Not permitted



8. Non-Destructive Testing (NDT)

Non-destructive testing is often used to inspect parts that cannot be checked internally without a destructive test.

For this reason, the personnel that performs such inspections has to be trained on specific modules for NDT. In general, the applicable standard for non-destructive testing is UNI EN ISO 9712 [28]. In this Standard, three levels of qualified personnel are foreseen:

- Level 1: the personnel certified for this level can perform the test, classify the results and write the report according to written criteria. The person cannot be responsible for the test method or for the interpretation of the test results.
- Level 2: the personnel certified for this level, in addition to what is foreseen for Level 1, can:
 - select NDT for the testing method,
 - write instruction sheets based on standards/specifications,
 - interpret the test results,
 - be a guide/supervisor for other personnel of same or below Level.
- Level 3: the personnel certified for this level, in addition to what is foreseen for Level 2, can:
 - be the responsible of a test centre and staff,
 - validate NDT instructions and procedures,
 - interpret the available standards, codes, specifications and procedures
 - decide for a particular test method that has to be used for NDT and write instructions accordingly.

All the levels, in order to obtain the certification, have to comply to specific requirements in terms of theoretical and practice examination as well as relevant industrial experience as defined within the specific non-destructive test. UNI EN ISO 9712 individuates 10 non-destructive tests that are listed, with their abbreviations, in the Tab. 11 below [28]:

Tab. 11 Non-destructive tests according to ISO 9712 (from [28]).

NDT method	Abbreviated terms
Acoustic emission testing	AT
Eddy current testing	ET
Infrared thermographic testing	TT
Leak testing	LT
Magnetic testing	MT
Penetrant testing	PT
Radiographic testing	RT
Strain gauge testing	ST
Ultrasonic testing	UT
Visual testing	VT

The methods used for checking welded aluminium alloys are ultrasonic testing, visual testing, radiographic testing, penetrant testing and the emerging technique which is the thermographic testing.

Non-destructive tests are often divided into volumetric tests and surface tests. Ultrasonic and radiographic tests are classified as volumetric while penetrant and visual tests as surface tests. In the following sections there will be a description of each of them.

8.1 Ultrasonic testing

Ultrasonic testing takes advantage on the ultrasonic waves that have a frequency greater than 20 kHz. The basic principle of this technique is to analyse the response after the material excitation.

In doing this operation it is worthwhile to note that when the part under test is excited its particles starts to vibrate around an equilibrium position determined by the electrostatic forces. Thus, the ultrasonic waves transmission is strictly dependent upon the means in which they are sent and propagate with a finite velocity.

There are different types of waves that can be used to intercept the flaws inside the welding:

- Longitudinal waves: they are also called compression waves and the particles oscillation is parallel to the wave propagation direction.
- Transversal waves: the particles oscillations are normal to the wave propagation direction.
- Superficial waves: they are also called Rayleigh waves and the particles vibrate in both the normal and parallel direction with respect to wave propagation. These waves are typical of a surface where there is the separation between the transmission medium, for example the metal and the air.
- Lamb waves: they are typical of means that have a thickness comparable to the wavelength.

An important parameter is the propagation velocity inside the medium. This is calculated in function of the Poisson ratio ν , the elastic module of the material E and the density of the material ρ . A specific formulation for each type of wave can be identified and in particular:

- For longitudinal waves: $V_L = \frac{E(1-\nu)}{\rho(1+\nu)(1-2\nu)}$;
- For transversal waves: $V_T = \frac{E}{2\rho(1+\nu)}$;
- For superficial waves: $V_R = \frac{0,87+1,12\nu}{1-\nu} \sqrt{\frac{E}{2\rho(1+\nu)}}$

Electrical transducers are specific devices that transform electric energy into mechanical vibrations of high intensity. They can be piezoelectric, electromagnetic, electro resistive or magneto resistive. The transducer and its frame constitute the probe. UNI EN ISO 16810 [29] states that the probe selection is based on material type and conditions (shape, thickness and surface aspect) and on the imperfection orientation. Indeed, the material transparency to the ultrasound wave can directly influence the instrument choice due to the opportunity to obtain high sensibility and high resolution (low damping phenomena).

Thus, the material thickness influences the full-scale setup during the probe calibration while the accessibility narrows the probe angle choice.

In welding inspection, a preliminary evaluation should be done. They are related to:

- Flaps preparation: in this case some hypothesis can be done on possible defects that can be found. As a general rule it's important to choose a probe angle that will detect the greatest number of defects.
- Welding process and position knowledge: can be useful to interpret some results.
- Joint superficial conditions have to be checked before starting the inspection. In this case a certain value of the superficial roughness may be required.

Regarding the equipment in UNI EN ISO 17640 [33] some useful ranges of the principal parameters in welding metallics are reported:

- The test frequency must be between 2MHz and 5MHz.
- Where the ultrasonic waves shall be reflected by an opposite surface, the angle of incidence for transverse waves between the normal to the reflective surface and the beam is between 30° and 70°.
- The gap between the probe surface and the tested part surface shall remain within 0,5 mm.
- The scanning volume is represented by the weld, the parent metal and the HAZ width.
- Sensitivity and range setting shall be corrected according to the values given in the Standard if the deviation is greater than 2dB or 1% of the range.
- The noise level shall remain 12dB lower than the testing level.

- Four techniques are used to set the reference sensitivity, as reported in the Tab. 12 below:

Tab. 12 Reference sensitivity setting for ultrasonic testing according to ISO 17640.

No.	Reference specimen	Remarks
1	side-drilled hole 3mm in diameter	based on distance amplitude curve (DAC)
2	disk-shaped reflectors with diameter D_{DSR} in function of thickness	based on distance gain size curve (DGS)
3	rectangular notch 1mm wide per 1mm in depth	beam angles greater than 70° thickness between 8mm and 15mm
4	flat-bottomed holes disk-shaped reflectors of 6mm in diameter	beam angle equal to 45° thickness greater than 40mm

During the inspection a signal reveals some indications inside the material. Such indications can be classified according to ISO 23279 [32], by using a 5-stage discriminatory technique:

Stage 1: at this stage echo amplitudes below the evaluation level do not need a characterization;

Stage 2: in second stage all the indications are considered as planar discontinuities if they exceed 6dB the reference level;

Stage 3: This stage applies only to indications that exceed in length:

- the thickness of the investigated material if the thickness is between 8mm and 15mm
- Half the thickness or 15mm if the thickness is over 15mm

This method is based on direction reflectivity criteria and echoes shall be compared when generated by the same reflector. For this reason, more than one probe is used:

- For normal-beam probes and beam-angled probes, the frequency has to be chosen in order to obtain same wavelengths for transversal and longitudinal waves.
- For two beam-angled probes, the difference between the refracted angles shall be equal or greater than 10° .

At this point the maximum echo value, detected along the discontinuity, is compared with the minimum one detected from all other directions to assess if a lack of fusion is present. To confirm the result, these conditions have to be satisfied:

- The maximum detected echo is greater than the reference level minus 6dB;
- The difference between the maximum echo and minimum echo is, in modulus, at least:
 - 9dB only if transverse wave probes are used;
 - 15dB if probes that produces transversal and longitudinal waves are used;

Stage 4: This stage aims to classify inclusions and it is based on echo static pattern. The discontinuity pattern in two directions of testing is compared to the pattern of a reference reflector with 3mm in diameter and side-drilled holes. The Standard states that to have an inclusion the pattern should be single and smooth.

Stage 5: This stage aims to classify cracks and it is based on the transverse echo dynamic pattern. The principle is to move the probe perpendicular to the discontinuity and to analyse echo behaviour. If the patterns identified at this stage do not match the patterns in 3 and 4, the discontinuity has to be classified as non-planar. The figures below show an example of echoes in single (Fig. 8.2) or cluster of (Fig. 8.1) non-planar discontinuities:

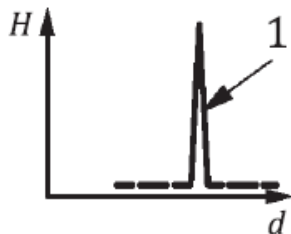


Fig. 8.2 single non-planar discontinuity according to ISO 23279 (from [32]).

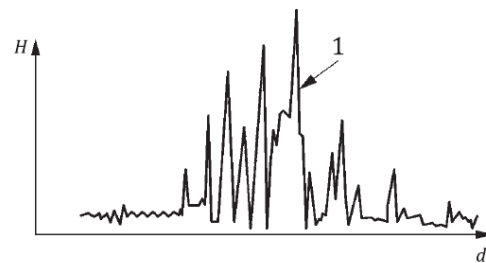


Fig. 8.1 clustered non-planar discontinuity according ISO 23279 (from [32]).

8.2 Radiographic testing

In inspecting welds in metallic materials, the radiographic method is very useful to detect internal defects that can, potentially, represent an initiation site for a crack.

The inspection can be done with both x- or gamma-rays that are electromagnetic waves with a wavelength much smaller than the wavelength of the light. They have the following advantages:

- High energy density that allows to examine bodies that are opaque to the light.
- They are adsorbed by bodies in function of the materials and their thickness.
- They can impress a photographic film.

These properties are essential to individuate internal imperfections such as cracks, porosities, slag inclusions and lack of penetration.

Two main means are in use in this field: x and gamma-ray with films and x and gamma-ray with digital detectors. The applicable standards for this technique are: UNI EN ISO 17636-1 [30] related to the film use and UNI EN ISO 17636-2 [31] for the digital detector use.

For both, a preliminary classification of the radiographic is the Class. Class A uses the basic technique while Class B uses an improved technique with enhanced parameters. A relevant constraint is set, based on the Class, on the density. Indeed, the density of the radiographs should have a minimum value of:

- 2 for Class A;
- 2,3 for Class B;

In general, in order to obtain a visible image, the image quality indicator (IQI) is used. Wire or step hole IQI shall be positioned close on the source side or on the film/digital detector side. Before starting the investigation, the following aspects have to be verified:

- If a wire is used, 10mm length of the wire are clearly visible on the base material. If a digital detector is used, this length value is visible in uniform grey section.
- If a step hole is used, at least two holes are clearly visible or the number of specified holes near the welding are visible if a digital detector is used.

Using the digital detector, the basic spatial resolution of the digital image have to be measured and it should not exceed the limit values given in the Standard in function of material thickness.

Then a comparison between the obtained results and the reference ones should be done in order to verify that the IQI value is the minimum acceptable.

The positioning of the radiation source can be achieved for different types of joints. Using the film technique for a butt welded joint penetrated by one side, as the one used in experimental investigations, a perpendicular positioning with the film behind the

joint can be used. A representative sketch with the main dimensions is reported in UNI EN ISO 17636-1 [30] and in Fig. 8.3:

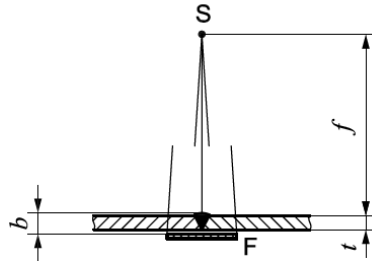


Fig. 8.3 Main dimensions for equipment disposal for a butt joint radiographic test (from [30]).

Positioning the source perpendicular to the joint to examine and exposing the part to the radiation source for a certain time called exposure time, it's possible to observe the x- or gamma-rays impression on the photographic film. This impression will be uniform for constant material thickness and no imperfections. Instead, if an imperfection is present, the outgoing radiation will be of higher intensity where the imperfection is located and the photographic film will appear darker in that zone.

The main relation between the dimensions in the above figure is related to the source-to-object distance if Class A is applied:

$$\frac{f}{d} \leq 7,5b^{2/3}$$

or if Class B is used will be:

$$\frac{f}{d} \leq 15b^{2/3}$$

Where:

- d is the focal spot size which is the size of the radiation source;
- b is the object-to-film distance
- f is the source-to-object distance;

In the Standard a nomogram is reported to determine the minimum source-to-object distance f_{min} in function of d and b .

Finally, a parameter of interest is the voltage for the x-ray tube. This is calculated, as reported in the diagram below (Fig. 8.4), considering the penetrated thickness w of the tested part and the material in both the cases of film and digital detector use.

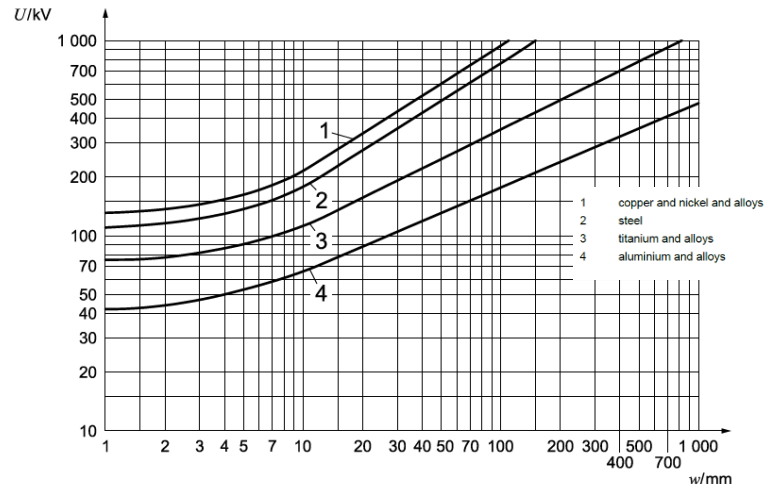


Fig. 8.4 Voltage selection in function of materials tested and penetrated thickness in radiographic testing (from [30]).

The Standard recommends that the voltage of the x-ray tube should be maintained as low as possible in order to obtain a clearly visible flaw.

8.3 Visual testing

Visual testing technique is one of the most used NDT in welding field because of its simplicity and readiness to use. In UNI EN ISO17637 [34] the minimum requirements to inspect a welded joint are specified and they are:

- Brightness of the surface: minimum 350 lx.
- Field of view: a minimum angle of 30° is recommended with a maximum distance for inspecting the part of 600mm. Whether this distance cannot be respected due to lack of accessibility, remote inspection should be considered

The test can be carried out:

- during the joint preparation to inspect the shape and dimensions of the joint according to the WPS applicable. In addition, the surface to be welded are clean and, if applicable, surface treatments are applied and the parts are fixed one each other in position as the joint requirement in WPS.
- during the welding to inspect:
 - cleaning of the single run when multi-pass welding is used;
 - any visible defect;
 - the gouging or any other repair gives as a result a welding that complies to the applicable WPS;
- After the welding process to inspect:
 - welding flush;
 - grinding marks to verify that the surface is not uneven;
 - slag, tool or bowl impressions are not present on the surface;
 - weld profile to check that is regular;
 - weld width to check the consistency and in case of butt weld the complete filling;
 - penetration, root concavity, undercuts, imperfections and arc strikes are within the acceptance levels defined on the drawing.

When the visual test fails, the welding can be repaired or completely removed.

In the first case the defect has to be removed completely and it is available full accessibility for the joint execution. Instead when the welding is completely removed the operator has to create the same conditions of surfaces (dimensions, shape and surface treatments) as the original welding as described in WPS.

8.4 Penetrant testing

The basic principle of this test is to use the penetration capacity of special liquids to identify indications on the surface of the part to be inspected.

The advantages of this technique are related to the readiness to use, economical convenience and the relative low time required for the inspection. However, the inspection can reveal only superficial imperfections and it is applicable only where the accessibility to the surface is good both for liquid application and the following visual inspection. Another limit is the surface roughness that gives false indications if too high.

Different methods can be used, depending on the product used. A complete classification is given in UNI EN ISO 3452-1 [27] and reported in the below Tab. 13:

Tab. 13 Penetrant testing: methods classification according to ISO 3452-1 (from [27]).

Penetrant		Excess penetrant remover		Developer	
Type	Denomination	Method	Denomination	Form	Denomination
I	Fluorescent penetrant	A	Water-washable	a	Dry powder
II	Colour contrast	B	Post-emulsifiable, lipophilic	b	Water-soluble
III	Penetrant Dual-purpose (fluorescent colour contrast penetrant)	C	Solvent-removable:	c	Water-suspendable
			— Class 1, halogenated		
			— Class 2, non-halogenated		
		— Class 3, special application			
D	Post-emulsifiable, hydrophilic	d	Solvent-based (non-aqueous for Type I)		
E	Water- and solvent-removable	e	Solvent-based (non-aqueous for Types II and III)		
			f	Special application	

For specific cases, it is necessary to use penetrant testing products complying with particular requirements with regards to flammability, sulfur, halogen and sodium content and other contaminants. See ISO 3452-2.

The main steps of inspection procedure are:

- 1- Cleaning the surface: this operation can be done with alkaline solutions, vapour with high pressure and/or sanding. This latter technique can occlude the superficial discontinuity where present on the part and for this reason it has to be used with care.
- 2- Drying: this step is applicable only if volatile cleaning solutions are not applied. This process is done with dry air to ensure the complete removal of water in order to avoid compromising penetration and so to hide the imperfection.
- 3- Penetrant liquid application: this step can be done by different means (i.e. spray application, brush application...) but an important parameter is the penetration

time. As reported in ISO3452-1 [27] this time is between 5 and 60 minutes depending on the application.

- 4- Excess penetrant removal: in this step, based on the product used, it can be possible to remove the penetrant liquid with water or emulsifier. In this latter case a post-emulsifiable product shall be used to remove penetrant. As shown in the above table, these products can be:
 - a. Hydrophilic: in this case a water washing is needed before the application. This product cannot be applied with brush due to the risk of removing the penetrant from the imperfection.
 - b. Lipophilic.

In both the cases a and b, the concentration and contact time shall be determined by experimental tests. In addition, a water washing shall be done after the application.

Care should be taken respect to this step because a deep washing can remove the penetrant liquid from the discontinuity but at the same time a bad removal can highlight false indications or hide the imperfection.

- 5- A drying cycle is required at this step.
- 6- Developer application: based on the developer type but in all the cases the surface of interest has to be covered in a uniform manner.
 - a. Dry powder developer is used only with fluorescent penetrants;
 - b. Water-suspended and water-soluble developers are applied by spray or by immersion. The immersion time should be as low as possible and it is followed by drying.
 - c. Solvent-based developer is applied by spray.

The development time is the time, between 10 and 30 minutes, after which the part can be inspected. This time is determined by tests and it is influenced by the temperature, the type of imperfection and the used developer.

- 7- Inspection can be done in two ways, depending on the penetrant applied:
 - a. Fluorescent technique: in a dark inspection area or with UV-A background light.
 - b. Colour contrast technique: with minimum 500lx on the surface to be inspected.

Further evaluation can be done after the inspection on the indications. They can be false indications mainly when there is a contamination of the surface under inspection. This could happen when the above procedure is not respected and excess of penetrant is not well removed or traces are present on the operator hands. Some indications can also be present at material discontinuity due to its shape. These indications are not considered because they are present on the drawing of the part.

Real indications are classified as linear (the length is 3-times the width) or non-linear. In welding inspections, linear indications can be represented as continuous line and they could represent lack of fusion, intended lines or even a crack. Non-linear ones are mainly related to superficial porosities.

9. Thermography: theory outline

As stated in [2] thermography is the study of the thermal patterns built from a distortion of the heat flow due to the imperfections that are present in the material.

Plank's Law [5] describe the base law for thermography because it illustrates the physical quantities of radiated energy due to the thermal effect from a back body through an empty space:

$$(i_{\lambda\varphi})_n = \frac{2c_1}{\lambda^5 \left(e^{\frac{c_2}{\lambda T}} - 1 \right)}$$

Where the two constants c_1 and c_2 are:

$$c_1 = 5,9548 * 10^{-17} \frac{Wm^2}{sr}; \quad c_2 = 1,43879 * 10^{-2}$$

and λ is the wavelength, T the temperature.

As it can be seen in the below Fig 9.1, whose curve are called black body isotherm emission spectrum, the blackbody irradiate in an ample spectrum of wavelengths and the monochromatic emission has a characteristic maximum at λ_{max} .

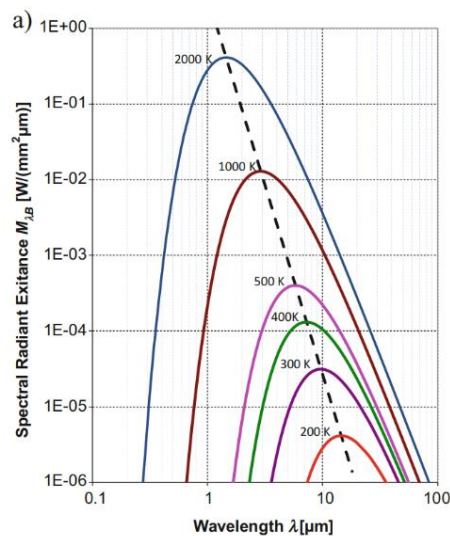


Fig. 9.1 Black body isotherm emission spectrum (from [5]).

This maximum value is lowered increasing the temperature. This is expressed by Wien law as follows:

$$\lambda_{max} T = 2898 \mu m K$$

This law establishes that the λ_{max} value is inversely proportional to the irradiating blackbody temperature.

Finally, it is useful to define the emissivity for a non-black body as follows:

$$\varepsilon = \frac{i_{\lambda\varphi}}{(i_{\lambda\varphi})_n}$$

Where $i_{\lambda\varphi}$ represents the emission of a generic body at a certain temperature and $(i_{\lambda\varphi})_n$ represents the emission of a blackbody at that temperature. This value ranges between 0 and 1. The value of 1 corresponds to the emissivity of a blackbody.

9.1 Thermography: techniques and acquisition systems

The thermographic investigation is divided into two major techniques:

- Passive thermography
- Active thermography

The above methods are used by the means of an acquisition system that allows to guarantee data detection and processing from the IR scene.

A thermal imaging camera is often used to estimate the temperature profile in a test with a field of functioning between the infrared and far infrared ($3 \mu m \leq \lambda \leq 13 \mu m$). The resulting profile is an approximation due to the reflection and transmitted radiation of the object.

A second optical camera is used to see the scene, but it does not measure the temperature.

In order to operate the image acquisition and processing, it is important to have a system as the one represented in the below Fig. 9.2 [17].

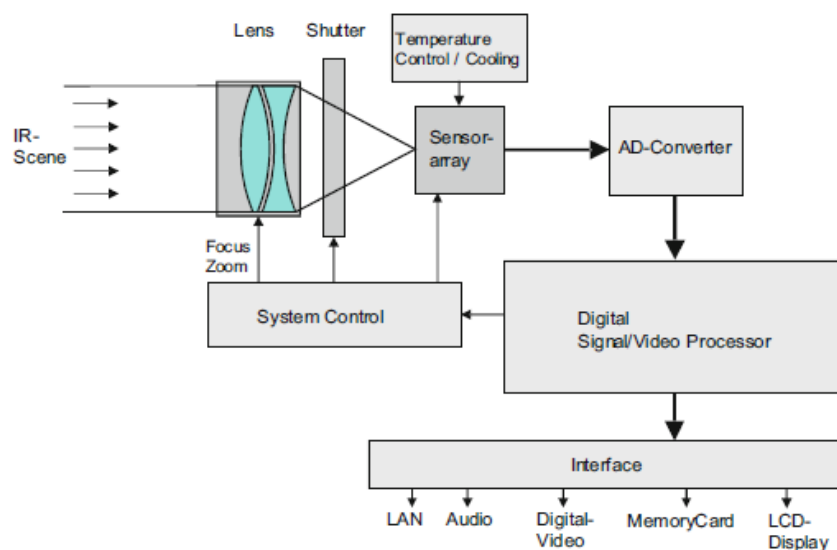


Fig. 9.2 Design of a thermal image camera (from [17]).

As it concerns the system, it is possible to identify:

- the lens;
- the shutter, of particular importance in uncooled systems that is cyclically closed to re-calibrate the system. In this kind of systems, during the measurement process the shutter is triggered to avoid disturbance. Instead in cooled cameras the shutter is not used or its cycle time is set to few hours;

- the AD converter in which signal is converted on a 14bit to 16bit basis;
- the video processor that elaborates the signal;
- the interfaces that are used to connect the camera to other systems (e.g. the audio/video interface to capture the most important points on the tested parts).

A general classification for the camera choice is based on the presence of a cooling system:

- Uncooled cameras use a thermal sensor with a Peltier element stabilized at room temperature. They are used for temperatures higher than 200 °C because the sensor has very low sensitivity.
- Cooled cameras use photon sensors with very narrow band.

The following Fig. 10.2 shows a comparison between a thermal and photon sensor depending upon two quantities: the wavelength and the BLIP detectivity.

This latter is defined in [17] and the background-limited infrared performance detectivity and represent the threshold of the absolute detectability (ref. Fig. 9.3)

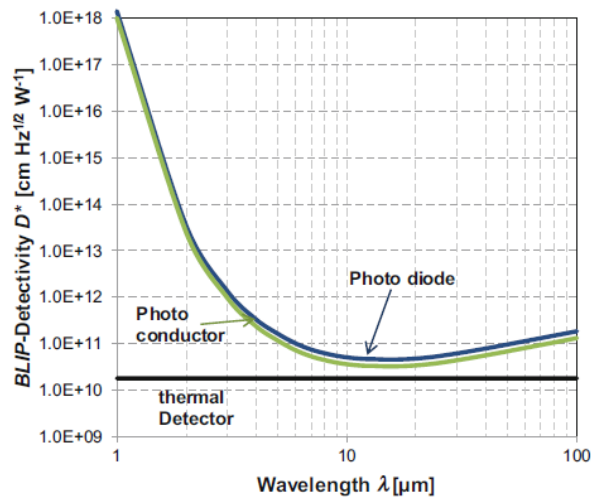


Fig. 9.3 BLIP detectivity in function of the sensors used (form [17]).

Comparing the two types of sensors, the detectivity of photon sensors is greater than the thermal one and for both it depends on the wavelength.

9.2 Passive thermography

This technique is used for an estimation of the thermal dissipation on the surface of the sample when subjected to a mechanical stress.

As stated in [17], passive thermography can highlight anomalies in the thermal profile of the surface of the sample. In this case the way to identify the material imperfections is to find the hot spots or temperature differences with respect to room temperature.

When the difference in temperature is of about 1-2 °C, a suspicious behaviour is considered. Instead when the hot spot is of about 4 °C this is a good proof of an anomaly inside the component. [2]

9.2.1 Fields of applications of the passive thermography

The passive thermography technique is widely used in lots of sectors from research and development departments to manufacturing ones, where the study is generally conducted in in-service conditions.

Of interest is the study [40] in the railway sector. In this case the experiment with the passive thermography technique has been carried out to obtain the temperature distribution on the brake disks in function of different forces, three different thicknesses of the brake pads and two simulated speeds. In this work it is underlined also how the emissivity value influences the obtained results. In particular the hot spot investigation will result attenuated when the value of the surface emissivity is too low. Also, in fatigue investigation of components, this method gives its advantages. As presented in the work [8] the notch in samples under fatigue load shows an increase in temperature. This allows to determine the relationship between the hot spot and the crack initiation site.

Finally, this technique is used even in the investigation of electric circuit. Indeed, as in [19] passive thermography can be used to inspect high-voltage cabling for electric traction motors in locomotive units. As in [22] some parameters will influence the inspection:

- 1) Spatial resolution: each camera lens has a geometric resolution that define the dimensions of the part of which you can take the temperature for a given distance. An insufficient camera resolution will lead to a wrong temperature measurement, underestimating the real temperature of the object. In the following Fig. 9.4 an example of the minimum dimensions of the object at different distances are taken into account for an objective with focal length of 35mm and geometric resolution of 1,4.

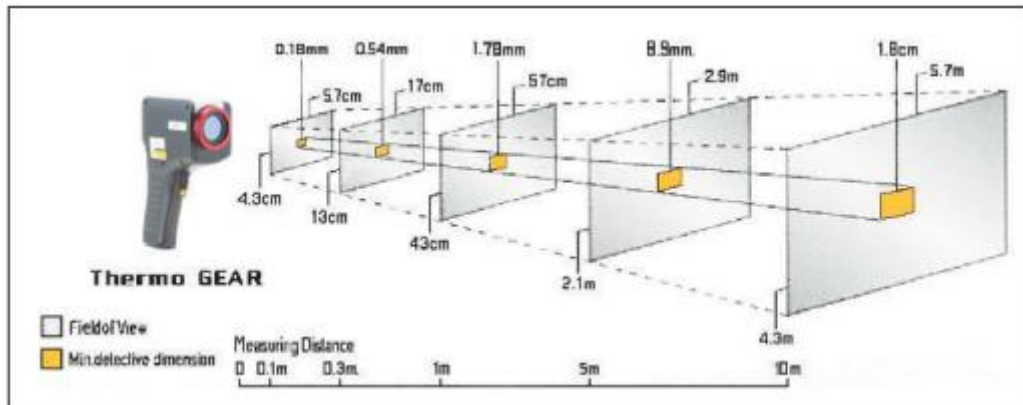


Fig. 9.4 Spatial resolution in function of the distance (from [22]).

- 2) Load: during the inspection of a three-phase circuit, it is important to compare the different phases temperature in order to assess if an anomaly has occurred. In the normal operating condition, all the phases should have the same temperature. The central phase has usually a slightly higher temperature due to the lower heat exchange with respect to the two adjacent ones.
- 3) Emissivity variation: the low emissivity of a component (e.g. with a shining surface) will result in a reflection of the surrounding sources of temperature.
- 4) Reflection: components with low emissivity will cause hot spots on the thermogram and this will result in a false indication. A good compromise to attenuate this phenomenon is to frame the object at different angles.
- 5) Solar heating: in case of high solar radiating, depending on the thermic capacity of the material, the thermic map could result in a temperature difference. The problem can be detected due to the fact that the temperature profile will coincide with the shady areas
- 6) Resistance increase: this problem is caused mainly by the tightening loose in bolted assembly where the thermic conductivity will cause a hot spot or by material oxidation.
- 7) Wind: the effect is to lower the measured temperature of the component. The inspection should not be done if the wind speed is above 8 m/s. For speeds lower than 8m/s a correction factor has to be considered to narrow the temperature value to the real one.

9.3 Active thermography

Active thermography technique implies an external heat source for the excitation of the material. This leads to a variation in the thermal conductivities and in the heat capacities of the samples under investigation and allows to recognize the response of the material discontinuity to that excitation.

9.3.1 Heating sources

As reported in [17] the sources for heating the component are:

- External: in this case the external surface of the component is heated by radiation, convection or thermal conduction. The excitation from the rear of the specimen is favourable with thin samples.

Internal: the heating takes place inside the volume of the specimen. The defects like cracks are heated and they are easily spotted.

The below Tab. 14 gives some examples of commonly used sources:

Tab. 14 Heat sources for active thermographic investigations (from [17]).

External sources	Radiation	Flash and photolamps Infrared emitters Halogen lamps Lasers Microwaves (electrically conductive materials) Sun (day/night change)
	Convection	Hot or cold air blowers Driers
	Thermal conduction	Heating plates Hot or cold water
Internal sources		Resistance heating (electrically) Inductive heating Sonic or ultrasonic excitation Chemical reaction Thermoelastic effect Microwaves (dielectrics)

9.3.1.1 Inductive heating

Inductive heating uses eddy currents that causes Joule dissipation and they heat the material. The method is non-contact, very low time spending and can be automated.

9.3.1.2 Ultrasound Heating

This source is typical of vibrothermography (contact process) and takes advantages on the material elastic properties for propagating the waves inside it. The defect is heated at its boundaries and can be measured on the surface of the specimen. Some limitations

are related to the samples of complex geometry and the high energy density that could result in a material damage.

9.3.1.3 *Microwaves heating*

A distinction has to be done between dielectric and metals. Indeed, the microwaves applied to metals excite only the surface by means of the induced eddy currents. Instead in dielectric materials the dielectric losses cause the specimen volume to heat.

9.3.1.4 *Laser heating*

The energy input is currently applied in point form, allowing the laser to be used in online thermography. In addition, the laser power can be modulated as well as the excitation vs time.

9.3.2 Active thermography techniques

The most common types of active thermography are:

- pulse thermography;
- pulsed phase thermography;
- lock-in thermography;
- step heating;
- vibrothermography;
- thermoelastic analysis of stresses;

9.3.3 Pulse Thermography

This method is the most used due to the rapidness of the test. Indeed, as stated in [2] for high conductivity materials like metals the test duration is about 3ms. Instead for low conductivity material this test can last up to 4s.

The working principle is based on the fact that where a discontinuity inside the material appears, the diffusion rate changes with a consequent variation of temperature in correspondence of the defect with respect to the whole sample. As consequence, deeper the defect longer will be the observation time and lower the contrast, according with the following formulation:

$$t = \frac{z^2}{\alpha}$$

$$C = \frac{1}{z^3}$$

Where:

- t is the observation time
- z is the discontinuity depth
- C is the contrast

- α is the thermal diffusivity of the material, defined in [17] as:

$$\alpha = \frac{\lambda}{\rho c_p}$$

- λ is the thermal conductivity
- ρ is the density
- c_p is the specific heat capacity

The contrast decay in function of the depth is reported in the Fig. 9.5 below:

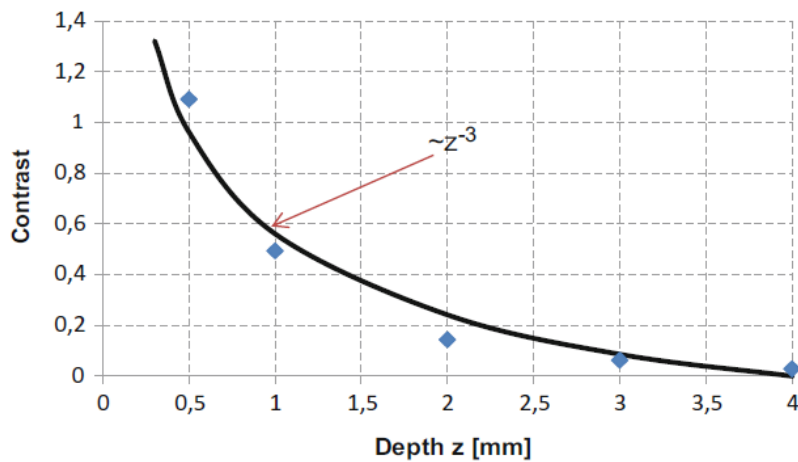


Fig. 9.5 Contrast decay of a thermal image in function of a defect depth (from [17])

As can be seen from the figure, there is a decrease in the contrast value increasing the depth.

Furthermore, as stated in [53], the thermal contrast is dependent upon the temperature and follows this relation:

$$K = \frac{T_{def}(t) - T_{def}(t_0)}{T_s(t) - T_s(t_0)}$$

Where:

- K is the thermal contrast
- T_{def} is the surface temperature of the sample over the defect
- T_s is the surface temperature
- t is the current time at cooling
- t_0 is the initial time instant

The paper [53] shows that the thermal contrast has one maximum in time during the cooling phase and its value are different depending on the defect size and depth. For this reason, knowing the defect size it is possible to determine the defect depth. The

samples considered in this paper are rectangular plates in austenitic steel with circular defects artificial made at different depth.

The Fig. 9.6 below plots the time at which the thermal contrast is maximum vs the defect depth in function of the defect diameter.

The maximum of the thermal contrast is increasing per increasing depth and increasing diameter of the defect. Indeed, the limit defect detection has been done for the maximum depth of 2mm with a defect diameter of 10mm.

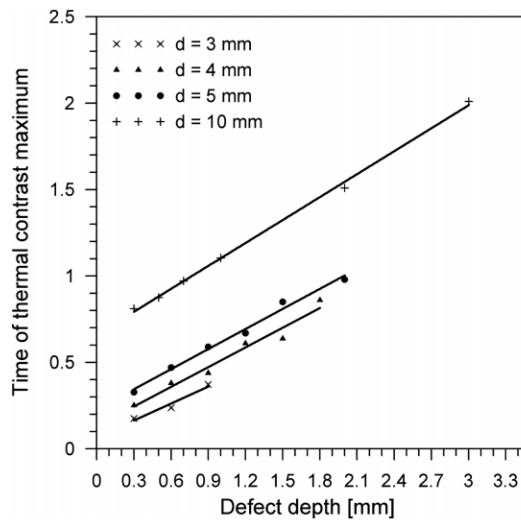


Fig. 9.6 Defect depth vs max thermal contrast (from [53]).

For pulsed thermography technique, an example of test bench that can be used is reported in the below Fig. 9.7 and represent a common configuration for the pulsed thermography investigation.

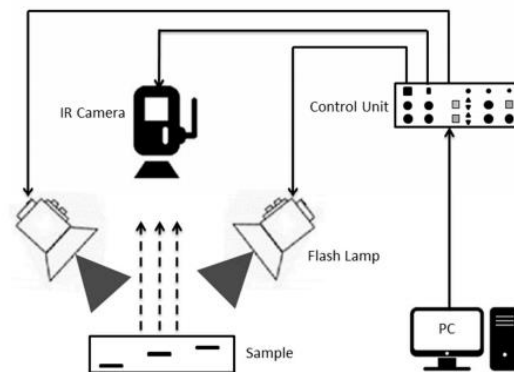


Fig. 9.7 Test bench example (from [54]).

The excitation source is the flash lamp. As stated in [54] the temperature in function of the time and the depth can be derived by the solution of Fourier equation for Dirac impulse propagation, under the hypothesis of semi-infinite solid material:

$$T(z, t) = T_0 + \frac{Q}{e\sqrt{\pi t}} \exp\left(-\frac{z^2}{4at}\right)$$

Where:

- T_0 is the initial temperature.
- $e = \sqrt{\lambda\rho c_p}$ is the thermal effusivity.
- Q is the energy deposited on the surface by the flash lamps.

Instead of flash lamps, a recent excitation mean is the inductor. Induction pulsed thermography is based on eddy currents that are generated inside the component under investigation. As Netzelmann et al. [26] have reported in their work, this technique is often used in place of magnetic test for ferromagnetic materials. The reason of this choice is to be found in the fact that relative magnetic permeability of materials that are ferromagnetic is high while the nonmagnetic materials have the relative magnetic permeability near one. The below Fig. 9.8 shows the setup for the experiment in [26]:

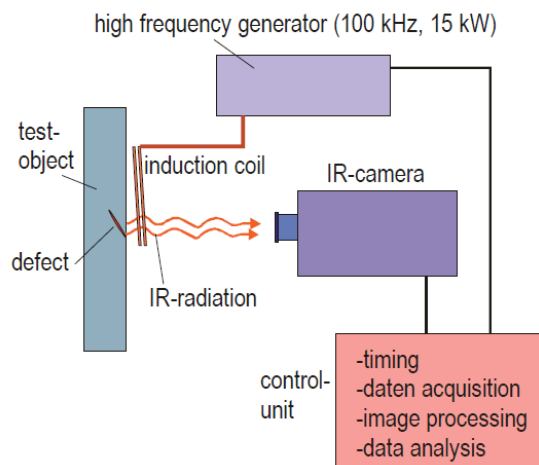


Fig. 9.8 Sketch of a test bench with inductors (from [26]).

The basic principle of the induction system is to use a high frequency generator with a pulse that is sent to the sample and then analysed by the IR camera in order to detect the temperature distribution.

In a simple one-dimensional case, the absorbed power density is:

$$S = \frac{1}{2\mu_0^2} b^2 \sqrt{\frac{\pi\mu_0\mu_R}{\sigma_e}} f$$

Where:

- b is the high frequency magnetic field
- σ_e electrical conductivity
- μ_0 is the permeability constant
- μ_R is the active effective permeability
- f is the electromagnetic frequency

What is stated above about the magnetic permeability related to the efficacy of this technique is also shown in the formulation of absorbed power. Indeed, the higher is the permeability, the higher is the signal strength that this method can achieve. Other two parameters have to be considered and they are electromagnetic skin depth δ and thermal penetration depth μ_T :

$$\delta = \sqrt{\frac{1}{\pi f \sigma_e \mu}} \quad \mu_T = 2\sqrt{\alpha t_{obs}}$$

Where:

- μ is the magnetic permeability
- α is the thermal diffusivity
- t_{obs} is the observation time.

These two parameters both express the capability of the induction thermography to detect a defect and the skin depth measures the depth of the current flow.

Common applications are related to small steel parts as well as very long rails with a movable equipment. With its capability for a fast detection, eddy current thermography has been tested also in railway field in particular for two applications: rail cracks detection and wheel surface damages. The damages are studied with an automated system in which a dedicated inductor is used and the surfaces is scanned with the wheel in rotation.

Instead the investigation on rail cracks has been carried out with a train in movement. In this case the thermal contrast diminishes as $1/\sqrt{v}$, where v is the train velocity.

9.3.4 Pulsed phase thermography

In pulsed phase thermography, a thermal wave is sent to the specimen and the transient heating and cooling state analysed. The test can be carried out by using one pulse at time and knowing the depth at which the defect is located.

D'Accardi et al [9] in their work on aluminium samples has explained that after the acquisition with an infrared camera, raw data must be analysed by using the Discrete Fourier Transformation (DFT), discretized in time and frequency domain. The relationship between time and frequency can be seen by the below equation:

$$F_n = \Delta t \sum_{k=0}^{N-1} T(\Delta tk) \exp\left(\frac{2j\pi kn}{N}\right) = Re_n + Im_n$$

Where:

- n is the frequency increment.
- Re and Im are the real and imaginary parts of the equation and they are used to compute the magnitude (A_n) and phase of the obtained signal:

$$A_n = \sqrt{Re_n^2 + Im_n^2}$$

$$\phi_n = \arctg\left(\frac{Im_n}{Re_n}\right)$$

The signal post processing gives a relation between the temperature and time once known the thermal effusivity e and the heating on the surface Q :

$$\ln(\Delta T) = \ln\left(\frac{Q}{e}\right) - \frac{1}{2}\ln(\pi t)$$

and the resulting graph is shown in the below Fig. 9.9:

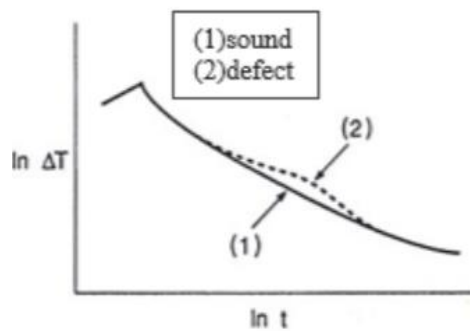


Fig. 9.9 Temperature difference vs time of a sound (1) and defective (2) parts (from [26]).

As it can be seen (Fig. 10.8), the trend in a defect-free condition is almost linear. However, when the signal crosses a defect, a perturbation occurs. In this case the perturbation is reflected also on the curve, that is no more linear. The thermal field alteration in presence of a defect can be quantified by the determination coefficient R^2 which expresses the deviation from the linearity of the considered system under investigation.

In a real case this approximation well fits to polynomial of degree n [23] as in the following equation:

$$\ln(T(t)) = a_n \{\ln(t)\}^n + a_{n-1} \{\ln(t)\}^{n-1} + a_1 \ln[t] + a_0$$

With a typical value of n of 4 or 5.

9.3.5 Lock-in thermography

The lock-in thermographic method is a non-contact inspection technique in which the laser beam periodically sends a wave to the portion of the material under investigation and a thermal imaging camera detects the signal that is post processed in a lock-in amplifier. The control method results in an objective evaluation of the defects because it can be identified with respect to dimensions, shape and depth. As reported in [52] an important parameter for this kind of investigation is the phase angle between the thermal response localized in the point of investigation and exciting signal. If a Fourier analysis is done pixel by pixel it is possible to calculate the magnitude and phase of the material response. The thermal load determines a sinusoidal oscillation of temperature with a frequency that is the same of the load and an amplitude A and a phase ϕ with respect to the imposed load [13].

The Fourier's law for one-dimensional solution under the hypothesis of propagation in a semi-infinite homogeneous material is expressed in [42] as:

$$T_{z,t} = T_0 \exp\left(-\frac{z}{\mu}\right) \exp\left(\omega t - \frac{z}{\mu}\right) = A(z) \exp i[\omega t - \phi(z)]$$

Where:

- T_0 is the temperature induced by the heat source;
- ω is the modulation frequency;
- $A(z)$ is the thermal amplitude;
- z is the defect depth;
- μ is the thermal diffusion length that generate the wave decay and it is defined as:

$$\mu = \sqrt{\frac{2\alpha}{\omega}}$$

- ϕ is the phase shift that can be correlated to the defect depth:

$$\phi = \frac{z}{\mu}$$

The thermal imaging camera acquires per each cycle four images with a phase shift of $\frac{1}{4}$ the period, as it can be seen in the Fig. 9.10 below:

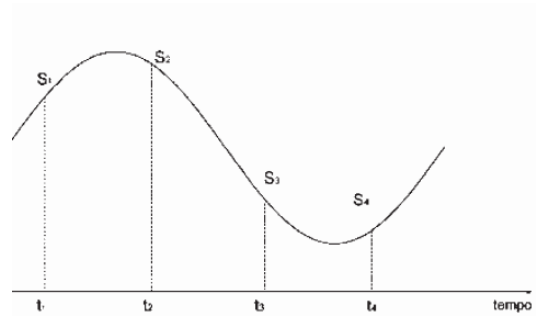


Fig. 9.10 sinusoidal behaviour of the four captures (from [13]).

Data are then recorded after an analysis in stationary regime and the magnitude and phase [13] are:

$$A = \sqrt{(S1 - S3)^2 + (S2 - S4)^2}$$

$$\phi = \arctg\left(\frac{S1 - S3}{S2 - S4}\right)$$

The magnitude image gives the temperature variations due to the non-uniform heating of the sample or due to the local variation of emissivity. The image phase instead provides, per each pixel, the value of the temperature phase shift with respect to the input signal sent to the system.

9.3.5.1 Lock-in thermography applications

A typical system for lock-in thermography with optical excitation is here reported in Fig. 9.11:

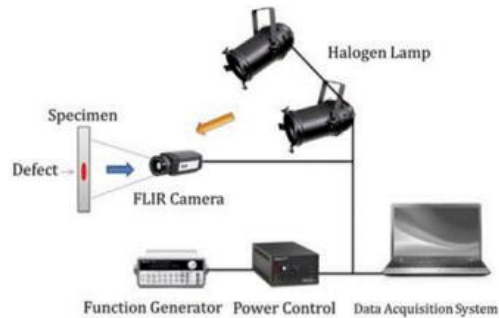


Fig. 9.11 Lock-in test bench (from [42]).

In the above schematic representation, halogen lamps generate the specimen excitation with the function generator and power control that modulate the sinusoidal waves. FLIR camera is then used to acquire the IR images.

In general, this kind of systems are used to monitor coatings or sandwich laminates [2]. In fact, the separation surfaces between the parts constitute a discontinuity volume in which the thermal conductivity worsen with respect to the whole sample, resulting in a more difficult heat dissipation inside the system.

The most interesting application in coatings is the measurement of the paint thickness. With this method it is possible to inspect paint thickness both in wet and dry conditions. The application has an immediate success in painting on metals but requires some calibration steps when the paint is on polymers. In this latter case, the coating and the substrate are very similar in terms of thermal impedance and this does not allow to the wave to be reflected.

Regarding the laminates, they are usually composed by carbon fibres embedded in a polymer matrix. In this case the inspection is not limited to the thickness of the layer that can be important but mostly to preventive maintenance. Indeed, when a point of the surface of the component is heated, the temperature field is disposed as the fibres orientation resulting in the detection of discontinuities. Some examples of what can be detected is related to damaging from an impact, delamination, corrosion and loss in tightening of the screws.

In [38], some steel welded specimens with root crack and lack of fusion were tested with laser spot technique. The researches have been demonstrated that exciting with a laser the welding surface and moving the laser beam on the whole welded path, in correspondence of a defect an abnormal thermic profile can be found. This fact is related to the low thermal conductivity of the defect inside the welding.

The ultrasound excitation source described in [38] is interesting due to its capability of defect detection and it uses ultrasounds with a typical frequency of 20 kHz. A reference sketch for this application is shown in Fig. 9.12:

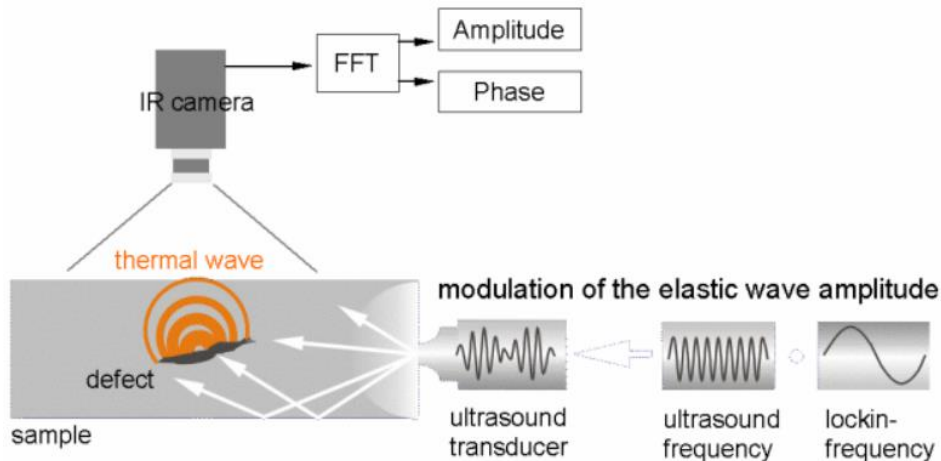


Fig. 9.12 Ultrasound excitation for thermographic investigation (from [14]).

In this case an ultrasonic source of excitation has been used and consist in propagating a mechanical wave inside the material. The ultrasonic transducer, attached to the sample, emits ultrasound at low frequency. When a material discontinuity has found, the wave is damped and there is a conversion of the wave in heat with a hot spot identification. As reported in [14], modulating the ultrasound frequency and fitting it to the sample, it is possible to make the defect a transmitter of a thermal wave generated by the hysteresis mechanism at discontinuity level. The phase of Fourier transformation contains the wave time propagation from the defect to the surface and this gives the information on the defect depth.

Then it is important to distinguish ultrasound lock-in thermography from vibrothermography and stress pattern analysis by thermal emission. Indeed, with these two techniques a periodical mechanical load is used and its effect is monitored during the application.

Another important application of ultrasound lock-in thermography is the crack identification in ceramics and metals but also delamination and corrosion [2]. In this case, despite the optical excitation sources, it is not relevant the crack orientation as the ultrasound waves will spread in all direction inside the material. It is useful to underline that, to be visible, the crack has to be closed. This make difficult to reveal cracks inside metals where the ductility of the material let the crack to open but it is very effective in ceramics where no opening occurs.

Last, to detect the corrosion this method exploits the local variation of mechanical behaviour of the oxidized material such that it is possible to see only areas affected by corrosion.

9.3.6 Step heating

This thermographic method uses a small amount of power to heat the surface. The temperature of surface is acquired by means of a thermal camera during the heating, resulting in a system that allows for a subsurface defect identification. In Fig. 9.13, a simple scheme of a test bench used with this technique has reported.

The goal of this technique is to obtain both the detect depth and the resistance in order to characterize the flaws.

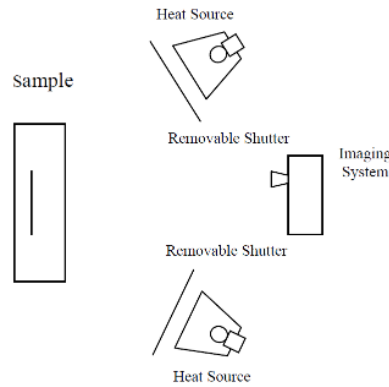


Fig. 9.13 Step heating test bench (from [40])

It can be possible to distinguish between high resistance and low resistance defects. In the first case it is assumed that the thermal wave does not pass through the defect and its depth is easily determined. In the latter as the thermal wave propagates through the material the signal is attenuated and it's more difficult to identify the material discontinuity.

As Badghaish and Fleming have demonstrated [4], the defect depth can be determined in both cases with an analytical approach that is the two-points correlation method.

The temperature distribution, while heating the surface in a finite thickness plate, will be the following:

$$T = \frac{2Q}{\lambda} \left(\frac{\alpha t}{\pi} \right)^{1/2} \left[1 + \sqrt{\pi} \sum_{n=1}^{\infty} 2 \operatorname{ierfc} \frac{nL}{\alpha t} \right]$$

Where:

- λ is the thermal conductivity
- α is the thermal diffusivity

- Q is the heat flux
- L is the plate thickness
- $ierfc$ is the integral of the complementary error function that for a generic element n in time t is defined as:

$$erfc(n) = \frac{2}{\sqrt{\pi}} \int_n^{\infty} e^{-t^2} dt$$

9.3.7 Vibrothermography

Vibrothermography bases its fundamentals in analysing the surface of a component when subjected to mechanical oscillations. This allows to have the material discontinuities heated. The heating process is due to the energy conversion caused by the interaction between the defect and the mechanical friction between crack tips. In [16] is shown as activating a device (laser vibrometer of Fig. 9.14) that allows to take the sample to a vibration near its resonance frequency for few seconds, the crack starts to increase in length and the temperature arises. The IR camera acquires the surface temperature contour that is then processed in a PC.

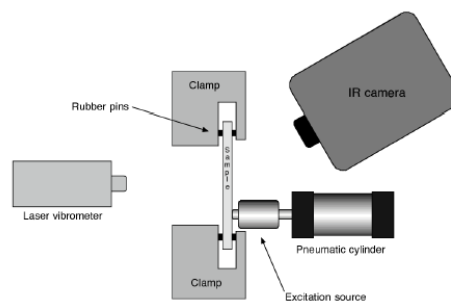


Fig. 9.14 Example of vibrothermography test bench (from [16]).

An application in welding inspections is reported in [38] where a ultrasonic vibration source has been used. In this work, lack of fusion and root crack has been successfully identified with vibrothermographic technique.

In [46] has been demonstrated that, even if vibrothermography has a high capability to detect cracks, porosity and voids are difficult to detect due to their shape. Indeed, there is no friction inside these defects when a vibration is applied and then no heating of the defect occurs.

9.3.8 Thermoelastic analysis of stresses

The thermoelastic analysis allows to derive the defect localization by mechanical stressing the sample. Indeed, in the elastic range and under cyclic load, the mutual conversion of mechanical to thermal energy is reversible under the hypothesis of adiabatic conditions and this allows for defect detection by the elaboration of the thermal signal recorded with a thermal camera.

In [13] the theory which related to this method is presented. Attention is given to the stress and the temperature related by this formula:

$$\frac{\delta T}{T} = -K_0 \delta \sigma$$

Where:

- T is the absolute temperature
- σ is the sum of principal stresses
- K_0 is the thermoelastic constant describes as:

$$K_0 = \frac{\alpha}{\rho c_p}$$

With:

- α is the thermic dilatation coefficient
- ρ is the material density
- c_p is the specific heat at constant pressure

By stressing the material, heat inside the sample is generated. The heat conduction is described by Fourier equation which, in adiabatic conditions, becomes:

$$q = -\rho c_v K_0 T_0 \frac{\partial \sigma}{\partial t}$$

Where c_v is the specific heat at constant volume and T_0 is the ambient temperature. Such a formulation, valid only in the elastic range, expresses that a cyclic load is related to an heat source q that is responsible for the temperature variation of the stressed zone.

The thermal diffusion length is the key parameter for this analysis and it is defined as:

$$\mu = \sqrt{\frac{2\alpha}{\omega}}$$

Where α is the thermal diffusivity and ω the pulse.

It is evident that, fixed α in the previous formulation, the only variable parameter to allow the thermal diffusion length to vary is the frequency, strictly related to $\omega = 2\pi f$: for high frequencies, the temperature signal is dependant only upon the generic point under examination and the other nearby disturbances does not interfere with it. For this reason, the resultant signal is expected to have 0 phase.

In metallic material the signal is attenuated due to the heat dissipation on the component, resulting in a signal with a phase different from 0. With a finite element analysis it is possible to derive the solution for the heat conduction equation and predict the relation between the signal attenuation and signal phase in order to properly interpret the results in investigation of metals.

10. The experimental equipment

In this section the description of the test plan will be provided.

10.1 Objective and description of the experimental procedure

The goal of the experimental investigation is to assess the presence of pre-determined defects inside the welding using non-destructive techniques and to evaluate the material response with thermographic investigation both with and without the presence of defects. Active and passive thermographic investigation techniques have been used:

- Passive thermography has been used in a fatigue test to assess the behaviour of the welded butt-joints under an LCF test to verify:
 - 1- If the life of the samples without any defects reflects the calculations outcomings.
 - 2- If the passive thermographic technique shows a temperature increment before the structural collapse.
- Active thermography has been used before and after the fatigue test to assess the material response to laser pulse after the fatigue test;

Regarding the defect characterization, different tests have been performed:

- Radiographic testing investigation for defects characterization;
- Penetrant testing investigation for surface defects identification;
- Ultrasonic investigation for defects characterization;
- Fatigue tests with passive thermographic investigation.

10.2 Samples description and identification

The final dimensions of the samples in all the tests are: 150mm x 300mm x 10mm. They are milled to have a chamfer of 10mmx45° and after that welded. The final step is to mill the samples to achieve the desired dimension. Because the samples are milled from a plate of bigger dimensions (300mm x 400mm x 10mm), to each sample name is added a suffix which identify the side of the bigger plate. This suffix is “L1” or “L2”.

Finally, the parts identification is done with the following criteria

- 1) Samples supposed to be without defects have been classified as “OK” followed by a progressive number.
- 2) Samples supposed to be with porosities have been classified as “PO” followed by a progressive number.
- 3) Samples with inclusions have been classified as “IN” followed by a progressive number.
- 4) Samples with incomplete root penetration have been classified as “MP” followed by a progressive number.

The first and the second batches are composed by 12 parts. For the second batch only 4 parts have been tested.

For the first batch visual, radiographic and thermographic examinations have been carried out.

For the second batch visual, ultrasonic, penetrant and thermographic tests have been performed to obtain a comparison with the results coming from the first batch examination. Radiographic and ultrasonic tests are in fact equivalent on the standard side and they are classified as volumetric inspections.

The only difference between the first and the second batch is that in the second one the weld seam has been grinded for all the samples in order to have the crack nucleation starting from the defect inside the sample and not from the weld toe.

Thanks to this difference, penetrant testing is only possible for the second batch because it could reveal false indications if used on the first one: indeed, the shape of the weld seam after welding and the surface roughness do not allow for a PT investigation.

Finally, the welded area has been covered with black paint to obtain an emissivity close to a blackbody (about 0,99) for the thermographic investigations.

10.3 Welding machine

The welding machine has been used to weld the butt-joint specimens. The model used was TPS500i by Fronius and its main characteristics are reported in Tab. 15 below:

Tab. 15 Main electrical characteristics of the welding machine generator

Characteristic	Value
Mains voltage (U1)	3 x 400V
Mains voltage tolerance	+/- 15%
Mains frequency	50/60 Hz
cos phi (1)	0,9
Max. permissible mains impedance Zmax on PCC1	49 mOhm
Welding current range for MIG/MAG/TIG	3-500 A

The below Fig. 10.1 highlights the main parts of the welding machine:

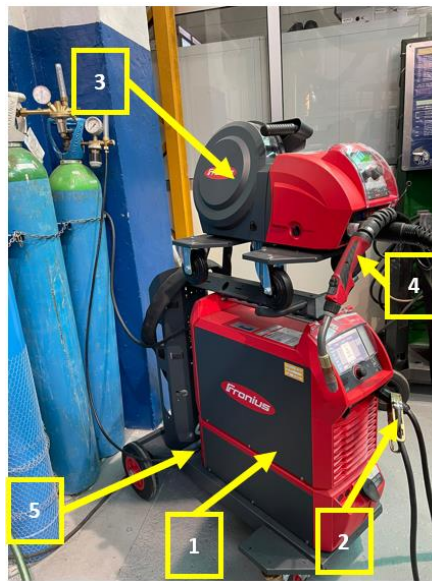


Fig. 10.1 Welding machine used during the experimental tests

The generator (1) is the core element because it provides to manage the whole system in terms of current and voltage generation and parameters compensation thanks to an embedded control unit.

The mass socket (2) is the cable to connect to the workpiece in order to have the negative pole for the arc. Instead, the wire feed unit (3) is used to carry the electrode wire and to supply it to the torch (4). Finally, the shielding gas supply (5) is connected to the proper entry of the generator.

The gas flow rate is instead controlled by a flowmeter connected directly to the gas cylinder, whose Fig. 10.2 is reported below:

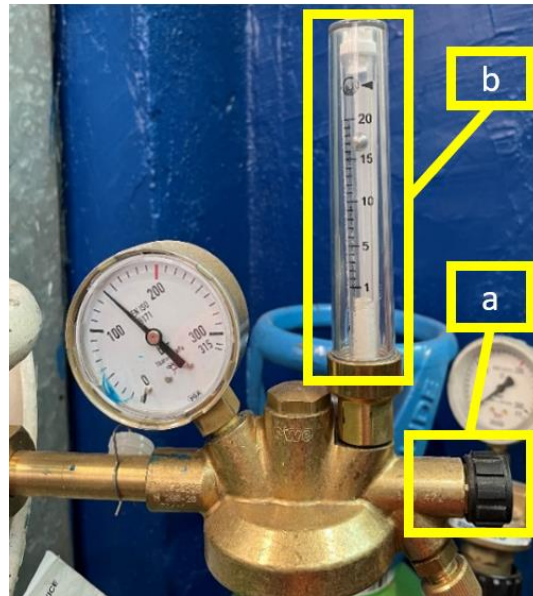


Fig. 10.2 Flowmeter for gas cylinder. The tap (a) and the flow meter (b)

As it can be seen from the above picture acting on the tap (a) the flow measurement (b) changes accordingly.

Last, to carry out the fatigue tests four types of joints have been welded, each composed by four specimens:

- 1) Joints without any defect;
- 2) Joints with incomplete root penetration;
- 3) Joints with an inclusion of another material of higher fusion temperature;
- 4) Joints with porosities.

For no. 1) and 3) no variation in WPS parameters have been adopted. In order to generate the inclusion defect, a 7mm nail steel has been introduced between the first and the second run.

Instead for incomplete root penetration the value of the current was lowered to 160A and the arc length to +5.

For what concerns the defects of porosity, only the gas value has been lowered to 5 l/min. The remaining parameters have been set according to the WPS.

The choice of such parameters is done to simulate an operator error during the semiautomatic welding process. Indeed, incomplete root penetration usually appears when the operator does not set a proper value of current and arc length at the first run.

Porosities depend on some welding parameters and on the cleaning conditions of the workpiece. For this reason, during the generation of this defect the gas flow rate is lowered with respect to the value indicated in WPS in order to reduce the gas protection of the weld bead and some water is added.

Once the parameters have been chosen, they have to be set on the welding machine in this order:

- to select the filler material and the gas composition used: in our case the filler was a 1.2mm AlMg5 wire combined with a mixture of shielding gas of 30%Ar + 70%He in weight. The machine display is shown in Fig. 10.3.

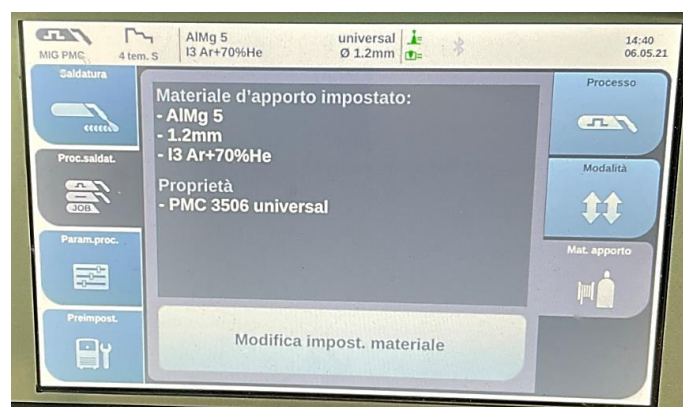


Fig. 10.3 Welding machine interface: summary of the gas parameters selection.

- to select the welding process: MIG PMC is a special process that uses a pulse arc and a rapid data elaboration to optimize the speed in welding.
- to select the MIG/MAG mode: in this case a *special 4-step mode* can be activated. In the Fig. 10.4 below is shown the graphic characterization of this mode:

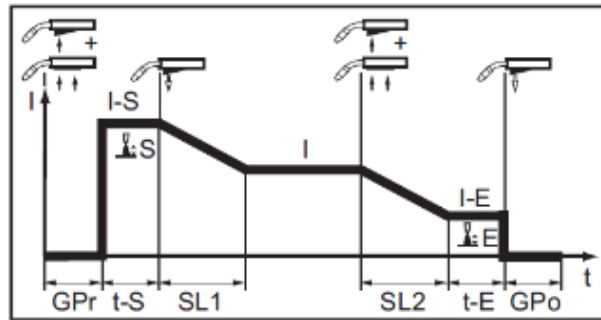


Fig. 10.4 Fronius special 4-step mode (from [12]).

The above graph shows the trend of current (I) vs time (t) as the button on the torch is pressed and then released. This function is particularly important because it takes into consideration the high conductivity of aluminium and modulates as consequence the arc length at the start and at the end of welding. As default setting the current (I) when starting to weld is 135% the nominal one set by the user. The two ramps have a duration SL1 and SL2 of 1s by default. While the final current is the 50% of the nominal one to avoid heat accumulation on the workpiece at the end of the welding process.

- to select the penetration stabilizer to obtain an optimal penetration. When the distance (h) from Fig. 10.5 is increased due to a prolonged stick-out (s_2), the resistance in the electric circuit formed by the electrodes diminishes and, at the same wire speed, there is a current drop that causes less penetration (x_2).

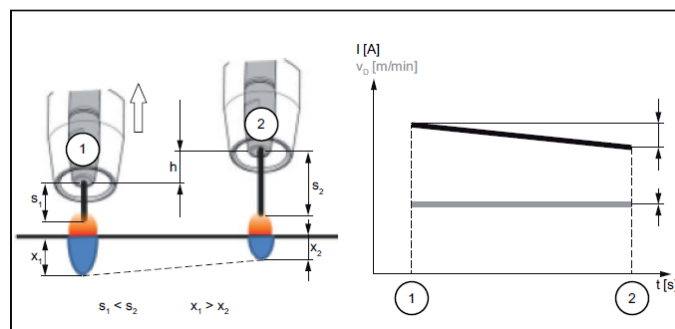


Fig. 10.5 Penetration stabilizer (from [12]).

Instead, if the penetration stabilizer is activated, there is a compensation on wire feeding velocity in order to minimize the current variation during the stick-out phenomenon. Fig. 10.6 shows, on the left graph the behaviour in presence of stick-out. The difference between the two cases is evident in the current stabilization (left graph of Fig. 10.6):

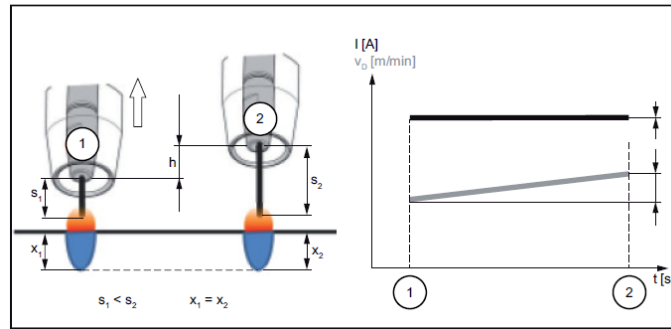


Fig. 10.6 Stick-out compensation (from [12]).

- to select the arc stabilizer to compensate the stick-out phenomenon and the external factors that contribute to the arc instability. The correction consists in reducing the arc length until short circuits happen, obtaining a more stable arc without dependence on the welding position. In Fig. 10.7 below three different situations have been reported:

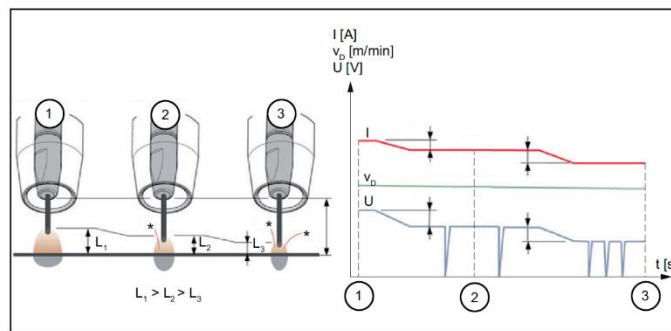


Fig. 10.7 Arc correction during the welding process (from [12]).

In the graph on the left of the above Fig. 10.7, in the situation 1 no arc length correction is adopted. As it can be seen in the solution 2, there is a small correction with a correction factor of 0.5 and, with the same feed rate, the current (I) and the voltage (U) are adjusted accordingly until the short circuit. Finally, the solution 3 represents a correction factor of 2 where the short circuits are more frequent due to the further reduction in current and voltage, keeping constant the feeding speed. For the experimental tests this value has kept to 0.

- to select the parameters required by WPS on the screen for the first and the following two runs. The figures below show the setting used during the experimental tests. On the display of the welding machine, highlighted by yellow rectangles (1) and (2), the real parameters values are reported. Indeed, as explained in the settings before, the values of current and voltage are corrected during the welding process to obtain a compensation for external factors that can have a negative effect on the final weld. The wire feeding speed is keep almost constant during the process. Instead, the yellow rectangle (3) highlights the parameters set by the user as input before to start welding. In Fig. 10.8, there are the values set for the first run:

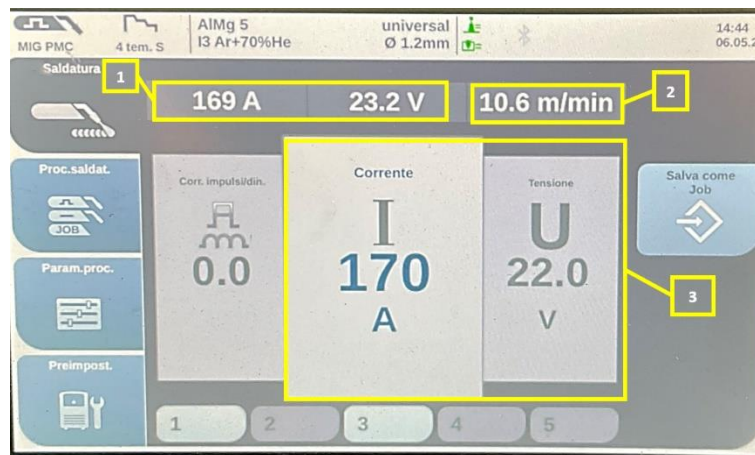


Fig. 10.8 Welding machine interface - parameters setting for the 1st

While in Fig. 10.9, there are the values set for the second and third runs:

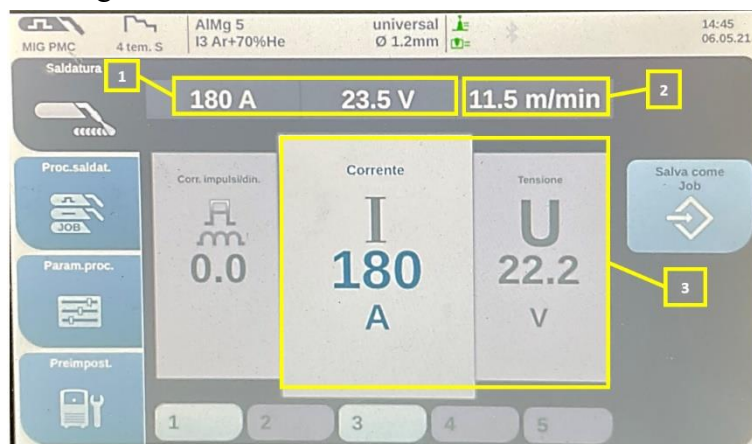


Fig. 10.9 Welding machine interface - parameters setting for the 2nd and 3rd run

10.3.2 Samples preparation

The plates are milled to obtain a chamfer of $10 \times 45^\circ$ and then, as per requirement in the WPS, a process for degreasing and brushing has been adopted.

In fact, after clamping the part, the surfaces that will be welded have to be degreased with alcohol as showed in Fig. 10.10 below:



Fig. 10.10 Degreasing phase of the samples

This phase is particularly important because an incorrect execution of this step could result in an increasing number of imperfections. After this first step, brushing is needed to remove aluminium oxide. The reason is that the fusion temperature of aluminium oxide is about 3 times the fusion temperature of aluminium and alumina could remain trapped into the weld seam and cause porosities. In this step is worthwhile to note that the brush bristles are in stainless steel to avoid rust transfer on the surface. A representative image of this process is shown in Fig. 10.11:

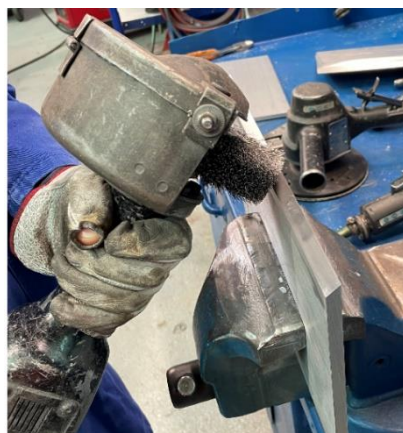


Fig. 10.11 Brushing phase of the samples.

The last step before to start welding is to position and clamp the final joint as in Fig. 10.12 below:



Fig. 10.12 Positioning of the sample.

As it can be seen from the above image the joint is positioned in front of the operator and in the upper right side the mass socket is connected. Finally, the welding beads are positioned at the start and the end of the welding to obtain the 100% of effective welded volume at the two plates sides.

At this point the sample is ready to be welded.

10.4 Ultrasonic equipment

During the ultrasonic test, a Gilardoni RDG-2500S machine has been adopted, paired with ATM70-4 probe from the same manufacturer.

The ultrasonic digital flow detector consists in a device capable to emit ultrasounds up to 12MHz and a system that detect the material response. The overall equipment configuration is given in Fig. 10.13:

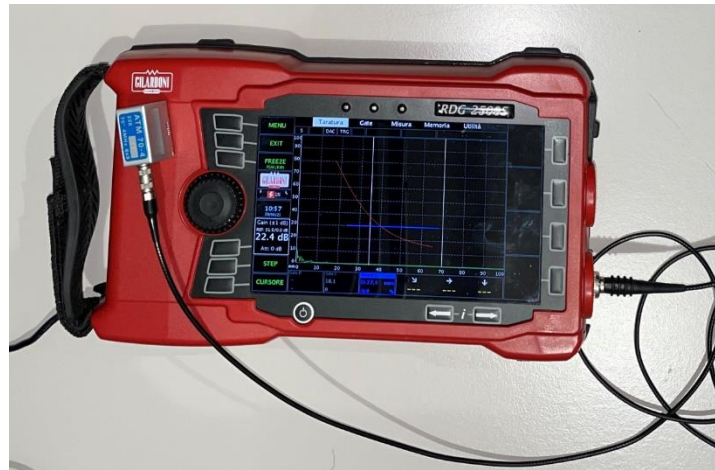


Fig. 10.13 Ultrasonic equipment: probe + device.

The detector has the possibility to set all the configuration parameters by acting on the buttons that are present on its board as showed in Fig. 10.14:



Fig. 10.14 Detector: main parameters setting

The power button (1) allows to start the system while buttons (2) with the scroll wheel (4) can be used for the selection of options present in the screen area. Finally, the measurement area is highlighted with the yellow rectangle (5).

The ATM 70-4 probe is a shear wave miniaturized probe with a frequency of 4MHz and an angle of 70°. This angle is capable to emit transversal waves. The manufacturer recommends this probe for inspection of butt welds with a maximum thickness of 15mm. It is also useful to note that in function of the probe angle the maximum inspectable thickness will vary. Thus, with a probe of 60° it is possible to inspect thicknesses from 15mm to 30mm and with a probe of 45° a sample over 30mm in thickness.

It is important to underline that the probes angles are conventionally set on steels and the effective angle on other materials like aluminium can be calculated by applying the Snell law:

$$\frac{\sin\alpha}{v_1} = \frac{\sin\beta}{v_2}$$

Where:

- α and β represent the angle of incidence and of transmission respectively;
- v_1 and v_2 are the sound velocities into the two means.

It is important to calculate the angle of transmission inside a mean different from steel because this parameter influences the defect detectability as well as the defect position identification inside the welding. Considering the following data:

- $v_1 = 3230 \text{ m/s}$ as the velocity of transversal waves inside steel,
- $v_2 = 3130 \text{ m/s}$ as the velocity of transversal waves inside aluminium;
- $\alpha = 70^\circ$ as the incidence angle declared by the probe manufacturer;

It can be concluded that the effective probe angle for aluminium is $\beta = 65,6^\circ$ and this is the parameter that have to be set on the detector setup after having connected the probe.

Finally, the selection of the acceptance curve is a key parameter to take into consideration. in this work a DAC curve has been chosen from the ones available in the instrument settings.

10.5 Test setup for passive thermography

In this work, two test benches have been used for the fatigue tests and the passive thermographic investigation at different testing frequency. The one that involve Instron 8801 machine has been used with a test frequency of 30Hz and the one with the ZwickRoell vibrophore with a testing frequency of 100Hz. In both the cases a mean load of 14,5kN and an alternate load of 4,5kN have been used.

The test bench for the 1st batch samples for passive thermography investigation is composed by:

- Instron servo-hydraulic machine.
- The special tool that allows for the four-point testing.
- IRTech thermal camera.
- Two PC: one for Instron machine control and one for the thermographic recording.

The whole system is represented in the below Fig. 10.15 in the unloaded condition:

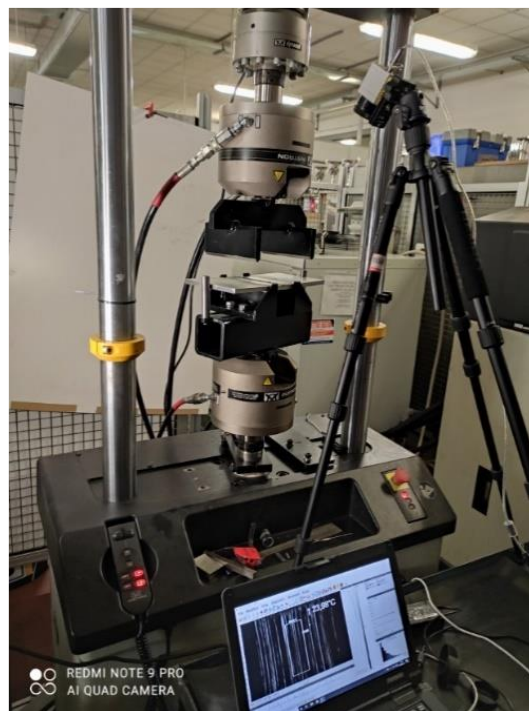


Fig. 10.15 test bench and sample in unloaded condition.

For the second batch samples the test bench is composed by:

- The ZwickRoell vibrophore;
- The three-points contact interface;
- IRTech thermal camera.
- Two PC: one for the vibrophore machine control and one for the thermographic recording.

The vibrophore and *IRTech* thermal camera are shown in the following Fig. 10.16



Fig. 10.16 Test bench for passive thermography investigation at 100Hz.

Also in this case two PC have been used: one for the control unit of vibrophore and one for the IR camera.

In the next paragraphs a deeper description about the two testing machines and the camera is given.

10.5.1 Instron 8801

Instron 8801 machine guarantees a test frequency of maximum 30Hz and loads up to 100kN. A picture from datasheet is reported in Fig. 10.17:



Fig. 10.17 Instron 8801 (from [18]).

The two-column actuation system allows to obtain the coaxial movement of the upper and lower cylinder.

However, to reach the four-point loading condition and assure the tensile stress in the welded joint, a special tool has been designed as interface with the machine. This steel tool is constituted mainly by two parts with respective seats to allow the connection with the upper and lower cylinder of the machine. The real assembly is reported in Fig. 10.19 (zoomed view) and in Fig. 10.18.

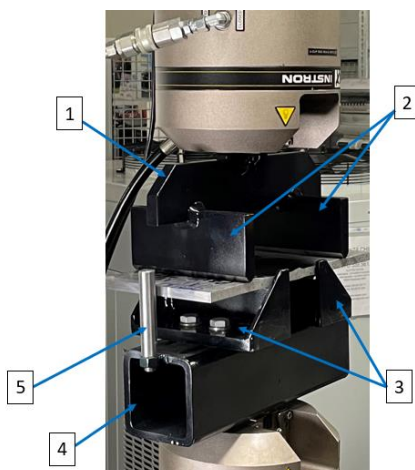


Fig. 10.19 Loading conditions for the tested specimen.

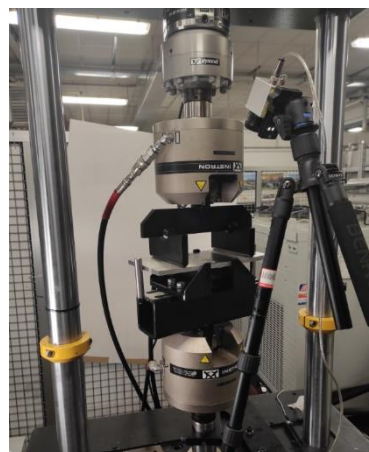


Fig. 10.18 Test bench and sample in loaded condition.

The first part is clamped in correspondence of the upper cylinder and a central beam (1) acts as support for two punches (2), both at the same distance from the beam clamp to have the uniform load distribution. The contact surface between each punch and the sample on the punch side is rounded to avoid notched surfaces on the sample side.

The lower part is clamped in correspondence of the lower cylinder and it is constituted by a supporting beam (4) on which two reaction supports (3) for the sample are located. The two supports are constrained by means of two screws each on the supporting beam (4).

Finally, two studs (5) are used in order to avoid uncontrolled movements of the sample during the test.

The machine cycle can be set using the software interface and a real time reporting shows information as the cycles, loads and position.

10.5.2 Vibrophore

The vibrophore machine by ZwickRoell is a machine that allows to use a testing frequency up to 100Hz in dynamic tests with loads up to 1000KN. The one used for these tests is shown in the following Fig. 10.20:



Fig. 10.20 Vibrophore used during the tests.

This machine is equipped with a 3-points contact punches that load the sample under investigation. The upper punches can be adjusted to obtain the desired loading for the weld seam.

10.5.3 IRTech camera

IRTech, Timage Radimatic “XT” has been used in evaluating the passive behaviour of the welding under cyclic loading.

The software interface for IR Tech camera is called *Timage Connect*. With this software it is possible to set some acquisition parameters like the acquisition time as shown in the Fig. 10.21 below:

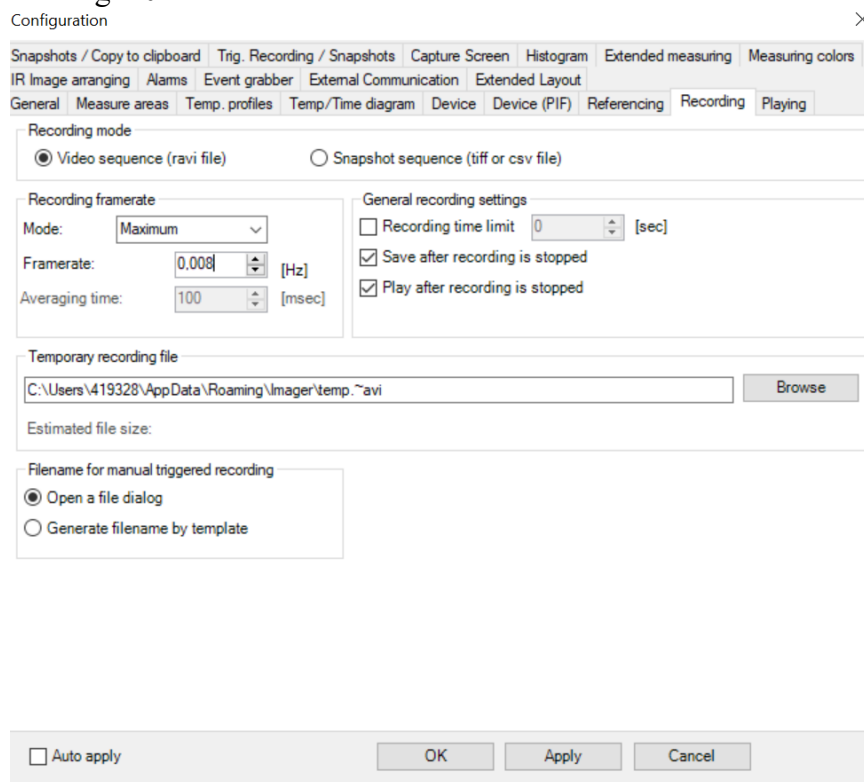


Fig. 10.21 Acquisition parameters in Timage Connect

Another important feature, necessary during the image post processing, is the area of investigation. In this case the area was set in a way to investigate only the welded and the heat affected zone.

The software allows to select an investigation area visible during the recordings. A representative image of the selected region of interest during the first batch analysis is shown in Fig. 10.22:

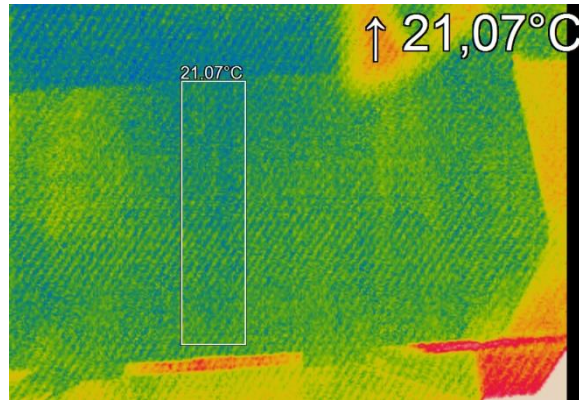


Fig. 10.22 Timage Connect: selection of region of interest (ROI).

10.5.4 Passive thermography: data collection and elaboration

After having started the test and having activated the recording on the PC side, the main quantities of output are:

- The cycles vs elapsed time, from the testing machines.
- The thermal map vs elapsed time, from the IR camera.

These data are stored in a PC for further post processing. Regarding the fatigue testing machines, the cycles data is the only needed information. Instead for the thermal camera, temperature data vs time have to be extracted from a region of interest (ROI) that is represented by the weld seam and the heat affected zone. The elaboration of these data consists in:

- Transforming the time instants in which the camera acquires the frames in the cycle domain, known the test frequency.
- Per each test, subtracting the environmental temperature, measured at the test starting, from the maximum temperature revealed by the region of interest at each acquisition instant.
- Plotting the elapsed cycles vs temperature difference ΔT .

10.6 Fatigue test: joint stress analysis

During this experimental setup a butt weld with full penetration and without backing has been chosen as reference joint to be investigated.

To reach this kind of joint two plates, 10mm thick, have been used with a chamfer angle of $10 \times 45^\circ$.

A representative joint section can be seen by the macrographic test in Fig. 10.23:



Fig. 10.23 Butt-joint section

Since the experimental investigation has been done with two different supports for the 2 batches of samples, the loading scheme changes to be adapted to the two different machines. However, acting on the support distances, the fatigue tests on the two batches have been carried out with the same stress condition for the weld seam. For this reason, both the static and fatigue verifications are valid in for the two tests.

10.6.1 Loading scheme for the 1st batch

In order to define the main parameters for calculations, a schematic representation of the test bench is reported in Fig. 10.24:

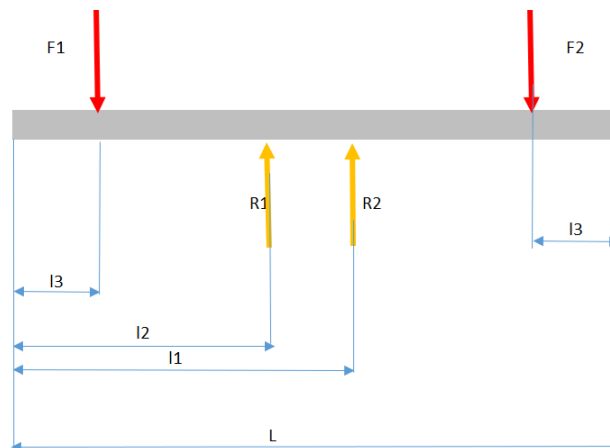


Fig. 10.24 Schematic representation of the test bench for 1st batch samples.

In Tab. 18 below are shown the geometrical parameters involved and the maximum forces adopted:

Tab. 18 Main geometrical parameters for the 1st batch loading condition.

Main dimensions:		
Thickness (t)	10	mm
Width (w)	150	mm
L	300	mm
l1	186	mm
l2	114	mm
l3	62	mm
maximum forces:		
F1	9500	N
F2	9500	N

Having the two reactions:

$$R1 = R2 = 9500N$$

At this point it's possible to calculate the bending moment diagram as the result of the loading conditions on the structure. The schematic representation of this diagram is reported in the below Fig. 10.25:

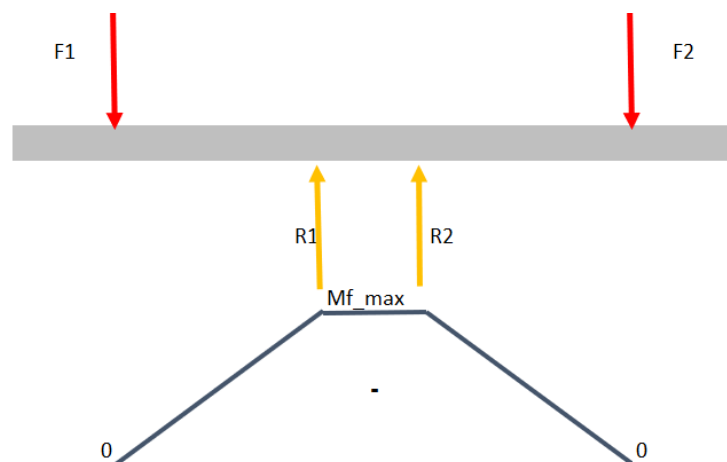


Fig. 10.25 bending moment on the structure – 1st batch samples.

From the above diagram it's clear that the maximum stress is located between the two reaction forces R1 and R2. In this region is also located the weld seam and the heat affected zone.

For this reason, the static verification should involve both the weld seam and the heat affected zone.

10.6.2 Loading scheme for the 2nd batch

In order to define the main parameters for calculations, a schematic representation of the test bench is reported in Fig. 10.26:

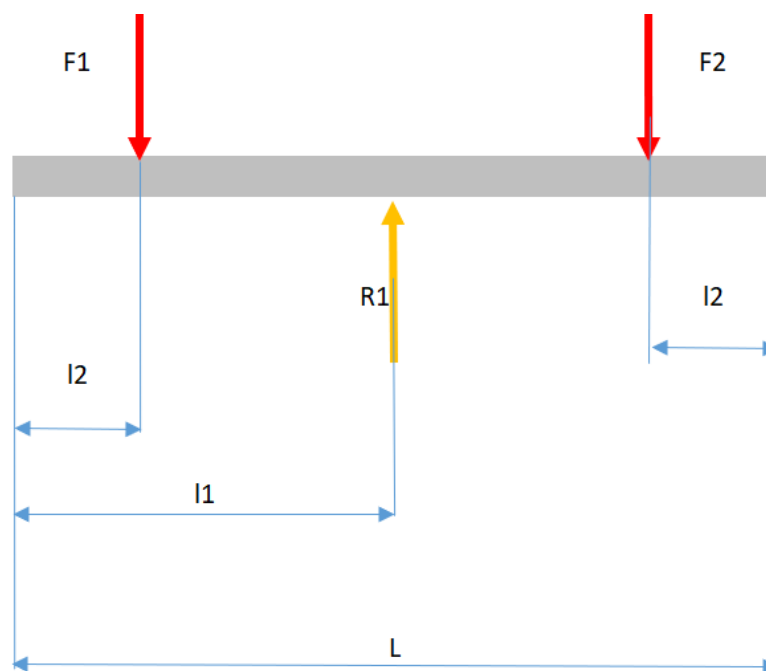


Fig. 10.26 Schematic representation of the test bench for 2nd batch samples.

In Tab. 19 below are shown the geometrical parameters involved and the maximum forces adopted:

Tab. 19 Main geometrical parameters for the 2nd batch loading condition.

main dimensions:		
thickness	10	mm
width	150	mm
L	300	mm
l1	150	mm
l2	98	mm
maximum forces:		
F1	9500	N
F2	9500	N

Therefore, the reaction R1 is:

$$R1 = 19000N$$

At this point it's possible to calculate the bending moment diagram as the result of the loading conditions on the structure. The schematic representation of this diagram is reported in the below Fig. 10.27:

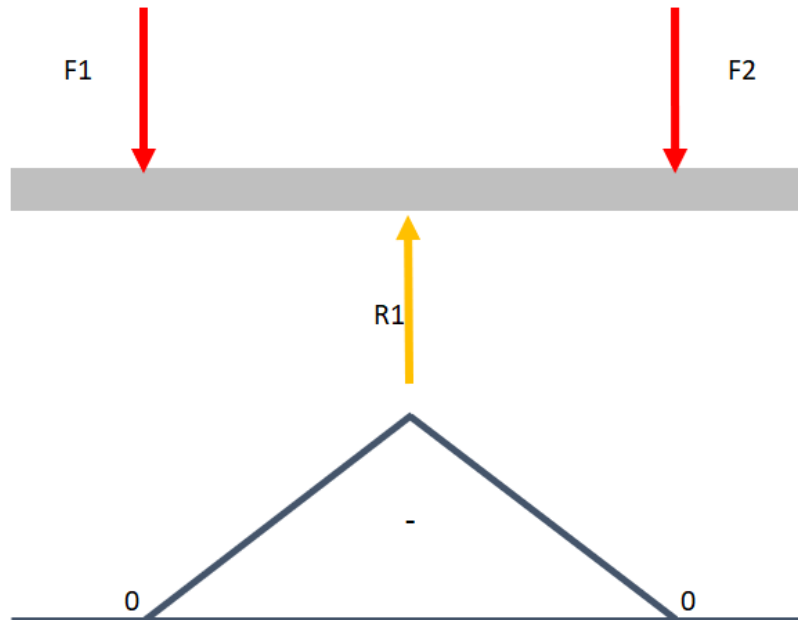


Fig. 10.27 bending moment on the structure - 2nd batch samples.

From the above diagram it's clear that the maximum stress is in correspondence of the reaction R1.

10.6.3 Joint static verification

For the identification of admissible values of normal stress inside the joint it's useful to refer to EN1999-1 [10]. This Standard is also called Eurocode 9, used in design of aluminium joints.

For butt weld joints, EN1999-1 establishes the stress limit values both for the weld seam and the heat affected zone when the joint is under normal stress.

For the weld seam:

$$\sigma_{\perp Ed} \leq \frac{f_w}{\gamma_{Mw}}$$

Where:

5) f_w is typical of the base material combined with filler metal;

6) γ_{Mw} is a safety margin that for welded joints is 1,25;

With a 5183-filler metal and AW6082 alloy as base material, $f_w = 210 \text{ MPa}$, thus:

$$\sigma_{\perp Ed} \leq 168 \text{ MPa}$$

For the heat affected zone, Eurocode 9 consider the ultimate strength of HAZ:

$$\sigma_{\text{haz},Ed} \leq \frac{f_u}{\gamma_{Mw}}$$

Where f_u is the ultimate strength for HAZ and the value for AW6082 is 185 MPa.

Considering the safety margin of 1,25 the result is:

$$\sigma_{\text{haz},Ed} \leq 148 \text{ MPa}$$

In order to do the joint static verification, it's important to calculate the section bending resistance modulus and the maximum bending moment as follows:

$$W_f = \frac{wt^2}{6} = 2500 \text{ mm}^3$$

$$M_{f_{max}} = 494000 \text{ Nmm}$$

Resulting in a stress:

$$\sigma_{max} = \frac{Mf_{max}}{W_f} = 198 \text{ MPa}$$

The calculated stress is higher than the admissible one and the inequality related to the weld seam is not verified.

The static joint verification is not verified under the assumptions of Eurocode 9 due to the low values of Rp02 considered by the Standard. The base material used during the tests has been tested by the Manufacturer obtaining the results showed in the following Tab. 20:

Tab. 20 Values of Rp02, Rm and hardness as declared by the manufacturer on the samples under test.

AW6082-T6 – as tested		
Parameter	Value	Unit of Measure
Rp02	331	MPa
Rm	355	MPa
Hardness	105	HB

Eurocode 9 proposes the minimum values of material strength as in Tab. 21:

Tab. 21 Reference (minimum) values proposed by Eurocode 9.

AW6082-T6 – as proposed in Eurocode 9		
Parameter	Value	Unit of Measure
Rp02	255	MPa
Rm	300	MPa

Comparing the tested values with the theoretical ones, it is possible to state that the mechanical strength is enhanced in the material used for fatigue investigation with an increment of 29,8% for yield strength and 18,3% for ultimate strength. Taking into consideration these values it is possible to re-consider the static calculations by increasing of 20% the f_w value given in Eurocode 9. With this operation a margin of 9,8% takes into account uncertainties and the new value of the characteristic parameter f_w is:

$$f_w = 252 \text{ MPa.}$$

Repeating the calculations and considering the safety margin of 1,25 proposed by Eurocode 9:

$$\sigma_{\perp Ed} \leq 201,6 \text{ Mpa}$$

Thus, verifying the static condition above for the base material.

In HAZ, even increasing by 20% the ultimate strength of HAZ, the static condition is not verified.

However, under the loading condition no static deformation has been observed with these loads.

10.6.4 Joint fatigue life calculation

The life estimation can be done with the guidelines contained in EN1999-3 [11]

In this case the maximum and minimum loads must be known. During the experimental test the following loads (Tab. 22) and consequent stresses have been used:

Tab. 22 Values of forces and stresses used in the experimental investigation

$F_{1_{\max}} [N] = F_{2_{\max}} [N]$	$F_{1_{\min}} [N] = F_{2_{\min}} [N]$	$\sigma_{\max} [\text{MPa}]$	$\sigma_{\min} [\text{MPa}]$	R	$\Delta\sigma_i [\text{MPa}]$
9500	5000	198	104	0,53	94

The stress ratio R is calculated as the minimum over maximum stress and $\Delta\sigma_i$ is the stress range.

Known the stress range, Annex F of EN1999-3 [11] can be used for an accurate life prediction under low fatigue cycles. Indeed between 10^3 to 10^5 cycles the following formula has to be applied:

$$N_i = \left(\frac{\Delta\sigma_c}{\Delta\sigma_i \gamma_{Ff} \gamma_{Mf}} \frac{1}{\gamma_{Ff} \gamma_{Mf}} \right)^{m_0} \cdot 20^{\frac{m_0}{m_1}} \cdot 10^5$$

- 1) N_i is the calculated number of cycles to failure of a stress range $\Delta\sigma_i$
- 2) $\Delta\sigma_c$ is the reference value of fatigue strength at $2 \cdot 10^6$ cycles depending on the joint category.
- 3) $\Delta\sigma_i$ is the stress range for the principal stresses at the detail and is constant for all cycles
- 4) m_0 is the inverse logarithm slope of the $\Delta\sigma$ -N curves between 10^3 and 10^5 . This value depends upon the detail category and R. For $R \geq 0$ its value is equal to m_1 .

- 5) m_1 is the inverse logarithm slope of the $\Delta\sigma$ -N and it depends upon the detail category.
- 6) γ_{Ff} is the partial factor allowing for uncertainties in the loading spectrum and analysis of response. A value of 1 is a recommended choice.
- 7) γ_{Mf} is the partial factor for uncertainties in materials and execution. A value of 1 is a recommended choice both for safe life and damage tolerant fatigue design.

In the examined case the detail category of Fig. 10.28 has been chosen:

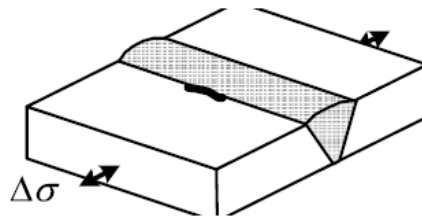


Fig. 10.28 Detail category chosen for the fatigue investigation (from [11]).

This detail category takes into account the fact that the welded joint is subjected to tensile stress and a potential failure will start from the weld toe.

At this point the calculation can be done with the known data and considering that:

- 8) $\Delta\sigma_c = 45 \text{ MPa}$
- 9) $m_1 = 4,3$

Developing the calculations with the above formula the result is:

$$N = 1,1 \cdot 10^5 \text{ cycles}$$

The detail category of the joint examined prescribes a minimum quality level both for the surface and the internal imperfections. As showed in paragraph relative to *Quality levels of acceptance* (chap. 7), this welding should be classified, according to UNI EN 15085-3, as high stress category because the ratio between the calculated over admissible stress is greater than 0,9:

$$\frac{\sigma_{\max}}{\sigma_{\perp Ed}} = \frac{198 \text{ MPa}}{201,6 \text{ MPa}} = 0,98$$

Knowing the stress category and the respective quality level, it is possible to determine in UNI EN ISO 15085 the weld performance class, the inspection class and the minimum required non-destructive tests to be performed on the welding.

10.7 Test setup for active thermography

Regarding active thermography, the test bench is constituted by three main components connected to a central unit, as showed in Fig. 10.29:

- Sub-system for infrared detection and its management software.
- Sub-system for laser head and its management software.
- Laser generator.

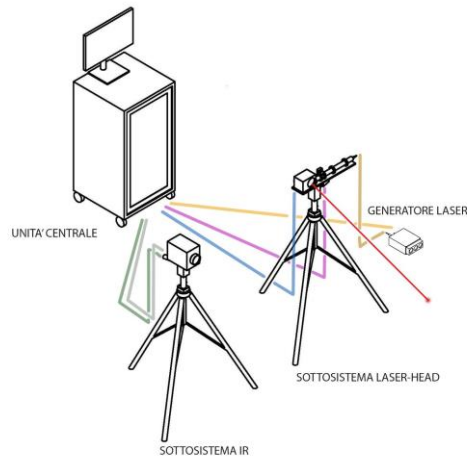


Fig. 10.29 Test bench for active thermography from [24])

Among the possible configurations, the one chosen for the tests is with the camera and laser on the same side. In the Fig. 10.30 below is represented the positions of the thermal camera (1) and the heat source (2):

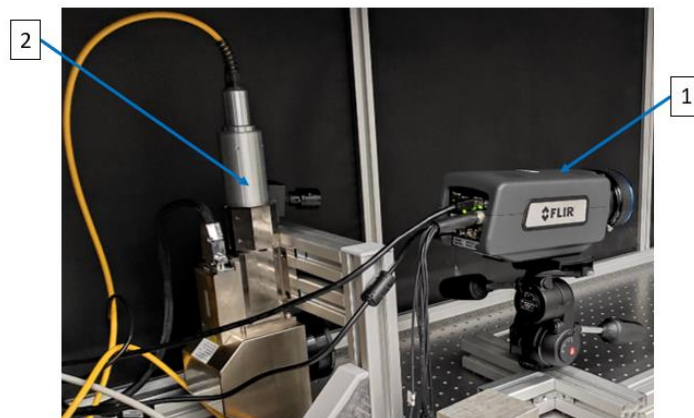


Fig. 10.30 Test bench for active thermography

Also, for the laser head (2) a dedicated software management is present. This software is called *MultiDES* and allows for activating and moving the laser head along the

designated path. In the *Type* section of Fig. 10.31, the available choices are: single pulse and train pulse.

In case of choice of train pulse, some additional parameters have to be set. These are the power percentage, the period of impulse that represent the period of the square wave and the number of pulses, that gives an indication of how many times to heat up the surface.

During the experimental tests, a power of 20% of the laser has been used. In addition, a single pulse and a period of 5000s has been set.

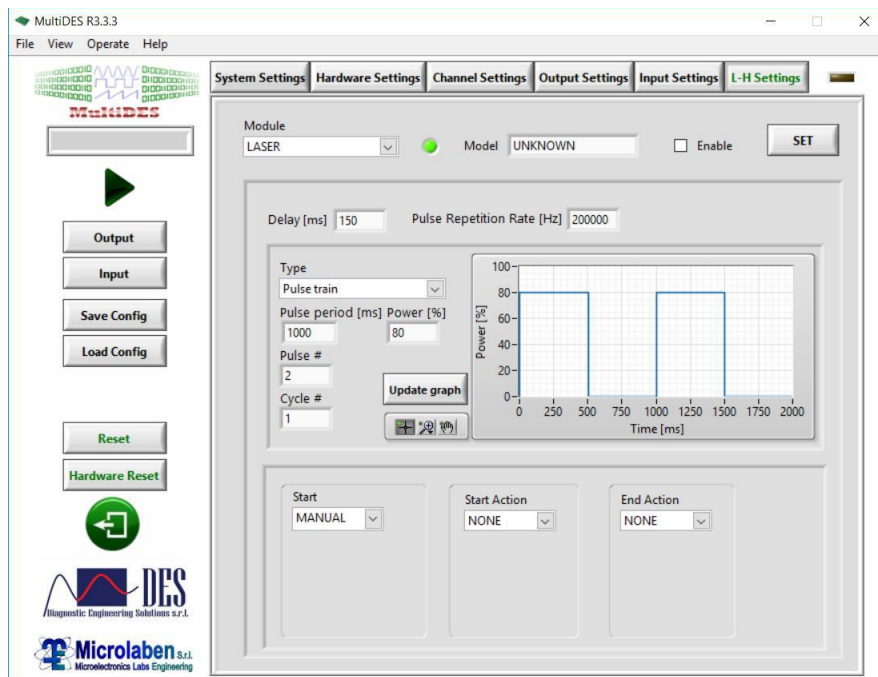


Fig. 10.31 MultiDES System - interface for parameters setting (from [24]).

Finally, the software allows to set the coordinates for path along which to move the laser on the sample in x and y directions. In the Fig. 10.32 below, is reported a screenshot of the software interface:

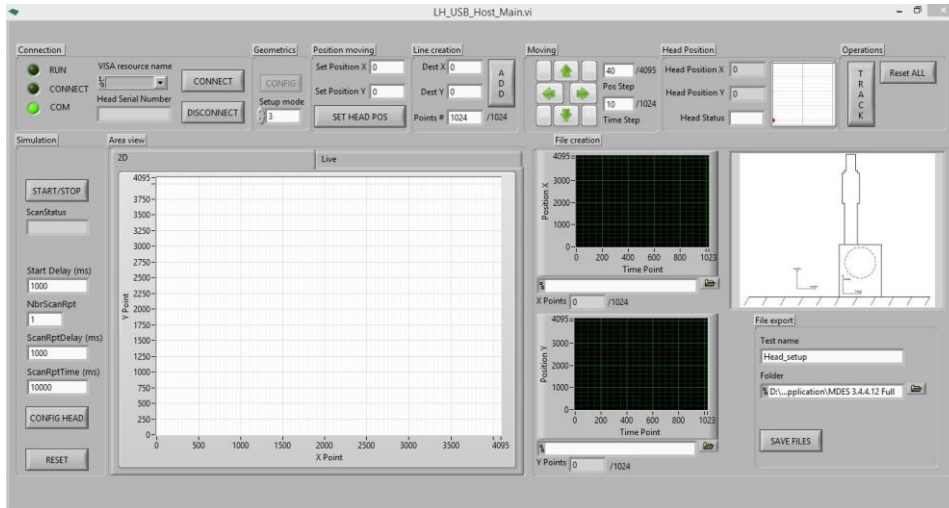


Fig. 10.32 MultiDes system – interface for coordinates setting (from [24]).

The complete configuration of the laser beam, infrared camera and sample under testing is reported in the Fig. 10.33:

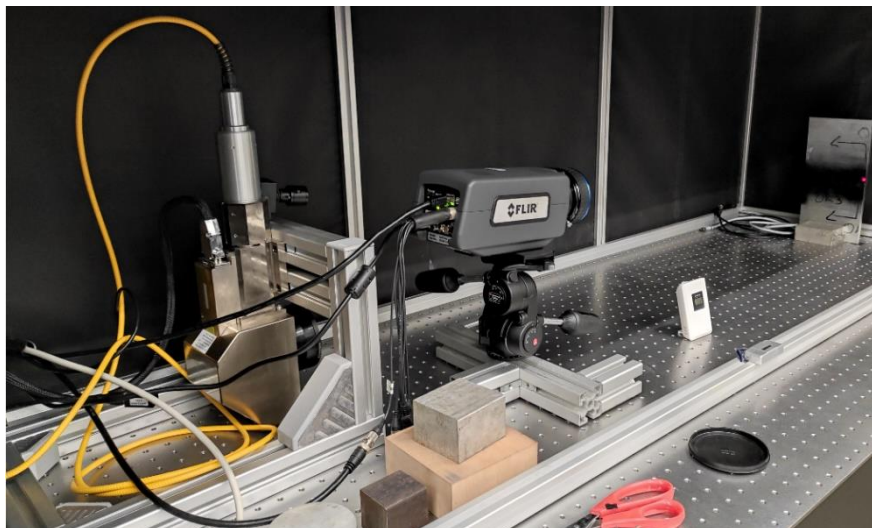


Fig. 10.33 Laser head, infrared camera and sample under investigation.

10.7.1 FLIR camera

The model used is FLIR A6751sc with a resolution of 640x512 pixel and a framerate from 0.0015Hz to 125Hz

The management software is called *ResearchIR*. With this software it is possible to set camera parameters to perform the tests.

The most important are: emissivity, distance from the object and reference temperature. In the below Fig. 10.34, a software representation of some setting parameters has been reported:

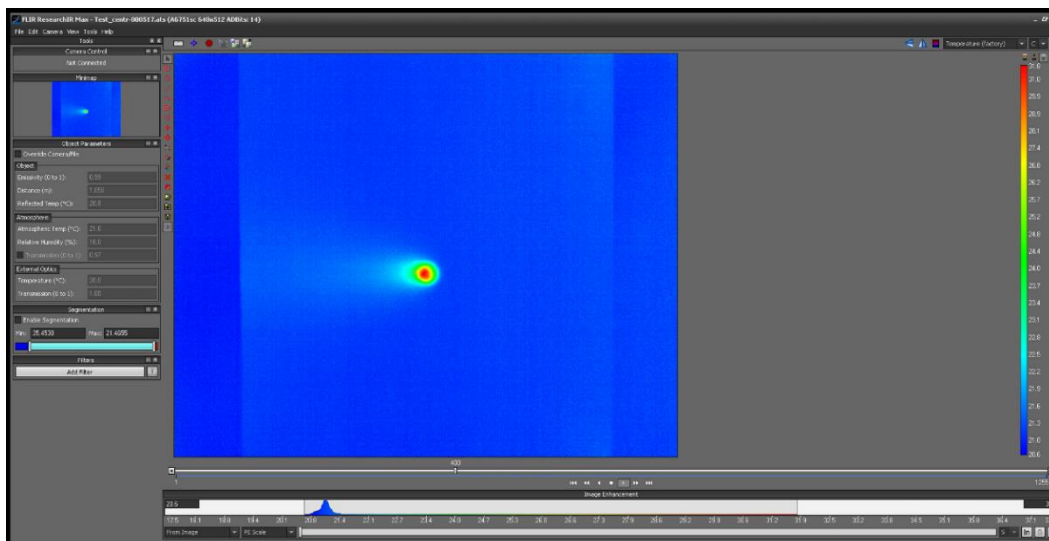


Fig. 10.34 Research IR software

10.7.2 Active thermography: data collection and elaboration

Before the fatigue tests and the investigation with passive thermography, a group of 4 samples have been investigated with active thermography. In this way it can be possible to compare the material response before the fatigue test on a selected number of samples. The 4 samples are chosen in order to characterize:

- 1) a sample without defects;
- 2) a sample with porosities;
- 3) a sample with an inclusion;
- 4) a sample with incomplete root penetration.

Regarding the parameters used during the investigations, these are strictly related to the heating source used as well as the infrared camera.

In particular, the heating source has been a laser beam whose period was set to 5000ms. During the setup phase, reflected temperature, ambient temperature, distance source-sample and humidity are used as input parameters for each test. In addition, some parameters have been settled: laser period, frame rate, emissivity, acquisition window, acquisition time and laser percentage. All these parameters are reported in the following Tab. 24 and they are valid for all the tests:

Tab. 23 Constant parameters for all the investigations with active thermography.

Parameter	Value	Unit of measurement
Laser period	5000	ms
Frame rate	125,57	Hz
Emissivity	0,99	-
Acquisition window	10 to 90	°C
Acquisition time	10	s
Laser percentage	20	%

Instead, in Tab. 25 and in Tab. 26 input parameters for the active thermographic tests before and after the fatigue tests respectively are reported:

Tab. 24 Parameters measured before testing the samples with active thermography before the fatigue assessment.

	Defect type	T reflected [°C]	T ambient [°C]	Humidity (%)	Distance source-sample [m]
OK3L1	No defect	20,8	21,6	16%	1,05
PO2L2	Porosities	20,6	21,3	18%	1,05
IN1L2	Inclusion	20,8	21,4	16%	1,05
MP3L1	Incomplete root penetration	20,8	21,7	16%	1,05

This acquisition has been done by heating the central part of the weld seam with a single pulse laser beam.

The same acquisition has been repeated after the fatigue tests on the same samples: the centre of the weld seam, with no visible damages and covered with black paint, has been tested pointing the laser beam as shown in Fig. 10.35, with the red line.

Tab. 25 Parameters measured before testing the samples with active thermography after the fatigue assessment.

	Defect type	T reflected [°C]	T ambient [°C]	Humidity (%)	Distance source-sample [m]
OK3L1	No defect	20,5	21	4%	1,05
PO2L2	Porosities	20,5	21	4%	1,05
IN1L2	Inclusion	26,9	27,5	45%	1,11
MP3L1	Incomplete root penetration	26,7	27,3	41%	1,11



Fig. 10.35 Centre of laser for investigation with active thermography.

The laser head moves from the left to the right side of the sample and the FLIR infrared camera reads the temperatures on the sample. Once stored, this information can be extracted in form of thermal map per each frame and then post-processed with Matlab. With *ResearchIR* software it is possible to investigate the temperatures in a *Box* window as shown in Fig. 10.36.

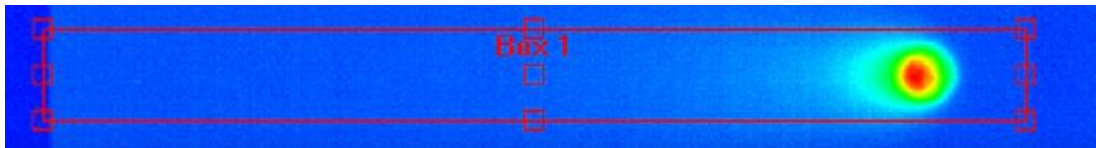


Fig. 10.36 Box object of a frame in *Research IR*.

In particular, the investigation on the mean temperature on the sample without defects is needed to build the base image that represents the base material response. Indeed, for a sample without defects, a characteristic mean temperature is detected and the related thermal image built up.

Since the laser head moves along the weld seam, the laser position will be different per each frame and the thermal map has to be reconstructed in the time domain to obtain a unique thermal image. Thus, a 3D matrix is imported in MATLAB and in this matrix:

- the first two dimensions represent the thermal map of the sample;
- the third dimension represents the time domain in which the thermal map evolves.

The following figure 10.37 represents this situation:

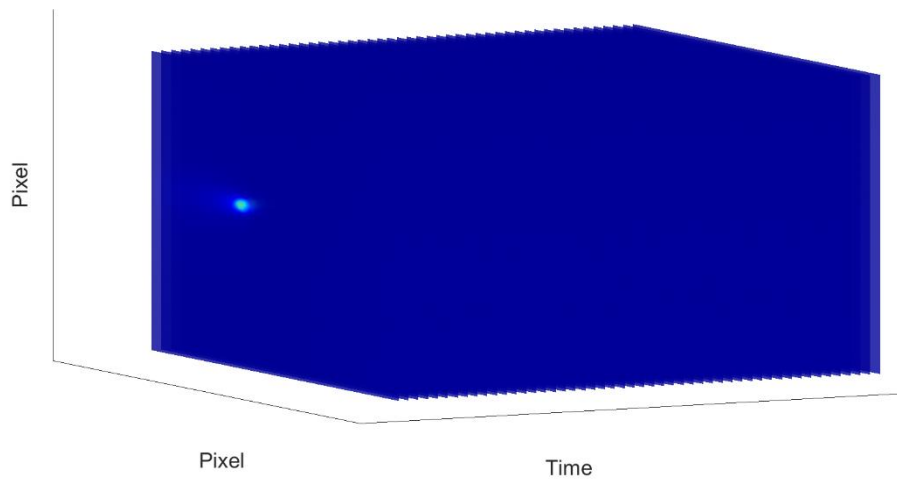


Fig. 10.37- 3D image of the subsequent frames.

A subsequent elaboration consists in cropping off the same box used for the mean temperature evaluation. At this point it is possible to reconstruct a unique thermal map for the whole weld seam and to subtract the base image with the base material information for each sample. During this step it is also possible to eliminate the environmental temperature influence by subtracting a thermal image in which each pixel is at the environmental temperature. This latter is measured with a digital thermometer before each test.

Finally, it is possible to plot the results and to compare the tests done before and after the fatigue test.

11. The experimental results for the 1st batch samples

In this chapter the results for the first batch sample are discussed. The radiographic test has been used to assess the presence of the defect inside the material.

11.1 Radiographic investigation for defect characterization

As seen in the section related to NDT, the radiographic test is useful to detect imperfections into the volume of welding.

For this reason, after the welding phase, a radiographic test has been carried out with the goal of verifying that what has been produced resembles the desired parts. In fact, the scope is to test welded samples with only one type of indication. The dimension of the tested plate is 300mmx400mmx10mm and two samples per each have been cut.

The radiographic method has used the following parameters:

- 5) source-to-object distance: 1200mm;
- 6) gain: 100;
- 7) voltage: 70kV;
- 8) amperage: 5mA;

Because of the use of the digital detector instead of the film, it's possible to have enhanced results due to image software improvement. *Rhythm Diconde Viewer* has been used to view and to enhance the contrast and/or brightness of the radiographic capture. In the below Fig. 11.1 is showed a software screenshot interface:

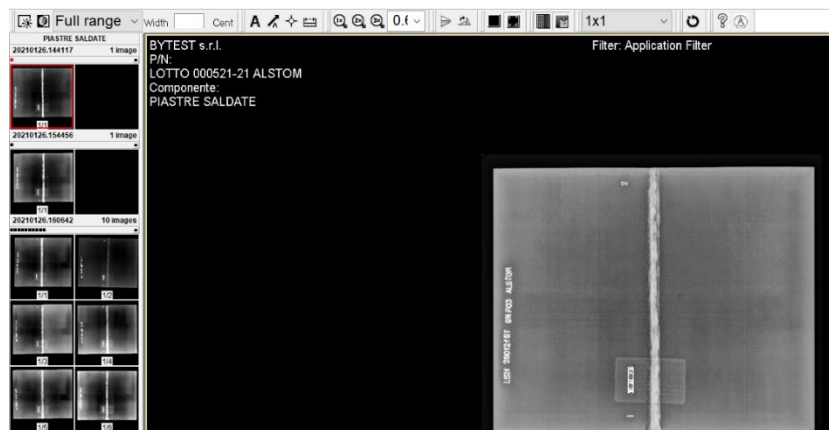


Fig. 11.1 Rhythm software to view radiographic images

On the left there is the image selection while on the right the capture selected on which to detect indications. To help into the detection phase, the upper bar gives some instruments. A zoomed view is here reported in Fig. 11.2:

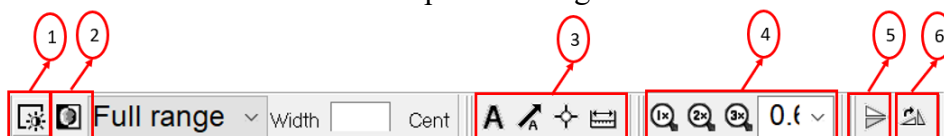


Fig. 11.2 Rhythm software parameters.

The buttons 1 and 2 are used to enhance brightness and contrast respectively while buttons group 3 is to set annotations both as text and dimensions. Instead, the buttons group 4 is used to zoom in/out the image. Finally, the buttons 5 and 6 are used to flip and to rotate the image respectively.

The radiographic test has been demonstrated its validity in detecting porosities, inclusions and incomplete root penetration.

The requested quality level for imperfections is B. The limit values are the one described in *Quality levels of acceptance* (chapter 7).

The results, with dimensional annotations, are presented in the following:

- 1) Samples without defects (Fig. 11.3):

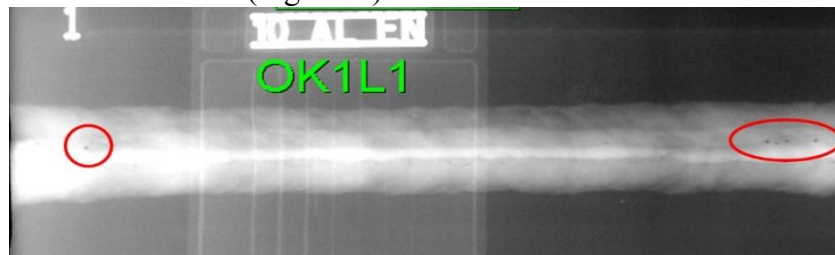


Fig. 11.3 Radiographic image of defect free sample 1 of 3

As it can be seen from the above image the sample shows few pores. In this case the imperfections can be considered acceptable and so the welding is defect-free.

The other two samples without defects are shown in Fig. 11.4 and in Fig. 11.5.

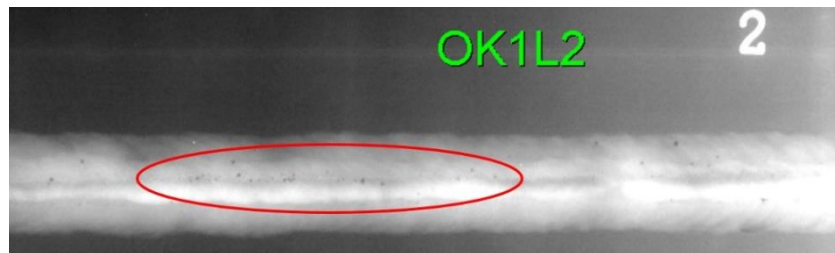


Fig. 11.4 Radiographic image of defect free sample 2 of 3

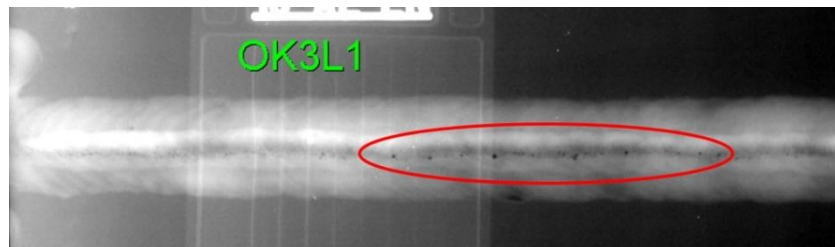


Fig. 11.5 Radiographic image of defect free sample 3 of 3

Also, in the two cases the pores are acceptable because for they are within the limit of 2% as described in Annex A of UNI EN ISO 10042 [47] and reported in Fig. 11.6:

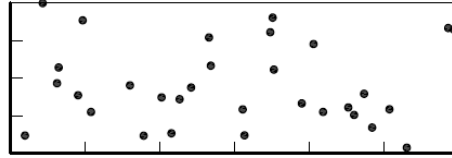


Fig. 11.6 - 2% of porosities according to ISO 10042 (from [47]).

2) Samples with inclusions:

The three samples with inclusions are represented in Fig. 11.7, Fig. 11.8 and Fig. 11.9:



Fig. 11.7 Radiographic image of samples with inclusion 1 of 3

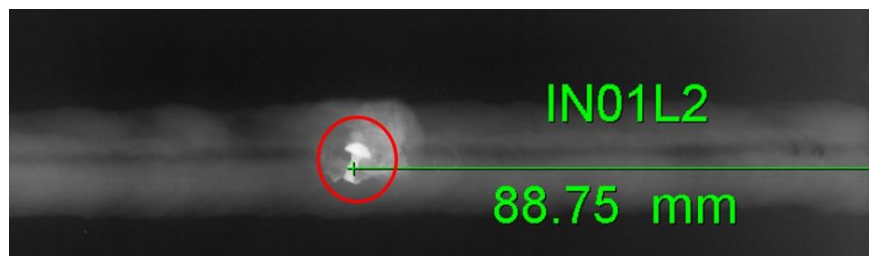


Fig. 11.8 Radiographic image of samples with inclusion 2 of 3

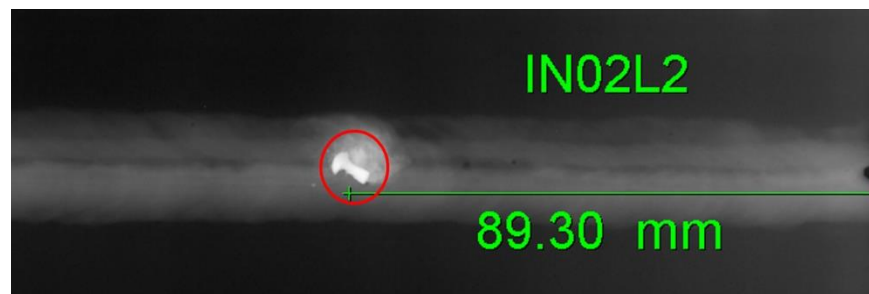


Fig. 11.9 Radiographic image of samples with inclusion 3 of 3

The red circles in the above images show the inclusion of a steel nail of about 7mm. In UNI EN ISO 10042 the metallic inclusions can be present for maximum 3mm and for this reason the imperfection has to be considered as not acceptable.

- 3) Samples with incomplete root penetration are presented in Fig. 11.10, Fig. 11.11, Fig. 11.12:

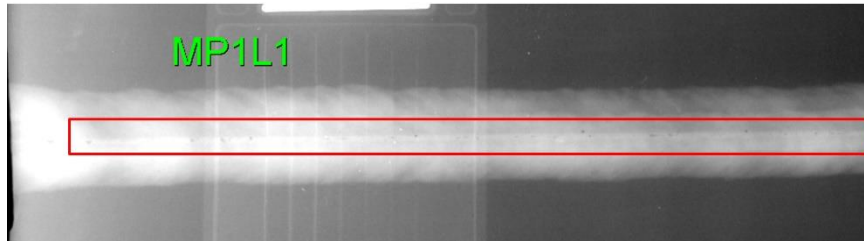


Fig. 11.10 Radiographic image of samples with incomplete root penetration 1 of 3

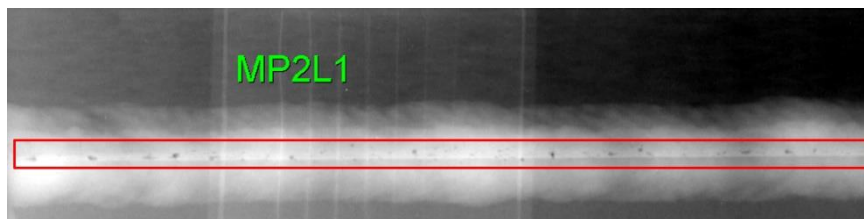


Fig. 11.11 Radiographic image of samples with incomplete root penetration 2 of 3

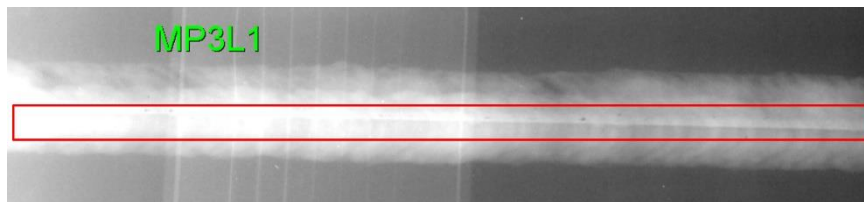


Fig. 11.12 Radiographic image of samples with incomplete root penetration 3 of 3

As it can be seen by the above images, the incomplete root penetration is evidenced by the darker line at the centre of the weld seam, highlighted by the red rectangle. This kind of imperfection is not acceptable for the quality level considered and therefore this is a defect.

4) Samples with porosities are presented in Fig. 11.13, Fig. 11.14 and Fig. 11.15:

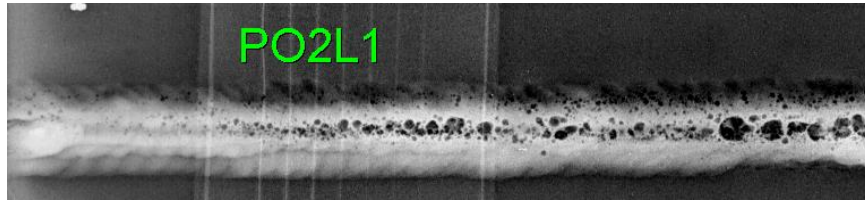


Fig. 11.13 Radiographic image of samples with porosities 1 of 3

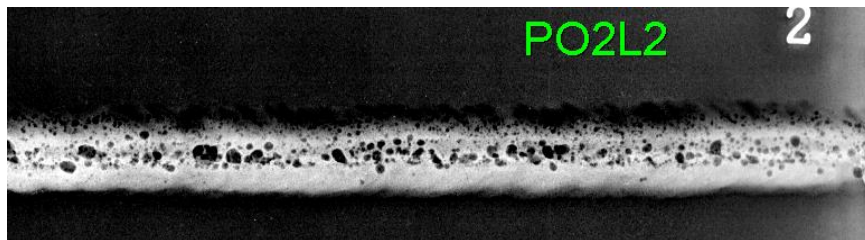


Fig. 11.14 Radiographic image of samples with porosities 2 of 3

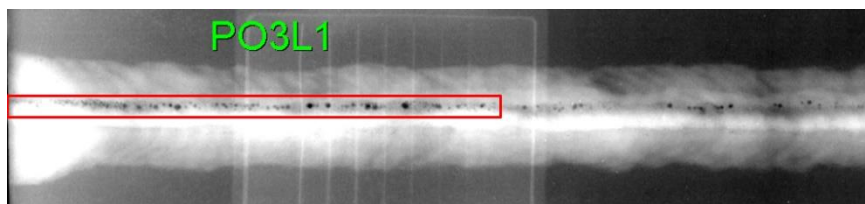


Fig. 11.15 Radiographic image of samples with porosities 3 of 3

The above captures show samples with different porosities. The first two samples (PO2L1 and PO2L2) are characterized by at least 10% of porosity, considered not acceptable for the quality level selected.

In the following Fig. 11.16 is reported the sample to which compare the porosities from ISO10042 [47]:

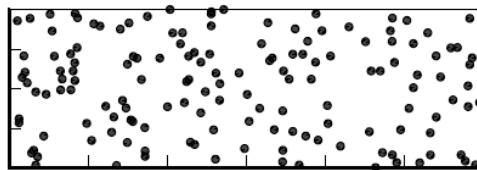


Fig. 11.16 - 10% of porosities reference sample according to ISO 10042 (from [47]).

The third sample (PO3L1) is characterized by linear porosity, a not acceptable imperfection.

11.2 Fatigue and passive thermographic test results

The results obtained in terms of life in number of cycles during the tests are higher than the calculated ones.

The graph of Fig. 11.17 shows the lives after the tests:

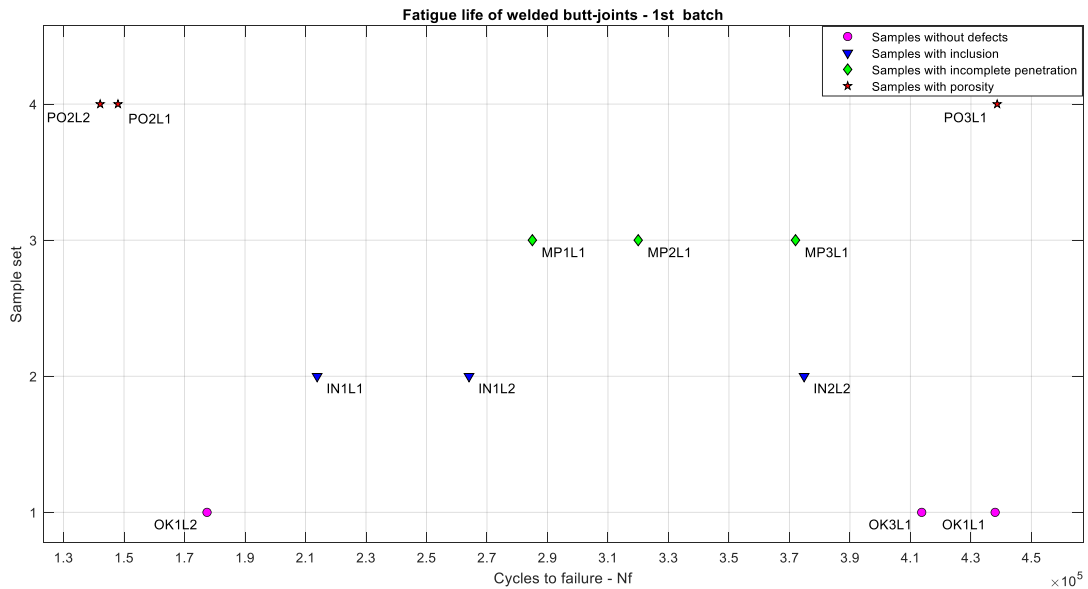


Fig. 11.17 Fatigue test results of 1st batch samples: cycles to failure.

Even if no work on inclusions in butt weld aluminium joints are present in literature, similar results have been obtained for the other three joint category. Indeed, as showed in [41] there is a correlation between the pores present in the weld seam and the life of the sample. A prediction model has been developed and it takes into consideration also the residual stresses of the welded component.

Thus, obtaining a number of cycles N :

$$N = \frac{1}{a(1 + \beta)} \left(\frac{\sigma_a(1 + d^c)}{1 - b\sigma_m} \right)^{-\beta}$$

Where:

- 1) the parameters a, b, c and β have been identified by several fatigue tests of defect-free components.
- 2) d is the pore diameter.
- 3) σ_a and σ_m are the alternate and mean stress respectively.

With this practical approach it is possible to trace S-N curves varying the pores diameters as identified in [41] and reported in Fig. 11.18:

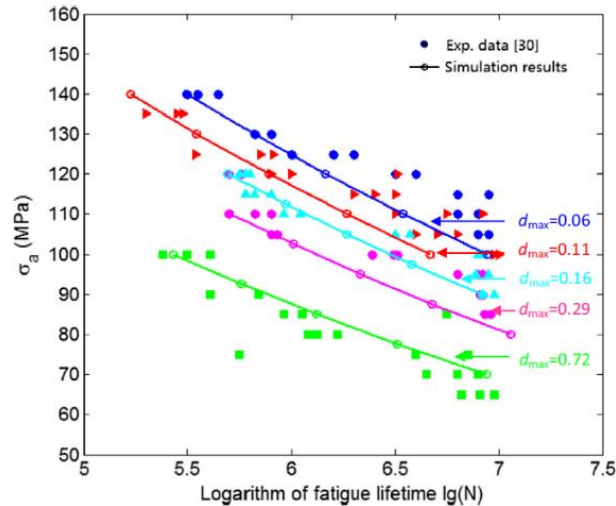


Fig. 11.18 S-N curves in presence of pores (from [41]).

As it can be seen from S-N curves, decreasing the pore diameters, the admissible stress increases. Thus, the obtained results for what concerns the porosities are in line with the experimental results obtained in the work [41].

In [35] instead it is possible to compare the obtained results with the ones of samples containing porosities and samples with incomplete penetration. In this case the joint type, the materials used and the weld process are comparable with the ones used during the experimental investigation. Even if the work [35] is intended mainly for assessing the life of welds subjected to a repair process, it is possible to take only the fatigue test results for welded specimens without repair.

These values are showed in form of histogram in Fig. 11.19:

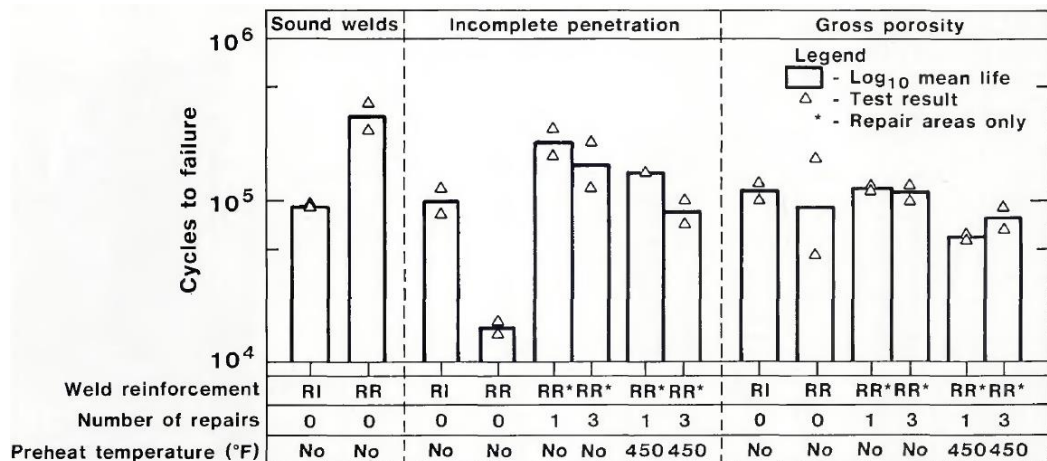


Fig. 11.19 Cycles to failure in presence of porosities and incomplete root penetration (from [35]).

From the above graph it is useful to observe only the results with zero-number of repairs and the mean cycles to failures are in the range of 10^5 cycles.

Finally, in the work of Maddox [39] some results for fatigue assessment of defect-free components are shown. In fact, some experimental results are compared with Eurocode 9 and International Institute of Welding design curves. The S-N curves as well as the experimental outcomings are reported in Fig. 11.20:

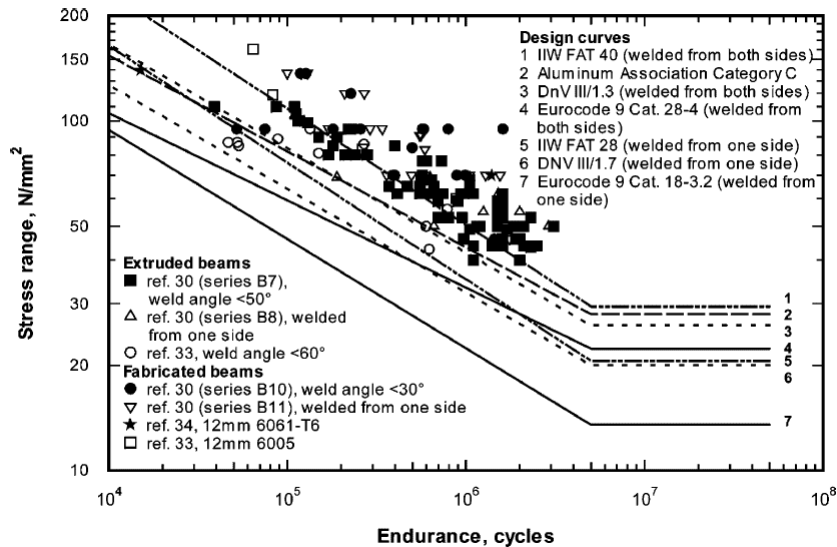


Fig. 11.20 S-N curves for defect free samples (from [39]).

To compare the results in [39] with the experimental ones, it's important to choose a stress range of 94Mpa.

Even in this case the endurance of the specimens is a little higher than 1×10^5 cycles.

Overall, the sample life resulted during the fatigue testing is in the order of magnitude of 10^5 , the same highlighted during the calculation steps and present in literature.

However, Eurocode 9 calculations have a margin that allows to take into consideration the imperfections identified for the quality level of imperfections as described in ISO10042 both on the surface and internally.

By taking the ratio between the number of cycles found during the experimental tests and the calculated number of cycles, the fatigue life ratio can be determined.

The values for the 12 samples are reported in Tab. 26.

Tab. 26 Eurocode 9 vs real values: estimation of safety factors for the 1st batch samples.

TEST	Defect type	Sample denomination	Nbr. Of cycles to failure observed during experimental tests	Nbr. Of cycles to failure calculated - Eurocode 9	Fatigue life ratio
1	No defects	OK1L1	438000	110000	4,0
2	No defects	OK1L2	177441	110000	1,6
3	No defects	OK3L1	413718	110000	3,8
1	Inclusion	IN02L2	374847	110000	3,4
2	Inclusion	INO1L1	231000	110000	2,1
3	Inclusion	IN01L2	264063	110000	2,4
1	Porosities	PO2L2	142121	110000	1,3
2	Porosities	PO2L1	148000	110000	1,3
3	Porosities	PO3L1	438676	110000	4,0
1	Incomplete root penetration	MP1L1	285000	110000	2,6
2	Incomplete root penetration	MP2L1	320000	110000	2,9
3	Incomplete root penetration	MP3L1	372000	110000	3,4

Finally, it is possible to see that:

- 1) the samples with inclusions and porosities have a mean life that is in mean two times the calculated one;
- 2) the samples without defects and the ones with incomplete root penetration have a similar mean life, about three times the calculated one.

Some other considerations can be done about the different samples tested:

- 1) In two of the samples with porosities the fatigue life is very low if compared with the third sample. This aspect is to be ascribed to the different severity of defects inside the welding. Indeed, as showed in the radiographic test, the samples cut from the PO2 plate have a greater number of porosities with respect to the other sample.
- 2) The root incomplete penetration samples have been tested with the welding in tension, resulting that the root is always in compression. For this reason, their lives are similar to the samples without defects.

In all the samples the weld toe represents a discontinuity between the base material and the welding. In addition, also the excess of metal is a discontinuity on the weld surface. Indeed, during the fatigue tests, the weld toe as well as the surface of the welding are preferred locations in which the crack has started and propagated.

In Fig. 11.21 below is evident this phenomenon:



Fig. 11.21 crack in weld toe.

As it can be seen, depending on the surface flatness the crack is present or not in the middle of the welding. Only in one case of a sample with the inclusion the crack has propagated also inside the inclusion, as showed in Fig. 11.22 below:



Fig. 11.22 Crack in a sample with inclusion.

The thermographic investigation has been performed by sampling the temperature profile of the specimen under examination at a specific frequency. This process is completely automatized thanks to the acquisition software of the camera.

An example of this acquisition is represented in Fig. 13.23 where the sample in its bench seat is represented:

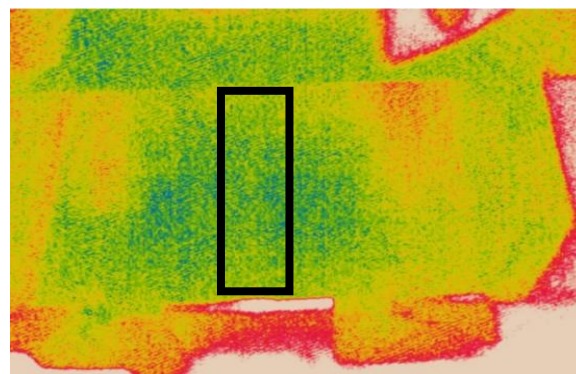


Fig. 11.23 Area of investigation in passive thermographic test

The sampling frequency was 0.008Hz for one half of the samples and 1Hz for the other half.

Even if a clear temperature profile is defined on and around the sample, a specific region of interest, painted with black and delimited by the black rectangle in the figure, has been considered.

By using the camera software function, it is possible to extract the temperature data and obtain the temperature profile during the test. The basic post-processing technique consists in subtracting the environmental temperature from each temperature value and obtaining a value that is relevant to be plotted vs the elapsed cycles.

The result for one of the samples with inclusion with a sampling frequency of 0.008Hz is reported in the graph of Fig. 11.24:

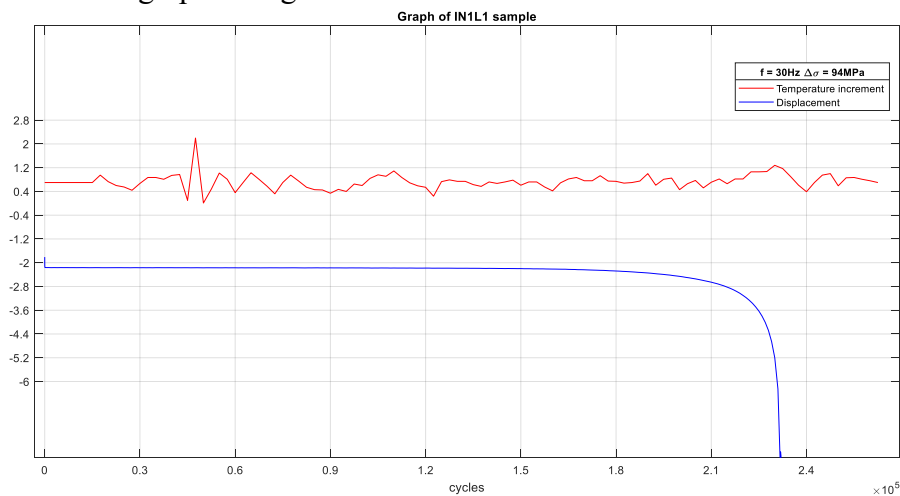


Fig. 11.24 Temperature increment and displacement for a sample with inclusion sampled at 0.008Hz.

Increasing the sampling frequency to 1Hz there is a data increase as shown in the below Fig. 11.25:

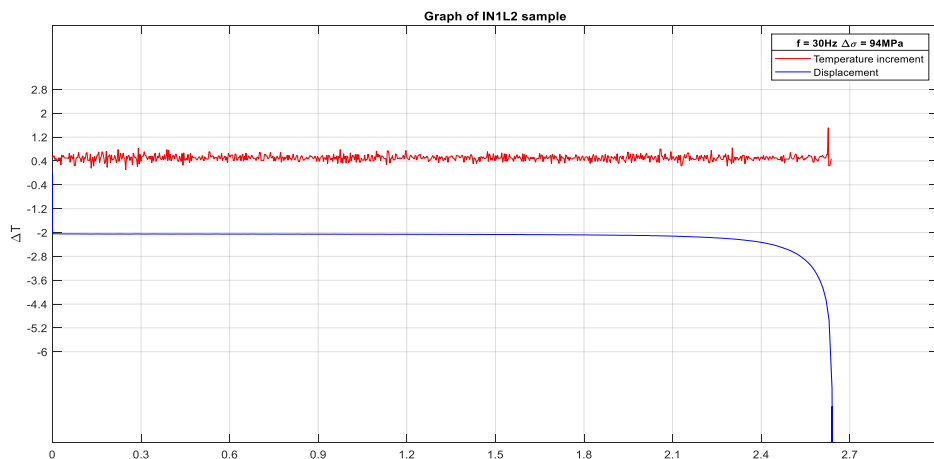


Fig. 11.25 Temperature increment and displacement for a sample with inclusion sampled at 1Hz.

However, even with a greater acquisition frequency, the calculated temperature difference with respect to the environment does not show a significative increase

during the test. In addition, even in the final part of the test, where the displacement curve is steeper, the temperature increment is the same order of magnitude of the rest of the test.

The same behaviour is present in the case of a defect-free sample and in samples with porosities and incomplete root penetration:

Finally, the complete dataset of the 12 samples is shown in Appendix A.

11.3 Active thermographic investigation

In the context of the active thermographic investigation, two tests have been done within this work, one before and one after the fatigue tests. As described in Chapter 11, this method allows to understand the material response in both the cases of a sample with or without a determined defect.

The FLIR camera used offers the possibility to extract, frame by frame, the thermal maps in the time domain in order to process them in MATLAB®. The four samples are chosen in order to have 3 different defects (porosities, inclusions and lack of penetration) and one sample without defects. In all the samples the test has been carried out at about 7mm far from the crack, at the centre of the weld seam.

After the post-processing described in section 10.7, the results, in which the temperature profile of the sample is plotted in function of the sample length, are shown in the following. The temperature profile has been deputed from the environmental temperature, having on the y-axis a delta of temperatures. In the upper part of the graphs, the radiographic image of the samples before the fatigue test has been reported.

The first sample analysed has been the one without any defect, as shown in the below Fig. 11.26:

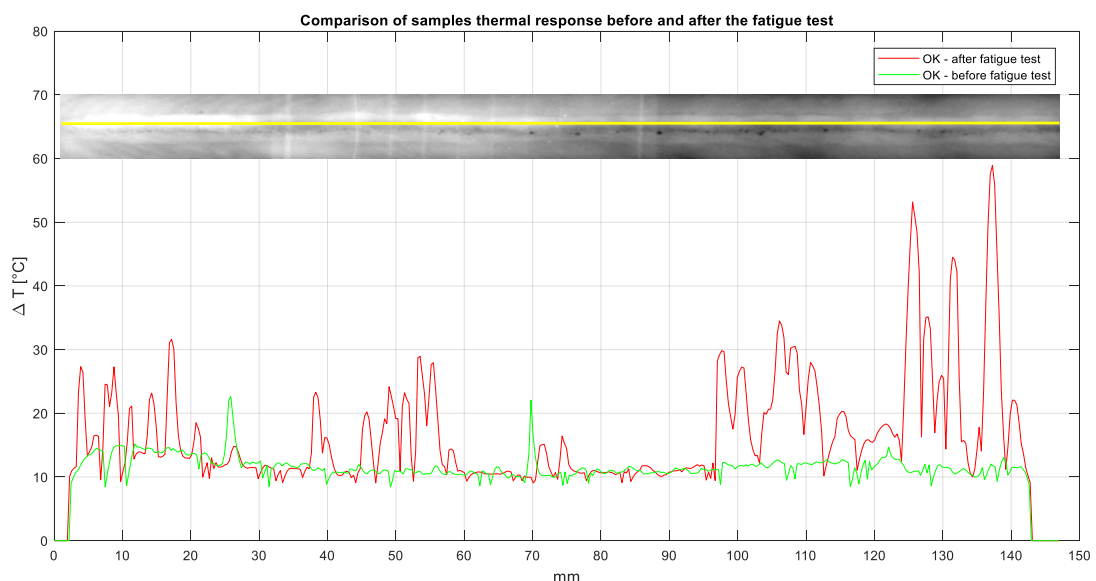


Fig. 11.26 Active thermographic testing of the sample without defects – OK3L1.

As it can be seen from the above figure, the sample without defects, shows an increase in the thermal response of the material along the tested area after the fatigue test. As it can be seen from the Fig. 13.26, the increment in temperature is marked at the right side of the sample (red thermogram).

To better understand this trend, it is important to analyse the surface of the sample as in Fig. 11.27.



Fig. 11.27 - OK3L1 weld seam after the fatigue test.

From the above figure, during the fatigue test the crack has started from the left side of the sample, propagating up to the right side. This has influenced the heat exchange inside the sample by modifying the material response to the excitation after the fatigue test. It is evident that the crack reduces the thermal conductivity of the sample and resulting in a response with an increased temperature.

In Fig. 11.28, the sample with an inclusion is shown:

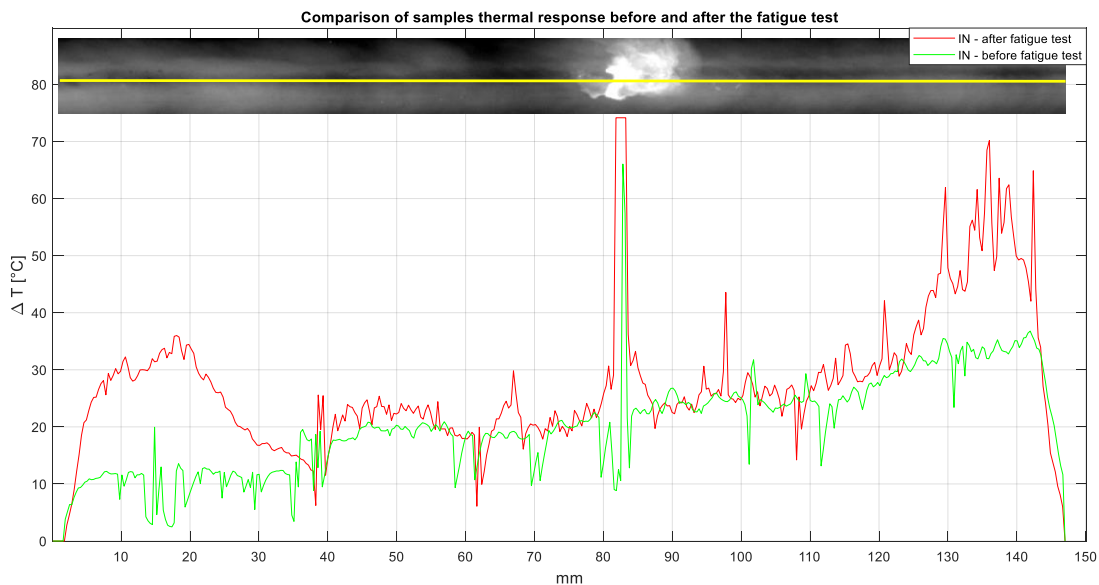


Fig. 11.28 Active thermographic testing of the sample with an inclusion – IN1L2.

As it can be seen from the above thermograms superposition, the inclusion found in the radiographic test, is also shown as a peak in both the thermograms before and after the fatigue test. It is important also to note that the red signal, that represent the material response after the fatigue test, exceeds the acquisition window in certain points of the sample. This phenomenon is called saturation.

The signal saturation in correspondence of the inclusion is mainly to be ascribed to the fatigue test that has decreased the heat conduction in the material in that points.

Even in this case, the results can be commented by looking at the surface crack image in Fig. 11.29.



Fig. 11.29 IN1L2 weld seam after the fatigue test.

Even if the central part of the red and green thermograms can be superposed without a significant difference except for the inclusion, the two ends show an increase in temperature. As the previous case, this aspect can be explained with a reduction in thermal conductivity of the sample due to the crack.

The third sample tested is the one with incomplete root penetration and its thermograms are shown in the below Fig. 11.30:

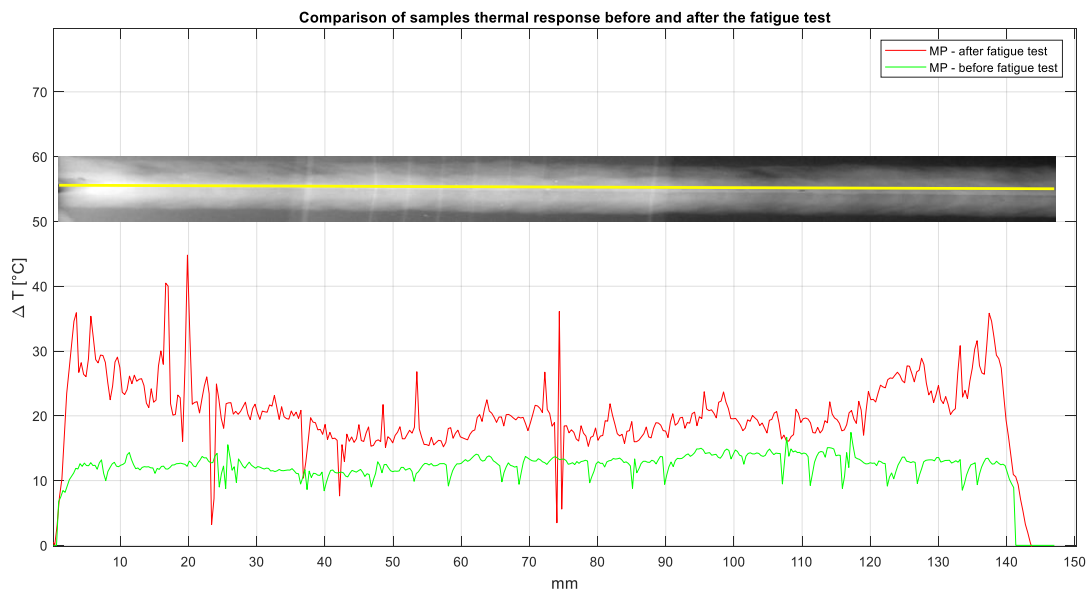


Fig. 11.30 Active thermographic testing of the sample with incomplete root penetration – MP3L1

In the sample with incomplete root penetration, the thermograms superposition shows a behaviour like the previous two samples related to the temperature increase. Also, it is important to show the crack image in Fig. 11.31 to better understand the trend of the red thermogram.



Fig. 11.31 MP3L1 weld seam after the fatigue test.

Indeed, also in this case the crack is present on the surface and the red thermogram is almost constant along the weld seam, demonstrating the thermal conductivity decrease in the sample.

The last sample analysed is the one with porosities defects and its thermograms are shown in Fig. 11.32:

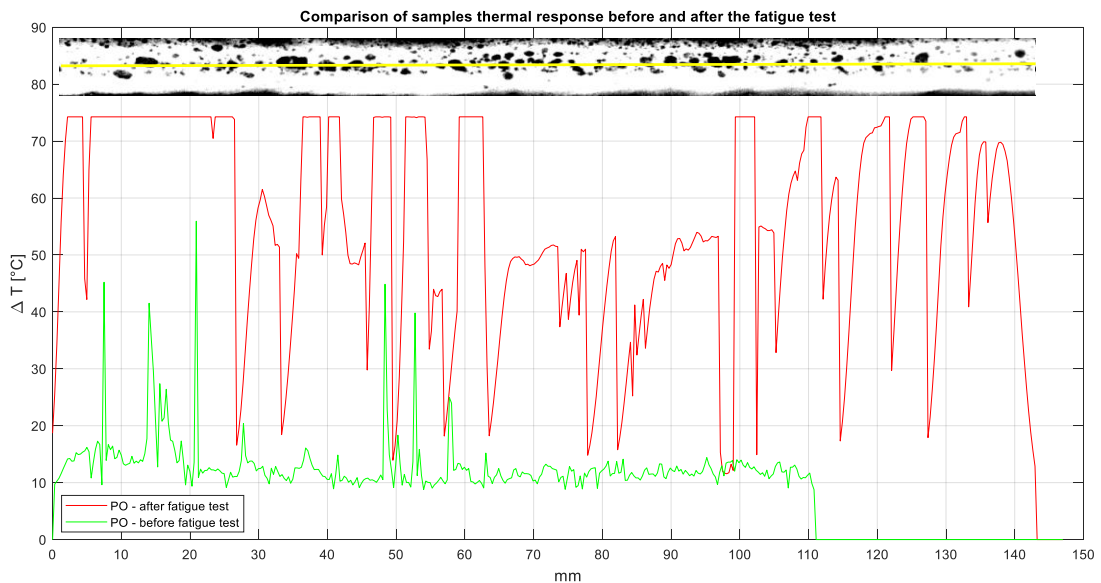


Fig. 11.32 Active thermographic testing of the sample with porosities – PO2L2

The green line represents the sample testing before the fatigue test. The straight line after about 112mm represents a laser misleading behaviour and no data are present from 112mm to 148mm.

It can be clearly seen that, testing the sample in the centre of the weld seam as shown by the yellow line, there is an overall increase of the temperature after the fatigue test. In the upper part of the graph is reported the radiographic test of the sample before the fatigue test to correlate the red signal with the porosities.

In the saturated points there is a low heat conduction due to the combination of the surface crack present on the material and the pores inside the weld seam. In this case, the saturated signal appears to be constant for the first 28mm of the sample, where the fatigue crack has started as shown in the following Fig. 11.33:



Fig. 11.33 Sample with porosities – PO2L2: crack at the surface.

However, it is not possible to have the exact correlation between each pore shown in the radiographic image and the thermographic test saturation because not all the pores dimensions are known. Indeed, the projection in 2-dimension of the porosity defect with the radiographic test, does not give the information on the depth of this defect neither its extension in depth.

12. The experimental results for the 2nd batch samples

In this chapter, the results for the second batch samples are shown. Penetrant and ultrasonic testing have been performed before the fatigue test to assess the presence of the defect inside the material.

12.1 Penetrant testing for surface defects identification

Penetrant testing is one of the most common tests to identify superficial discontinuities that, at a visual test, does not appear clearly.

In this specific case the test has been performed on 100% of samples, even if the production requirement according to UNI EN ISO 15085-3 is to inspect 10% of what produced.

The test was performed using ISO prescriptions described in section 8.4 and with the use of the following specific spray liquids:

- 1) K71B2p red penetrant;
- 2) D112A white developer;
- 3) BC1 cleaner remover;

These products are specific for colour contrast testing and allow to obtain a sensitivity level of 2.

In a preliminary phase, the samples have been cleaned firstly with water and then with BC1 cleaner in order to remove dust and residuals from welding process. The result of this process is shown in Fig. 12.1:

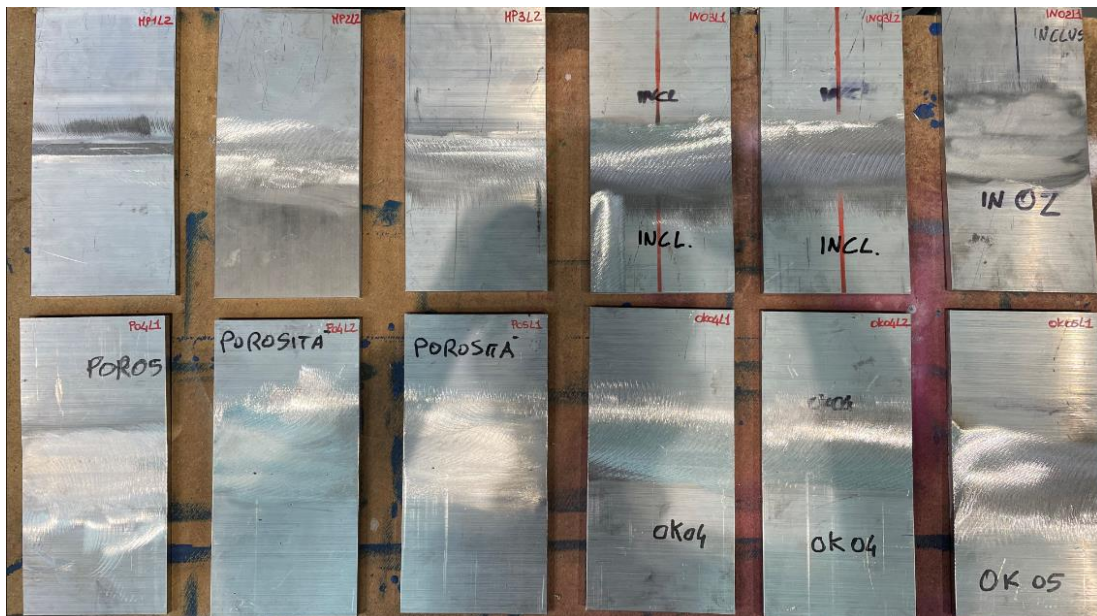


Fig. 12.1 Samples after the cleaning procedure

At this level, a visual test does not show relevant indications except for:

- 1) Samples with incomplete root penetration defects where, on the back side, is visible that the base material is unfused;
- 2) Samples with porosities, where, after the milling process, some surface pores are visible.

After this first step it is important to dry the samples with hot air to assure that all of them are dried in order to proceed with the application of the red penetrant.

The red penetrant applied is washable with water and allows to obtain faster results thanks to the intense red colour.

The results after the red penetrant application are showed in Fig. 12.2 below:

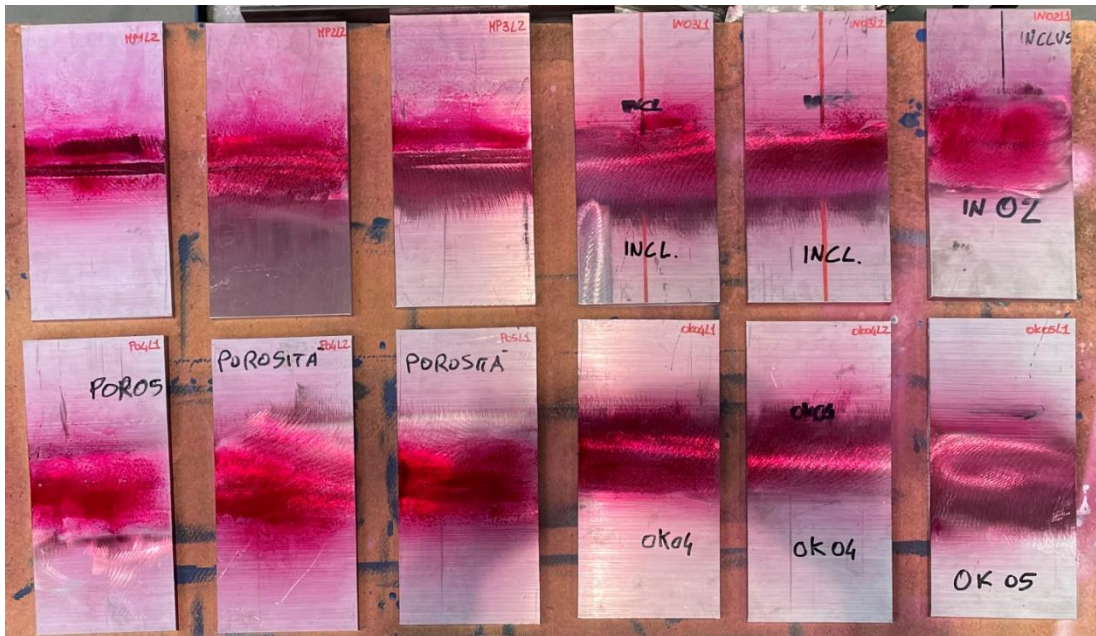


Fig. 12.2 Samples after the application of red penetrant.

Once applied, it's important to leave the red penetrant on the samples from 5 to 20 minutes depending on the environment temperature. For an environment temperature of 20 °C the manufacturer suggests a time up to 10 minutes. This time is called penetration time and assure the correct penetration of the liquid inside a surface defect. After that it is possible to remove the excess of penetrant from the samples by using a cloth with a small quantity of cleaner or water with low pressure. In this step it is important to avoid spraying the cleaner directly on the samples because there is the possibility to remove the penetrant from the defects.

Finally, white developer can be applied and after the developing time that is the same time of penetration, the overall result is shown in Fig. 12.3:



Fig. 12.3 Samples after the application of white developer.

The fine spray white particles allow to obtain a clear visualization of some defects that are present on the samples.

Each weld seam is here analysed more in detail.

12.1.1 Defect-free samples

The samples without defects do not show any surface mark and the surface colour is uniform. The below images (Fig. 12.4, Fig. 12.5, Fig. 12.6) highlight the results on the three samples:



Fig. 12.4 Penetrant testing results for defect-free samples 1 of 3.



Fig. 12.5 Penetrant testing results for defect-free samples 2 of 3.



Fig. 12.6 Penetrant testing results for defect-free samples 3 of 3.

12.1.2 Samples with inclusion

Regarding the samples with an inclusion, they are welded with a multi-pass welding with the inclusion of a ferrous nail between the first and the second pass. The inclusion position was previously traced on the sample with a line. In the following Fig. 12.7, Fig. 12.8 and Fig. 12.9 indications found on the samples are shown:



Fig. 12.7 Penetrant testing results for samples with inclusion 1 of 3.



Fig. 12.8 Penetrant testing results for samples with inclusion 2 of 3



Fig. 12.9 Penetrant testing results for samples with inclusion 3 of 3

From the above images is visible at least one indication per sample. This superficial indication represents the inclusion inside the welding. The fact that the inclusion is visible also on the surface is to be ascribed to the grinding process after welding that has taken the weld seam thickness to the plate nominal value.

12.1.3 Samples with root incomplete penetration

Incomplete root penetration has been created on the samples by using a tiny arc that allows to artificially create the defect but at the same time simulate the results of a wrong parameter setting during the welding process. The images related to the penetrant test are below reported in Fig. 12.10, Fig. 12.11 and Fig. 12.12.

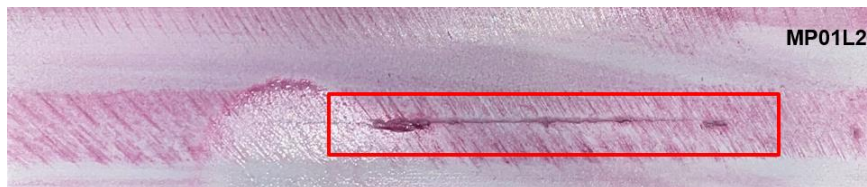


Fig. 12.10 Penetrant testing results for samples with incomplete root penetration 1 of 3

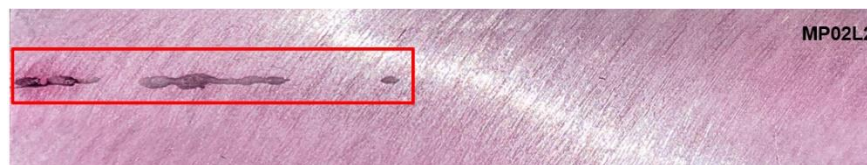


Fig. 12.11 Penetrant testing results for samples with incomplete root penetration 2 of 3

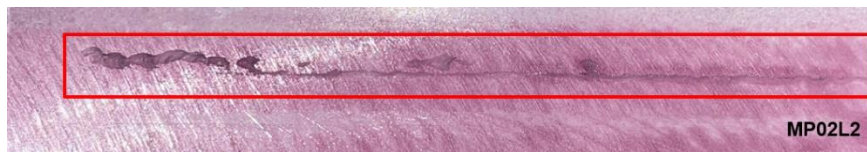


Fig. 12.12 Penetrant testing results for samples with incomplete root penetration 3 of 3

As it can be seen by red rectangles, the incomplete root penetration defect is present on the three samples at least for a length of 40%. The red penetrant makes in evidence the marks.

12.1.4 Samples with porosities

Porosities are defects that can be generated inside the weld seam even if they are unwanted. They represent a discontinuity inside the weld seam and can be allowed where an acceptance criterion is met. In Fig. 12.13, Fig. 12.14 and Fig. 12.15 the indications are shown:



Fig. 12.13 Penetrant testing results for samples with porosities 1 of 3

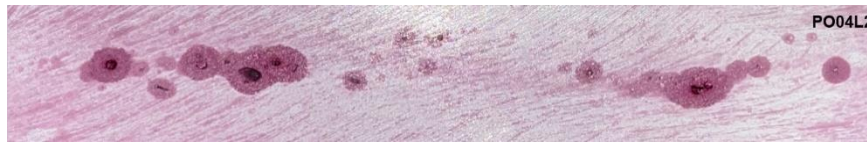


Fig. 12.14 Penetrant testing results for samples with porosities 2 of 3.

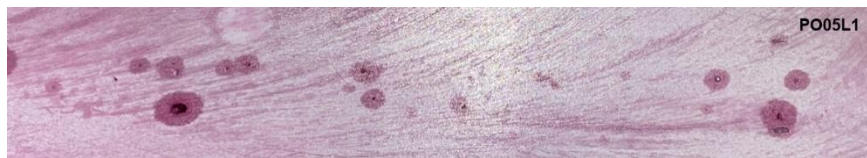


Fig. 12.15 Penetrant testing results for samples with porosities 3 of 3.

Overall, all the samples have some indications of porosity on the surface: the pore distribution and dimension vary on each sample. It is worthwhile to note that these results come from the previous grinding of the welding. Thus, it is possible to conclude that also inside the welding, some pores will be present.

12.2 Ultrasonic test

Before starting to analyse the samples, a calibration procedure has to be performed. This consist in calibrating the detector coupled with the probe in order to maximize echo and set the angle and the 0-scale. The ultrasonic scanning technique is based on the comparison of the response of the sample under examination to the one of a sample block with well-known discontinuities on which the system (probe + detector) is calibrated. This allows to evaluate the performances of the control apparatus guaranteeing the reproducibility of the results.

In addition, a correct choice of the sensitivity of the device in this phase will give advantages in the following control phase: a too high sensitivity gives a noisy signal that could not allow to distinguish real defects from the material structure.

Finally, even if the defect location can be determined, its entity can be determined by comparison with the one of a known geometry.

In this work, the calibration procedure for the angled probe have used V1 and V2 blocks.

V1 block it is used in two ways:

- To select the right refracted angle (transmitted in the examined sample): it is important to move the probe in a direction parallel to the graduated scale to identify on the device the maximum reflection peak from the 50mm hole of the sample block. This allows for a precise determination of the discontinuity inside the sample.

The below Fig. 12.16 shows the configuration:

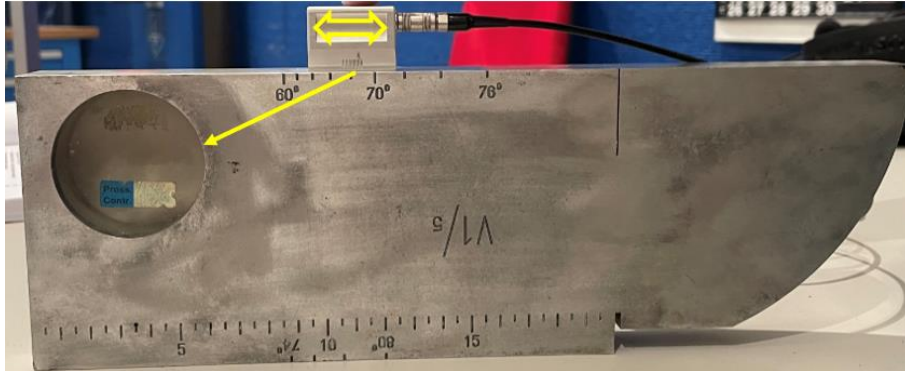


Fig. 12.16 VI block for probe and detector calibration.

- To select the 0 point of the angled probe: it is important to move the probe parallel to the flank of the sample block in order to obtain the maximum peak on the screen. In this configuration the reflection is maximum from the curved part (radius of 100mm) of the sample block. In the below Fig. 12.17 the system probe-sample block positioned for this calibration:

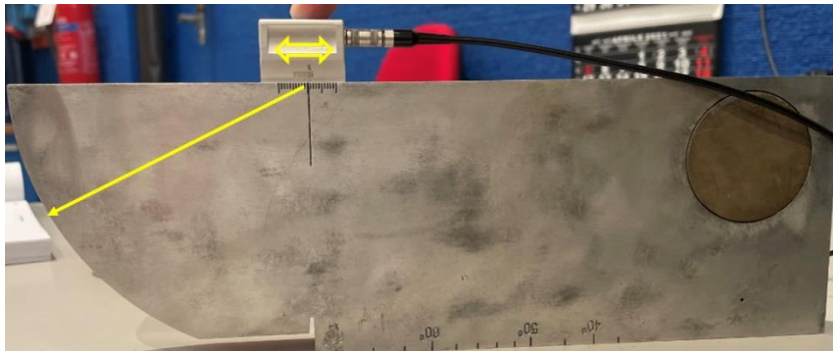


Fig. 12.17 VI block - probe angle calibration.

The same principle has been adopted with V2 block. In this case the probe angle determination and the 0-scale has been done with a sample that has lower dimensions and a different shape. In the following Fig. 12.18 the configuration for probe angle setting:

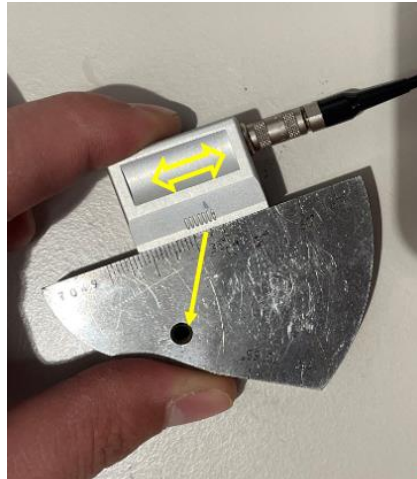


Fig. 12.18 V2 probe - angle and 0-scale calibration.

After the calibration procedure and having set the DAC curve, it is possible to start the measurements on the samples. During the inspection is important to cover all the welding volume from the root to the upper surface. This operation is done by moving the probe in a direction perpendicular to the weld section under examination. Considering the weld centre, two limit positions, a and b , can be determined by knowing the path of ultrasonic waves, as shown in Fig. 12.19:

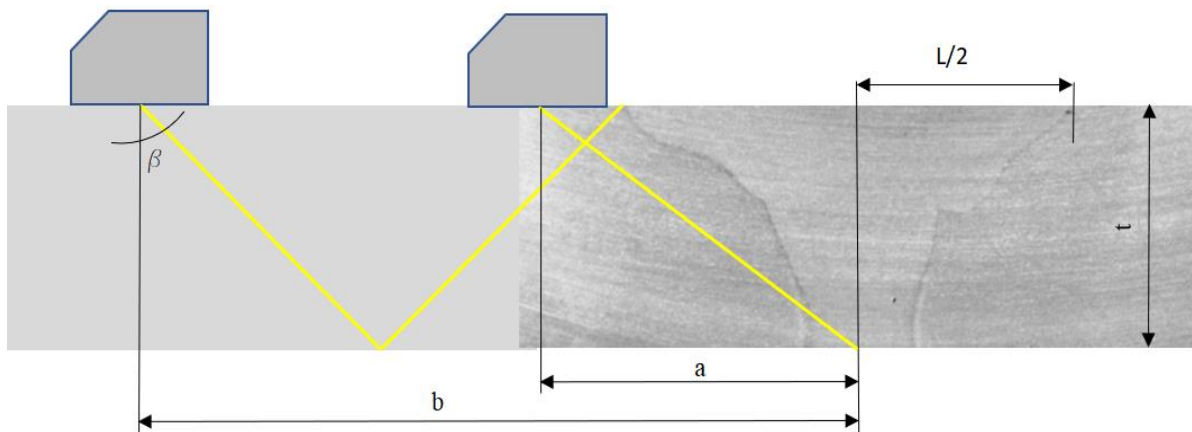


Fig. 12.19 Ultrasound testing: max and min positions of probe to cover the entire joint volume.

The above image shows with the two yellow lines the two limit paths for the welding volumetric inspection. The weld seam section can be considered as symmetric. Under this assumption, it is possible to set the 0-line at the weld seam section centre and to move the probe between the position a up to the position b in order to be sure of covering the inspection of the whole weld seam volume.

The positions a and b are calculated with respect the welding centre and in particular:

$$a = t \cdot \tan(\beta)$$

$$b = t \cdot \tan(\beta) + \frac{L}{2}$$

Where:

- β is the transmitted angle;
- L is the weld seam transversal dimension;
- t is the thickness of the joint:

Knowing the parameters dimensions:

- $\beta = 65,6^\circ$
- $L = 20mm$
- $t = 10mm$

The values of a and b are 22mm and 32mm respectively.

In order to verify the position of the defect, the device used has the possibility to reveal the path of ultrasonic waves up to the defect and with simple formulas it is possible to determine the defect depth. If we call p , the path showed on the device screen, t the plate thickness and β the transmitted angle, then the depth in first reflection d will be:

$$d = 2t - p \cdot \cos\alpha$$

While the depth in direct path will be:

$$d = p \cdot \cos\alpha$$

At this point it is important to identify the relevant results for each sample.

All the ultrasonic plots below are composed by several elements:

- On abscissas there is the ultrasonic field in the range of 0-100mm which is the maximum ultrasonic path that can be visible by the instrument.
- On ordinates there is the signal amplification in percentage.
- The red line is the DAC (distance amplitude compensation) curve: this curve is constructed as described in the Chapter 8. The calibration of the DAC curve

consists in amplifying the signal to take the signal of the first reflector of the master block at the 80% of the amplification. This allows to obtain a threshold of acceptability of the defect. All the points on this line has the same response in frequency, increasing the ultrasonic path.

- The blue curve is called *gate*: this curve is specific for the instrument and it is used to better read the values on the screen.
- The green curve represents the response of the material as the result of the ultrasonic test. The first 10mm length is considered noise and not taken into consideration.

12.2.1 Defect-free samples

In this paragraph the samples supposed to be without defects will be analysed. During the investigation the probe movement on the surface has highlighted some indications that can be considered acceptable because they lay over the DAC curve. The results of the three samples are reported below in Fig. 12.20, Fig. 12.21, Fig. 12.22:



Fig. 12.20 Ultrasonic testing results for defect-free samples 1 of 3.

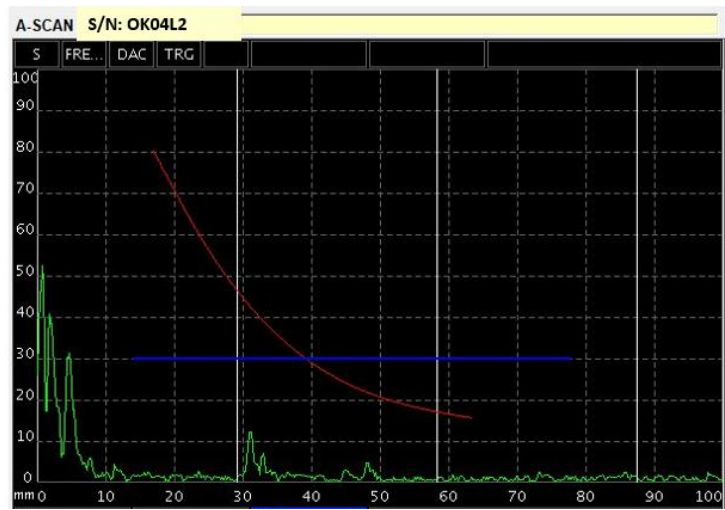


Fig. 12.21 Ultrasonic testing results for defect-free samples 2 of 3.

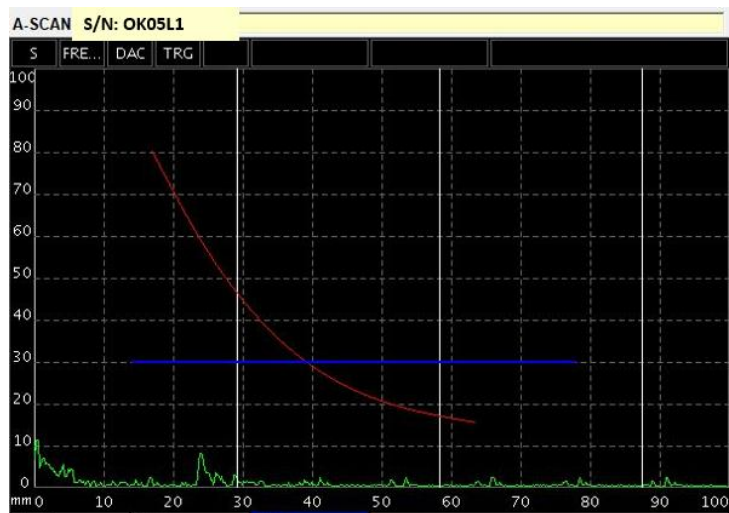


Fig. 12.22 Ultrasonic testing results for defect-free samples 3 of 3.

12.2.2 Samples with inclusion

The samples with the inclusion show an important peak in correspondence of the inclusion. In this case is clearly shown the overcoming of the red DAC curve and the imperfection is considered a volumetric defect that is not acceptable. The results are shown in Fig. 12.23, Fig. 12.24, Fig. 12.25.



Fig. 12.23 Ultrasonic testing results for samples with inclusion 1 of 3.

Regarding this first sample, a marked single peak is at about 76mm from the plate side and reveals an inclusion inside the welding at a maximum depth of 8mm. This indication is accompanied by a series of smaller peaks that reveals the different response of the material due to the partial fusion of the inclusion inside the welding. The defect extension is about 10mm in a direction perpendicular to the welding.



Fig. 12.24 Ultrasonic testing results for samples with inclusion 2 of 3.

Regarding the second sample, a marked single peak is at about 72mm from the plate side and reveals an inclusion inside the welding at a maximum depth of 8mm. This indication is accompanied by a series of smaller peaks that reveals the different response of the material due to the partial fusion of the inclusion inside the welding. The defect extension is about 10mm in a direction perpendicular to the welding.

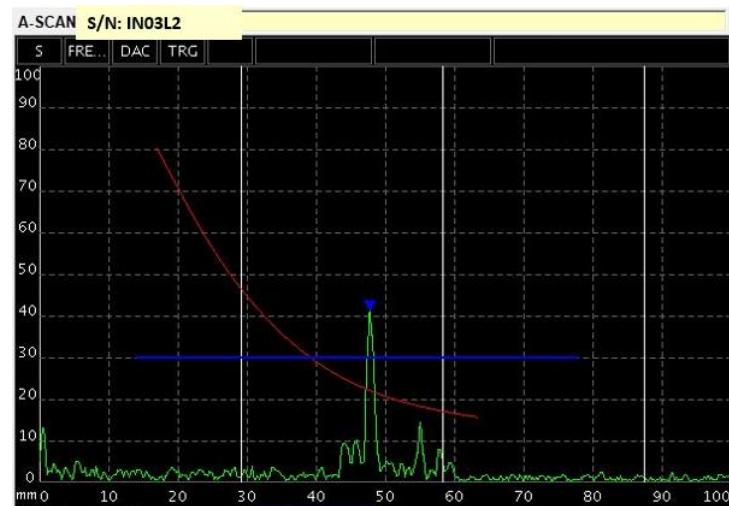


Fig. 12.25 Ultrasonic testing results for samples with inclusion 3 of 3.

Regarding this third sample, a marked single peak is at about 81mm from the plate side and reveals an inclusion inside the welding at a maximum depth of 8mm. This indication is accompanied by a series of smaller peaks that reveals the different response of the material due to the partial fusion of the inclusion inside the welding. The defect extension is about 10mm in a direction perpendicular to the welding.

12.2.3 Samples with incomplete root penetration

In the case of samples with incomplete root penetration, an in-depth analysis has been done at about 23mm from the weld centre. Even if some indications have been found, they are not relevant and the test has demonstrated poor detection of the incomplete root penetration, better visible with a surface test (both with visual testing and penetrant testing). The test results are shown in Fig. 12.26, Fig. 12.27 and Fig. 12.28.

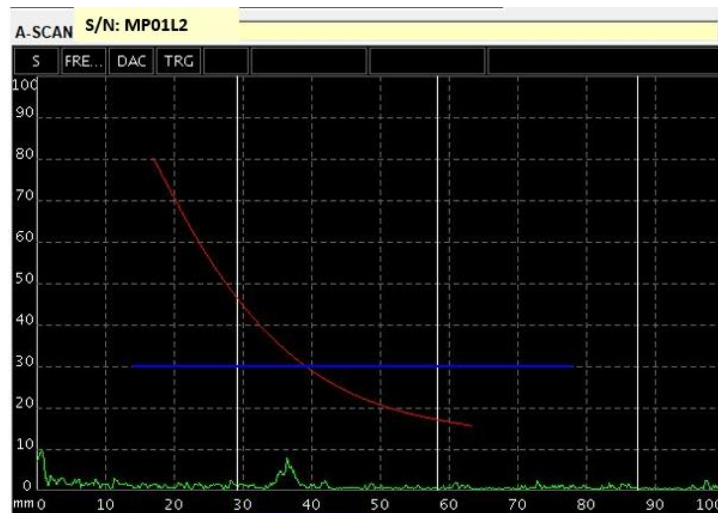


Fig. 12.26 Ultrasonic testing results for samples with incomplete root penetration 1 of 3.



Fig. 12.27 Ultrasonic testing results for samples with incomplete root penetration 2 of 3.

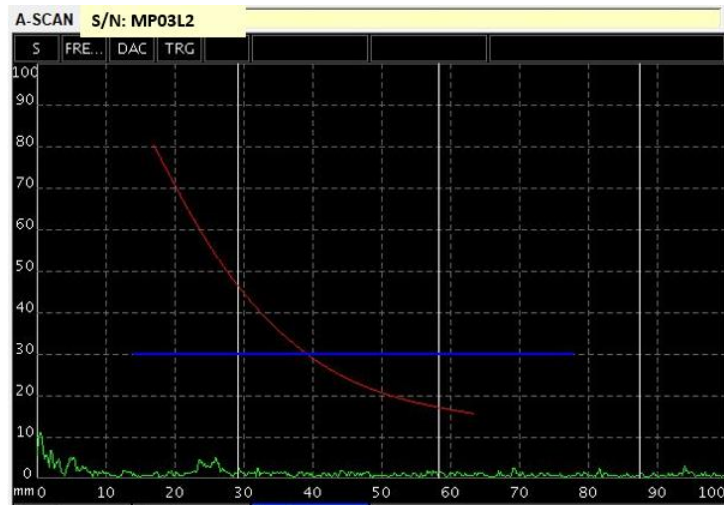


Fig. 12.28 Ultrasonic testing results for samples with incomplete root penetration 3 of 3

12.2.4 Samples with porosities

Finally, samples supposed to be with porosities have been investigated. In this case the evaluation of the entire weld seam has shown distributed porosity. The different dimensions of pores generate irregular peaks of echoes, resulting in a porosity distribution both in depth and width of the weld seam. The below Fig. 12.29, Fig. 12.30 and Fig. 12.31 show a portion of the weld seam investigated with this technique.

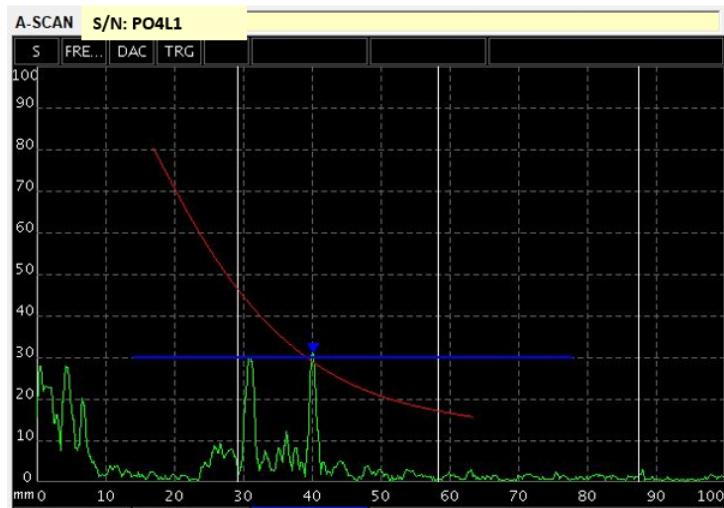


Fig. 12.29 Ultrasonic testing results for samples with porosities 1 of 3.

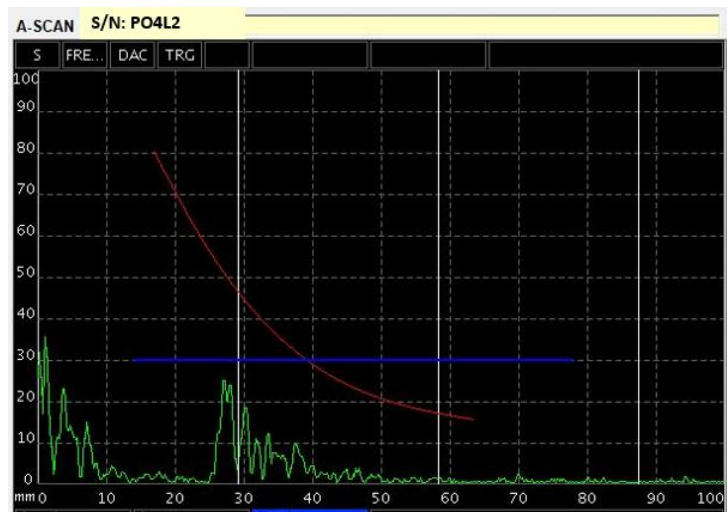


Fig. 12.30 Ultrasonic testing results for samples with porosities 2 of 3.

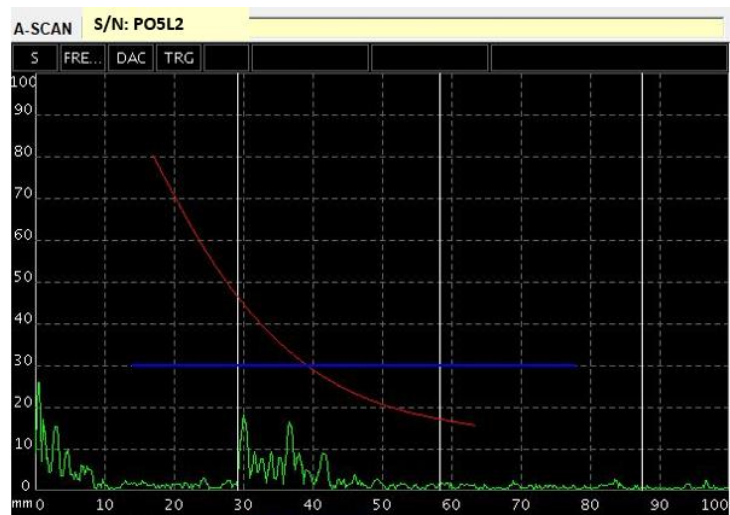


Fig. 12.31 Ultrasonic testing results for samples with porosities 3 of 3.

12.3 Fatigue and passive thermographic test results

The goal of a second fatigue test is to verify:

- If a greater testing frequency allows to obtain a marked temperature increment in passive thermography.
- If the life of the sample increases with respect to both Eurocode 9 calculations and the previous fatigue test when, by grinding the weld seam, the welded thickness is taken to the nominal value.

Even if all the 12 samples of the batch have been tested under penetrant and ultrasonic testing as reported in the previous paragraph, only 4 (one sample per type) have been chosen for the fatigue and the passive thermographic investigation.

The results of these tests are reported in the below Fig. 12.32:

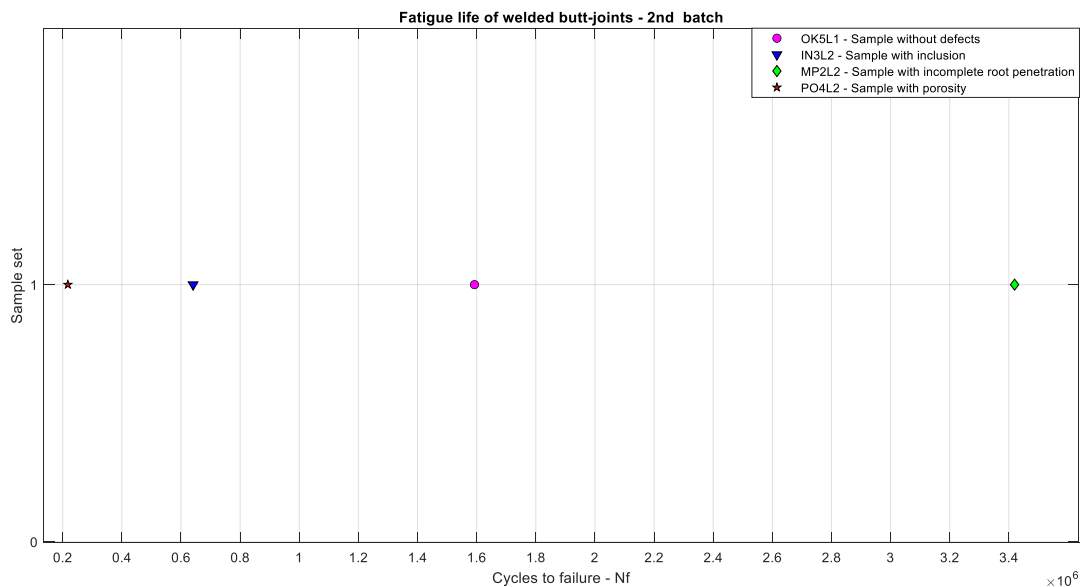


Fig. 12.32 Fatigue test results of 2nd batch samples: cycles to failure

By taking the ratio between the number of cycles found during the experimental tests and the calculated number of cycles, the fatigue life ratio can be determined.

The values for the 4 samples are reported in Tab. 27:

Tab. 27 Eurocode 9 vs real values: estimation of safety factors for the 2nd batch samples.

TEST	Defect type	Sample denomination	Nbr. Of cycles to failure observed during experimental tests	Nbr. Of cycles to failure calculated - Eurocode 9	Fatigue life ratio
1	No defects	OK05L1	1592656	110000	14,5
2	Inclusion	IN03L2	641062	110000	5,8
3	Porosites	PO4L2	217455	110000	2,0
4	Incomplete root penetration	MP2L2	3419348	110000	31,1

As reported in Tab.27 the lives of the samples show an overall increase with respect to the previous fatigue test. This aspect is justified by the improvement done in removing the excess of metal from the weld seam so that it does not represent a discontinuity point. For what concerns the results of the sample with porosity, the number of cycles identified during the test is very similar to the one found in the first fatigue test but still higher than the calculated one. However, while in the previous case the fracture has occurred at weld toe level, in this case the diffused porosity on the surface constitutes a site for crack initiation. This can be clearly seen from the below Fig. 12.33:



Fig. 12.33 Crack after the fatigue test on the specimen with porosity.

For what concerns the thermographic investigation, the same technique of post-processing has been used. In this case, the acquisition frequency has been of 1Hz for all the samples.

The main results are reported in the following Fig. 12.34, Fig. 12.35, Fig. 12.36 and Fig. 12.37:

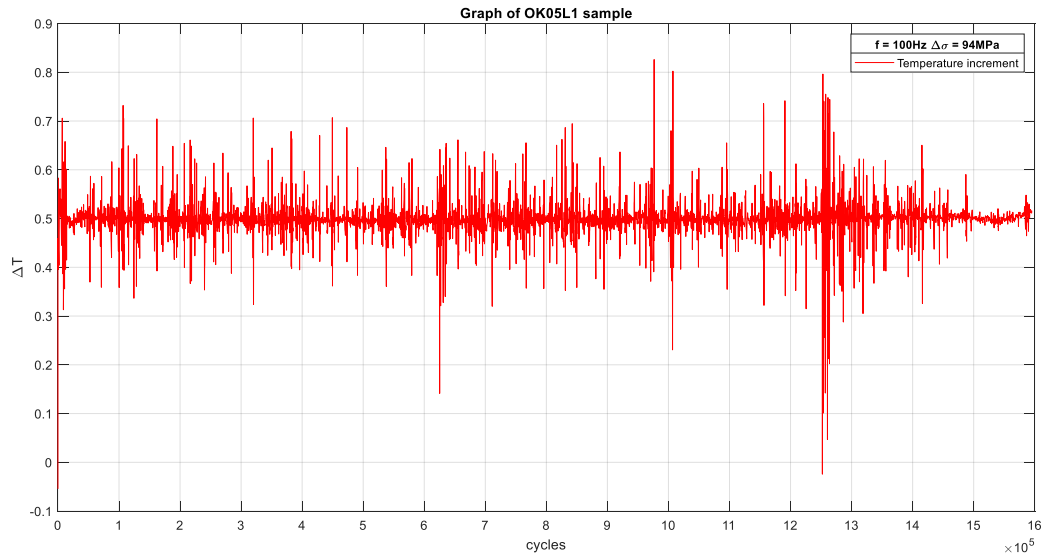


Fig. 12.35 Passive thermographic test on OK5L1 sample

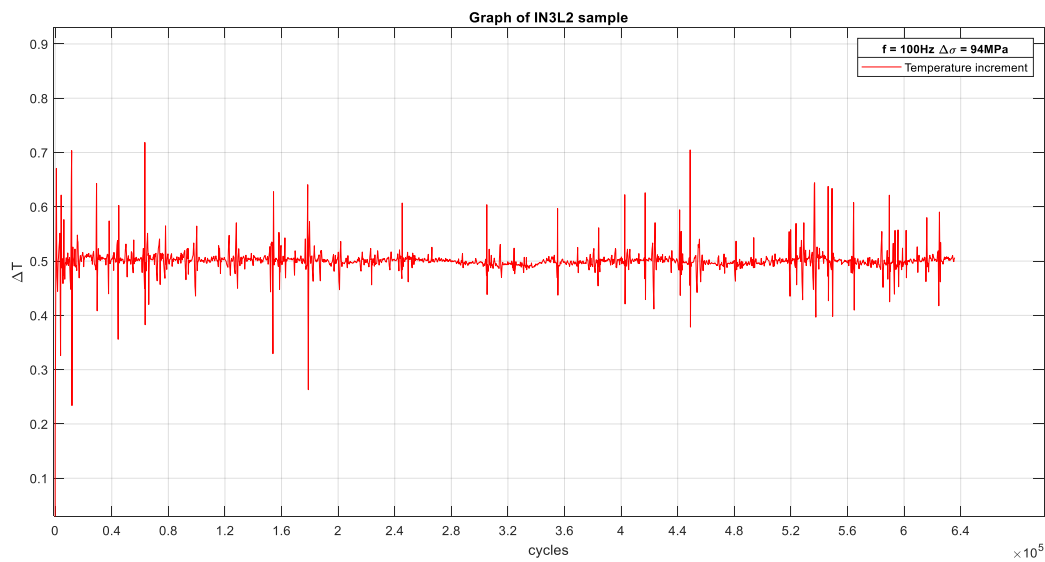


Fig. 12.34 Passive thermographic investigation on IN03L2 sample.

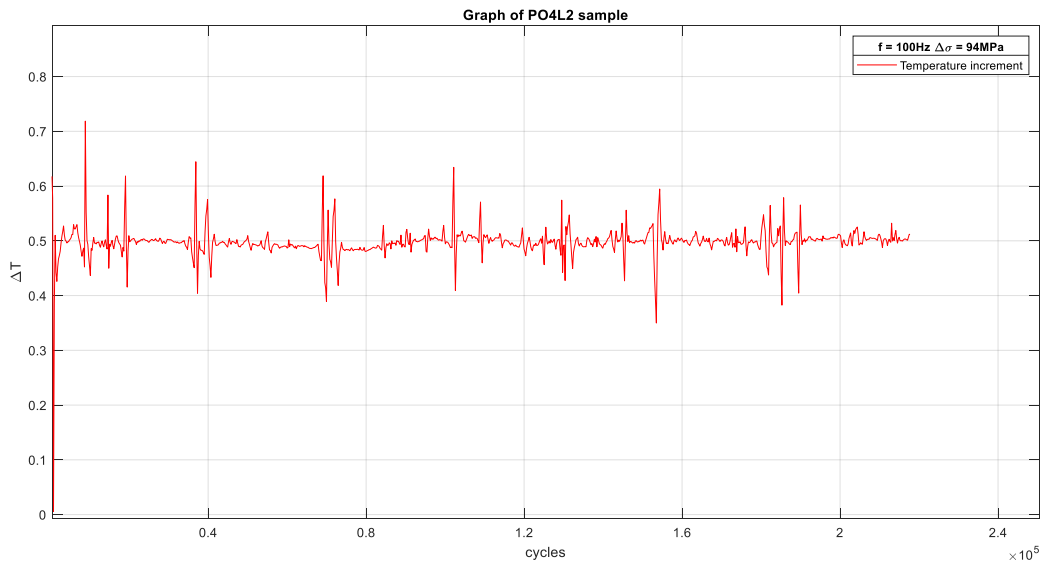


Fig. 12.36 Passive thermographic investigation on MP02L2 sample.

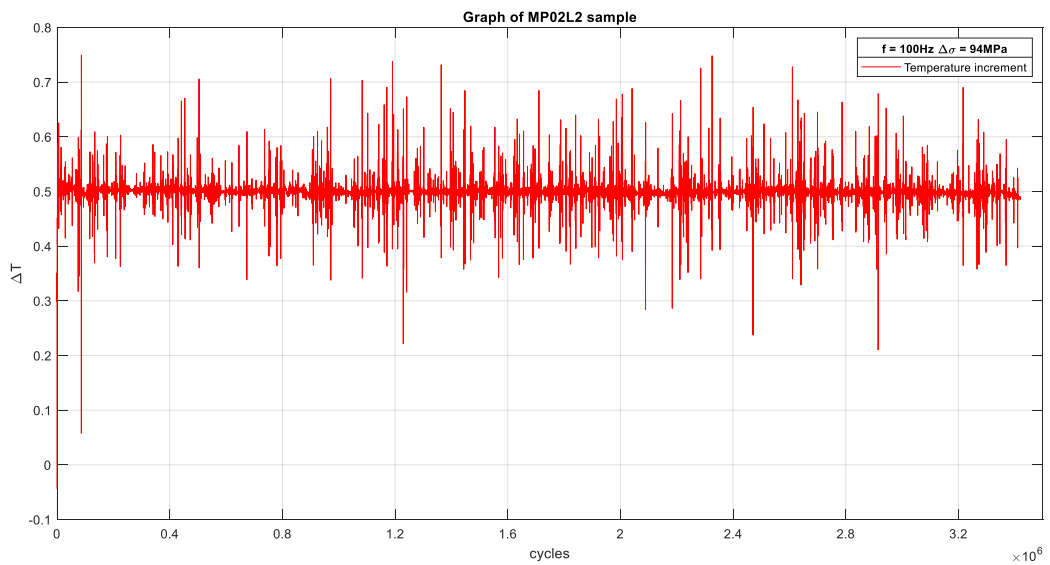


Fig. 12.37 Passive thermographic investigation on PO4L2 sample.

As it can be seen from the above figures, the signal shows a mean ΔT of 0,5 $^{\circ}\text{C}$ with local peaks between 0,7 and 0,8 $^{\circ}\text{C}$. In all the four cases there is not the expected thermal increment that shows the crack nucleation and propagation. This is probably due the high thermal conductivity of aluminium that, for the thickness under examination, disperses the heat wave inside the base material.

13. Conclusions

In this work non-destructive tests have been applied to two sets of samples in order to investigate both the presence of the defect and the material response to an excitation with the thermographic methods.

Two different volumetric tests have been performed to assess the presence of the defects inside the weld seam: radiographic and ultrasonic tests. In addition, penetrant and visual tests have been used to examine the surface of the samples. The success of these standardized methods has set the basis to start a deeper thermographic investigation once known the position of the defects for each weld seam.

At this point, with two different fatigue tests the passive thermographic method has been adopted. The results are then post-processed, eliminating the influence of the environmental temperature.

The first test, at a loading frequency of 30Hz, have revealed an increment of the temperature positive, with an increase in the weld seam area of the sample in the range of 0,5 °C up to 1,2 °C. This first result, common to all the samples, has demonstrated that the high heat conduction capacity of aluminium of about 6 times the one in steels does not allow to reveal the starting point of a crack neither its propagation. Indeed, as seen, the temperature of the investigated area has remained almost stable during the tests. Also, the acquisition frequency set on the thermal camera has revealed that, even with an increase of the acquisition frequency up to 1Hz, which corresponds to 1frame/s, the results do not change significantly. In addition, the cracks have started in all the samples from the weld toe, which represents a point of stress intensity increase, affecting the total life of the component.

The second fatigue test, at a loading frequency of 100Hz, has been used to validate the results obtained on the first test but with an improvement: grinding the weld seam there was an higher probability that the crack would have started from a discontinuity inside the material or at least from the centre of the weld seam. For this second test, only one sample per type of defect and one defect-free sample have been used. In addition, the increase in testing frequency has been done in order to increase the heat generated during the fatigue test. Also, in this second case, the numeric values of the temperature increase have not changed from the previous fatigue test, with an increase in noise due to the higher testing frequency.

In addition, the testing frequency does not affect the fatigue life of the component and in all the cases the improvement done by grinding the weld seam has resulted in an increased life of the samples

All the cracks have been developed at the defect level and in any case at the centre of the weld seam.

The real life under fatigue is in both the tests at 30Hz and at 100Hz, even where a defect is present, higher than the calculated one.

During the test at 100Hz, the fatigue lives detected are up to 31,4 times the calculated ones by Eurocode 9, demonstrating a significant increase in life. Due to the weld seam grinding, the second batch of samples have demonstrated an increase in sample life up to 7 times with respect to the first batch.

Finally, the active thermographic investigation has been performed. In this case, using a pulsed laser beam, four samples of the 1st batch have been investigated. The test has consisted of two steps: an acquisition has been done before the fatigue test and one after the fatigue test of the samples. It is worthwhile to underline that with these tests, it is identified the right combination of the setting parameters in order to verify a significant temperature increase of the sample. Moreover, the thickness of 10mm has resulted in an unfavourable factor because of the higher volume in which cool the laser excited samples. The two investigations before and after the fatigue test have shown a different response of the material, having an increment in the temperature response after the fatigue test. This factor is to ascribe to the change in heat conduction of the material due to the crack inside the weld seam.

In the sample with porosities there is a superposition of the effects of the crack and of the pores, leading to the temperature signal saturation.

A future development can involve the study of the defects dimensions on the samples starting from the thermal response. The porosity defect is the most dangerous in terms of sample life among the defects considered. In this context the investigation of the material response in function of the pores depth can be an important step for the defect detection. Also, it can be of interest the material response in function of the pore volume and if there is a characteristic dimension of the pore that can influence the thermal response of the sample.

Further development of the active thermography technique will be investigated in the PhD in collaboration with Alstom Ferroviaria Spa.

14. Appendix A

In this sections thermograms and displacements are presented for the whole number of the samples under fatigue test.

14.1 Defect-free samples

In Fig. 14.1, Fig. 14.2 and Fig. 14.3 the passive thermography results are shown for defect-free samples. In all the samples the acquisition frequency was 0.008Hz

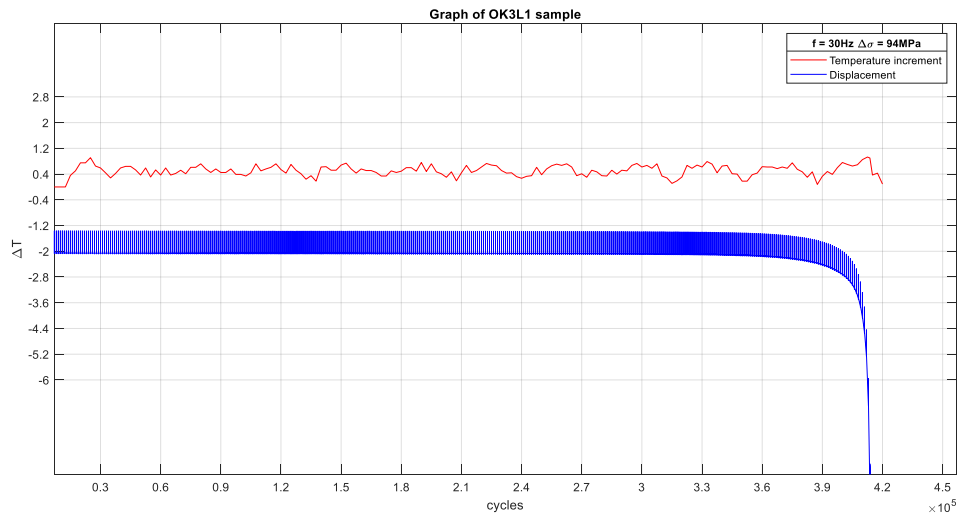


Fig. 14.1 Passive thermography results for defect-free samples 1 of 3. Temperature increment and displacement vs elapsed cycles.

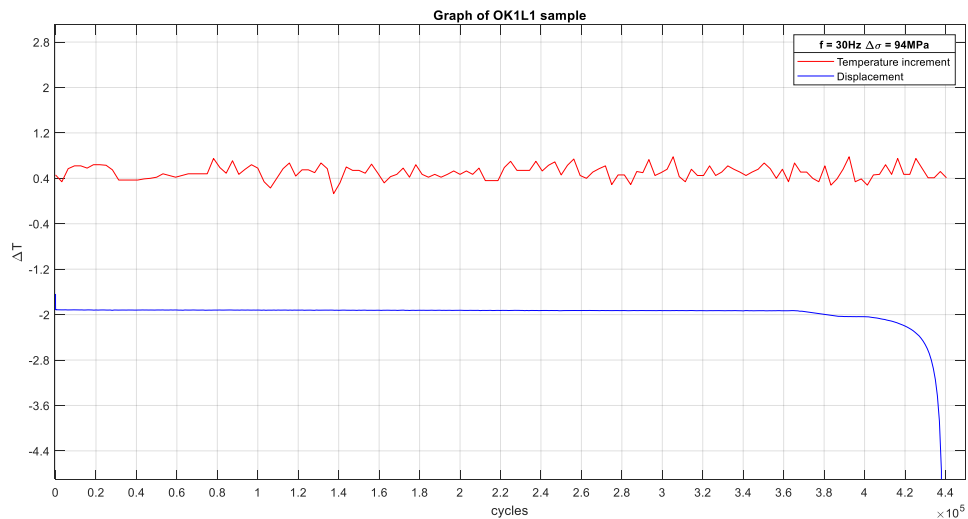


Fig. 14.2 Passive thermography results for defect-free samples 2 of 3. Temperature increment and displacement vs elapsed cycles.

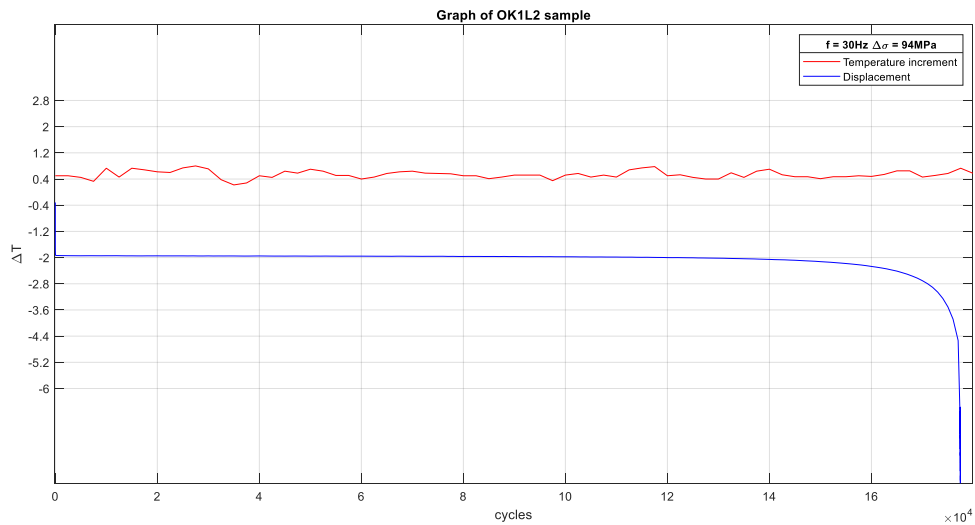


Fig. 14.3 Passive thermography results for defect-free samples 3 of 3. Temperature increment and displacement vs elapsed cycles.

14.2 Samples set with inclusions

In this section in Fig. 14.4, Fig. 14.5 and Fig. 14.6 the passive thermography results are shown for samples with inclusion. The acquisition frequency was 0.008Hz for the samples IN1L1 and IN2L2 and 1Hz for IN1L2.

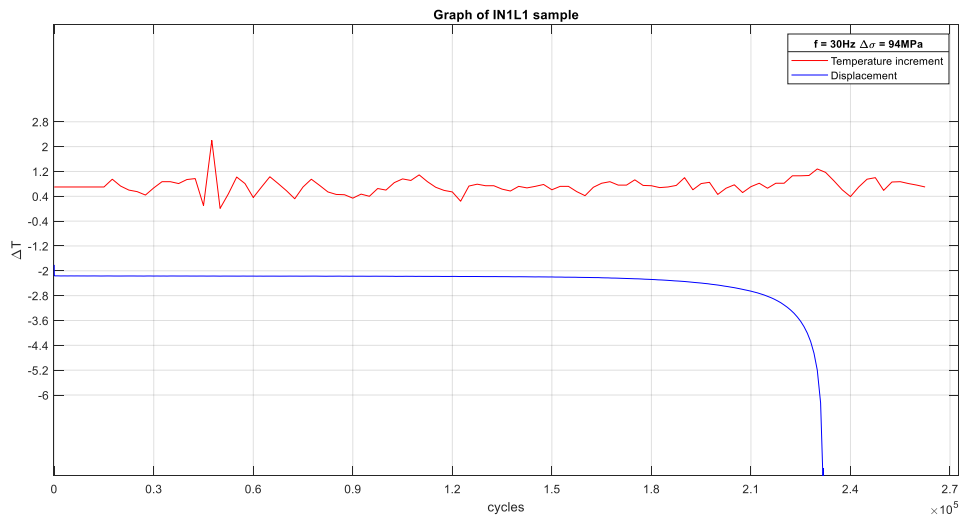


Fig. 14.4 Passive thermography results for samples with inclusion 1 of 3. Temperature increment and displacement vs elapsed cycles.

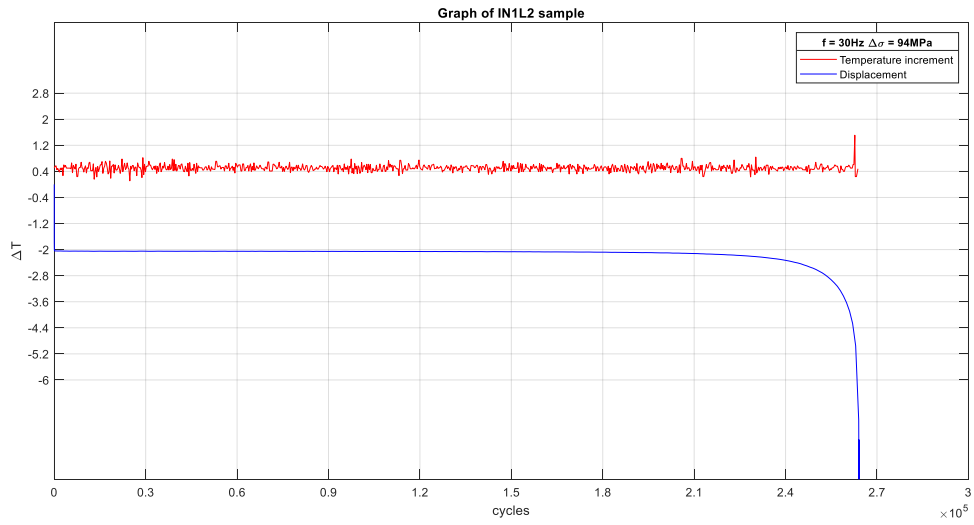


Fig. 14.5 Passive thermography results for samples with inclusion 3 of 3. Temperature increment and displacement vs elapsed cycles.

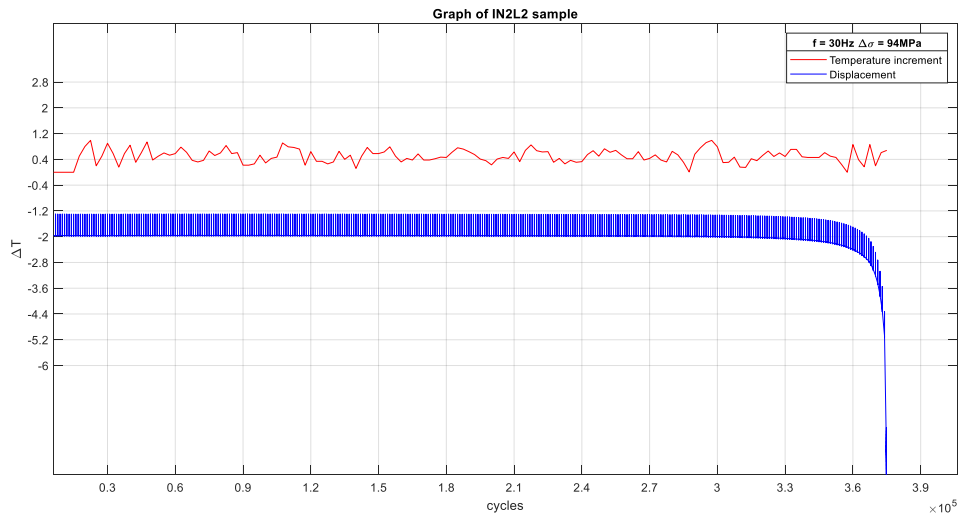


Fig. 14.6 Passive thermography results for samples with inclusion 2 of 3. Temperature increment and displacement vs elapsed cycles.

14.3 Samples set with incomplete root penetration

In this section in Fig. 14.7, Fig. 14.8 and Figure 14.9 the passive thermography results are shown for samples with incomplete root penetration. The acquisition frequency was 1Hz.

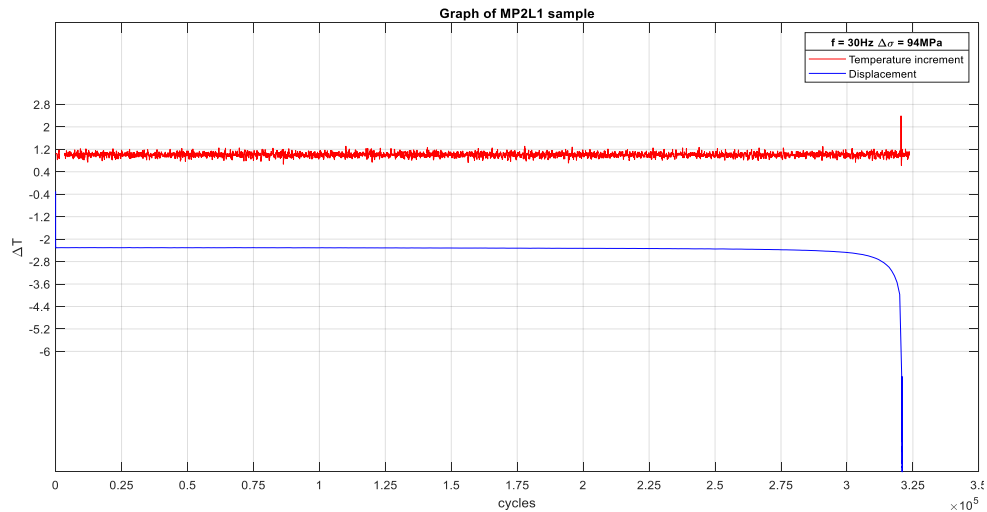


Fig. 14.7 Passive thermography results for samples with incomplete root penetration 1 of 3. Temperature increment and displacement vs elapsed cycles.

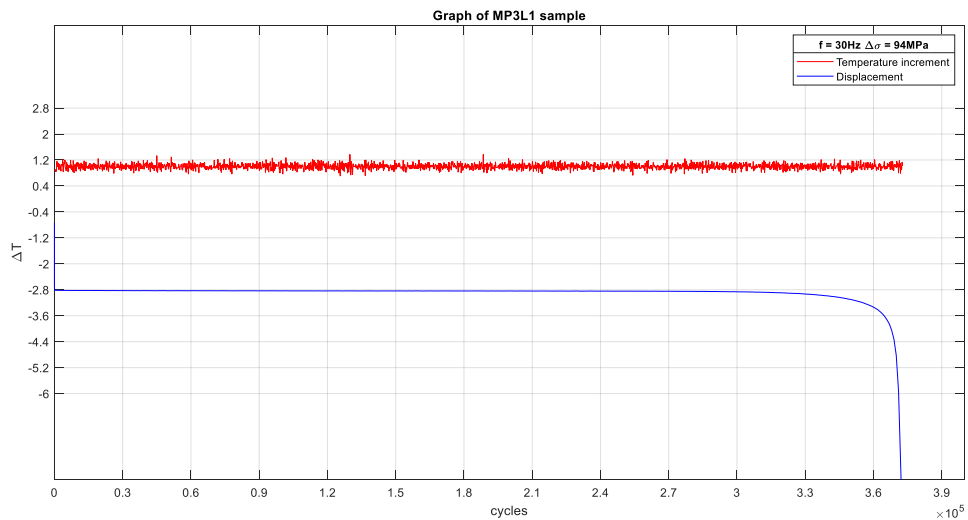


Fig. 14.8 Passive thermography results for samples with incomplete root penetration 2 of 3. Temperature increment and displacement vs elapsed cycles.

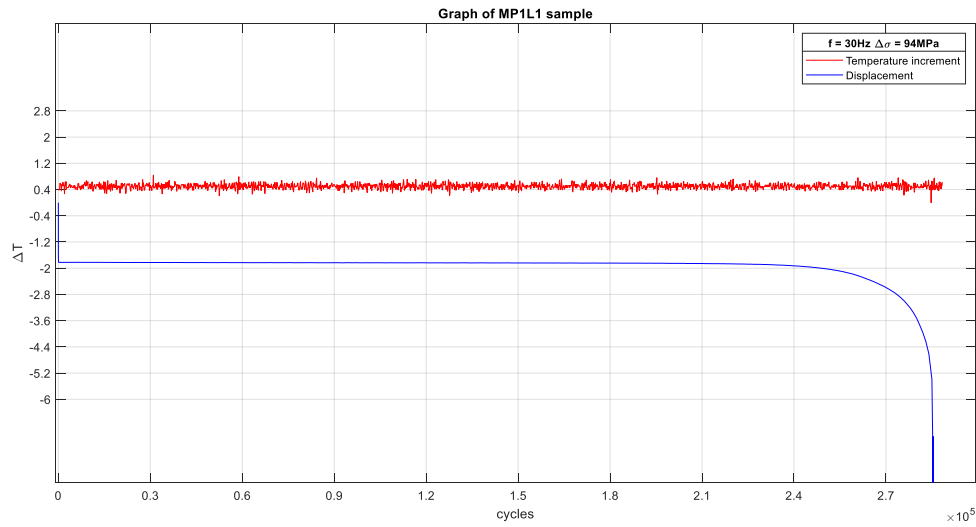


Fig. 14.9 Passive thermography results for samples with incomplete root penetration 3 of 3. Temperature increment and displacement vs elapsed cycles.

14.4 Samples set with porosities

In this section in Fig. 14.10, Fig. 14.11 and Figure 14.12 the passive thermography results are shown for samples with porosities. The acquisition frequency was 0.008Hz for PO3L1 and 1Hz for PO2L1 and PO2L2

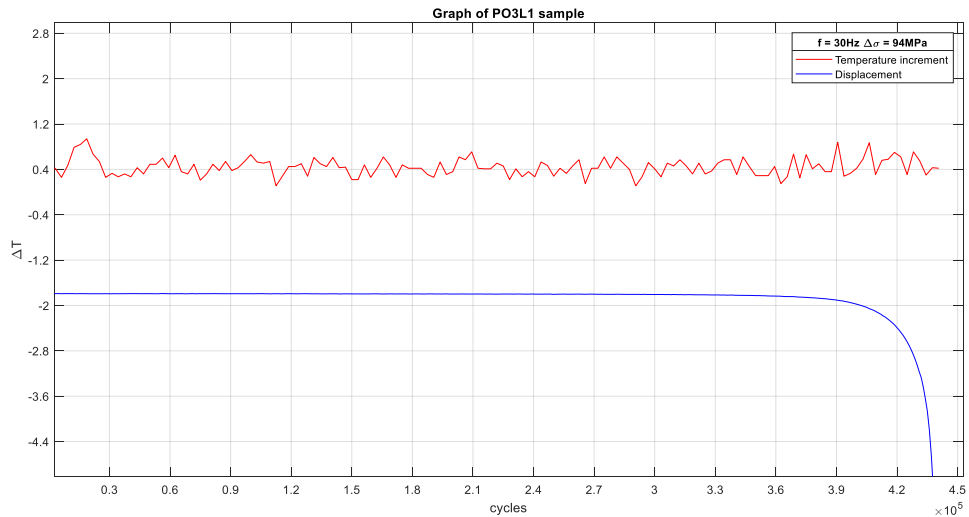


Fig. 14.10 Passive thermography results for samples with porosities 1 of 3. Temperature increment and displacement vs elapsed cycles.

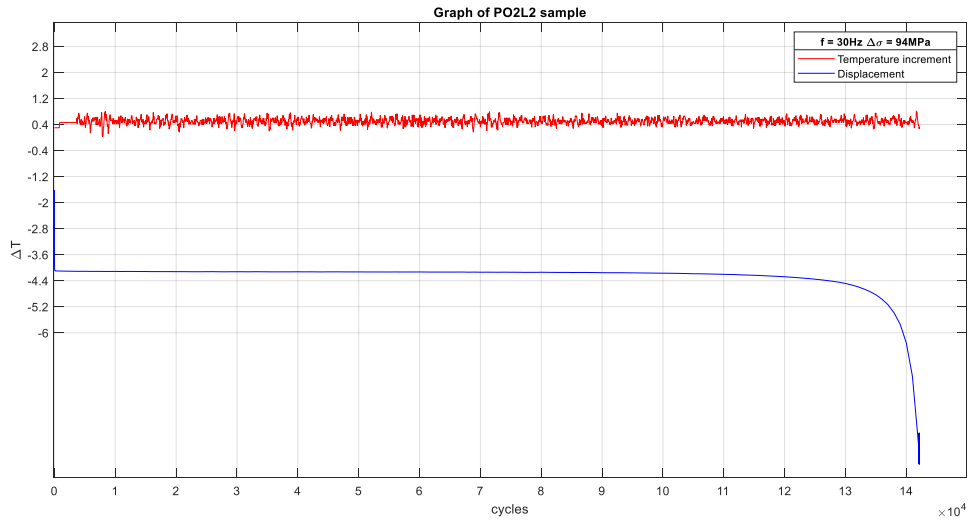


Fig. 14.11 Passive thermography results for samples with porosities 2 of 3. Temperature increment and displacement vs elapsed cycles.

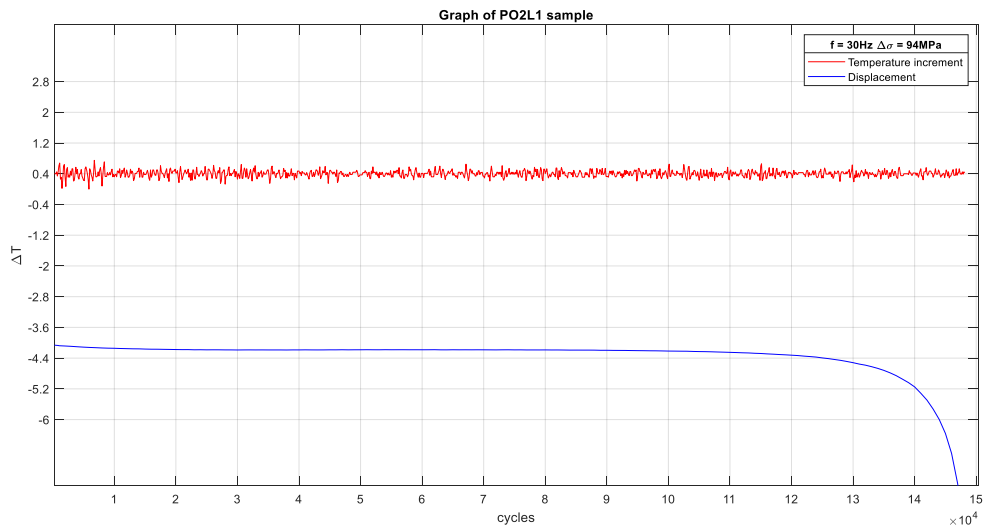


Fig. 14.12 Passive thermography results for samples with porosities 3 of 3. Temperature increment and displacement vs elapsed cycles.

15. Bibliography

- [1] Aluminium and aluminium alloys - Wrought products - Temper designations, UNI EN 515, Milan, Unificazione Italiana, 2017.
- [2] American Society for Nondestructive Testing, Infrared and Thermal Testing – Volume 3 – 3rd Ed., Maldague I., Xavier X.P., Moore O., Ohio (USA), 2001, 307-342.
- [3] American Welding Society, Welding Handbook - Volume 1 - 9th Ed, Jenney C. L. and O'Brien A., Miami (USA), 2001, 71-78 & 452-476.
- [4] Badghaish A. A., Fleming D. C., Quantitative characterization of resistive defects in thick composites using step heating thermography, SPIE Defense and Security Symposium, 6939(693916), Orlando (USA), March 16-20, 2008, 1-12.
- [5] Bonacina C., Cavallini L., Mattarolo L., Trasmissione del Calore, Padova, CLEUP, 1989, 423-427.
- [6] Coniglio N., Cross C. E., Michael T., Lammers M., Defining a Critical Weld Dilution to Avoid Solidification Cracking in Aluminum, Welding Journal, 87(8), 2008, 237-247.
- [7] Cross C. E., Coniglio N., Schempp N., Mousavi M., Critical Conditions for Weld Solidification Crack Growth, Hot Cracking Phenomena in Welds III, New York, Springer, 2011, 25-41.
- [8] Curti G., Cura' F., Sesana R., Analisi termografica di provini intagliati sollecitati a fatica, Salerno, XXXII Convegno AIAS, 3-6 September 2003.
- [9] E. D'Accardi, D. Palumbo, R. Tamborrino, P. Cavallo, U. Galietti, Pulsed Thermography: evaluation and quantitative analysis of defects through different post-processing algorithms, 14th Quantitative InfraRed Thermography Conference, 2018, 1-10.
- [10] Eurocode 9 - Design of aluminium structures - Part 1-1: General structural rules, UNI EN ISO 1999-1, Milan, Unificazione Italiana, 2014.
- [11] Eurocode 9: Design of aluminium structures - Part 1-3: Structures susceptible to fatigue, UNI EN ISO 1999-3, Milan, Unificazione Italiana, 2014.

- [12] Fronius – Manuale: TPSi – (www.fronius.com).
- [13] G. Fantoni, L.G. Merletti, A. Salerno, Stato dell'arte della termografia Lock-In applicata a componenti di elicottero: analisi termoelastica e rilevazione di difetti, Giornata di studio "Stato dell'innovazione del metodo Termografico nelle sue applicazioni industriali, civili e dei beni culturali, Padova, October 1st, 2018, 30-34.
- [14] Gleiter A., Riegert G., Zweschper T., Busse G., Ultrasound-Lockin-Thermography for Advanced Depth Resolved Defect Selective Imaging, *Insight - Non-Destructive Testing and Condition Monitoring*, 49(5), 2007, 272-275.
- [15] Han Y., Xue S., Fu R., Lin L., Lin Z., Pei Y., Sun H., Influence of hydrogen embrittlement on impact property and microstructural characteristics in aluminium alloy weld, *Vacuum*, 172(109073), 2020, 1-8.
- [16] Holland S. D., Uhlb C., Ouyang Z., Banteld T., Lie M., Meekere W. Q., Livelyc J., Braschef L., Eisenmannf D., Quantifying the vibrothermographic effect, *NDT & E International*, 44(8), 2011, 775-782.
- [17] Ida N., Meyendorf N, *Handbook of Advanced Nondestructive Evaluation*, Cham (Switzerland), Springer, 2019, 1396-1400.
- [18] Instron – Datasheet: Instron 8801- (www.instron.us).
- [19] Jeongguk K., Nondestructive evaluation of railway components using infrared thermography technique, *Quantitative Infrared Thermography Journal*, 2017, 1-2.
- [20] Kah P., Hiltunen E., Martikainen J., Investigation of Hot Cracking in the Welding of Aluminium Alloys (6005 & 6082), 63rd Annual Assembly & International Conference of the International Institute of Welding, Istanbul, AWST-10(128), July 11-17 2010, 373-380.
- [21] Lampman S, *Weld Integrity and Performance*, Ohio (USA), ASM International, 1997, 3-21.
- [22] Ludwig N., Marchetto L., Ricca R., *La termografia: teoria e applicazioni*, Milan, *Le Point Veterinaire Italie*, 2015, 165-182.

- [23] Maldague X., Galmiche F., Ziadi A., Advances in pulsed phase thermography, *Infrared Physics & Technology*, 43(3-5), 2002, 175–181.
- [24] MiltiDES – Manuale: MultiDES System Laser – (www.desinnovations.com).
- [25] Mrówka-Nowotnik G., Sieniawski J., Nowotnik A., Effect of heat treatment on tensile and fracture toughness properties of 6082 alloy, *Journal of Achievements in Materials and Manufacturing Engineering*, 32(2), 2009, 162-170.
- [26] Netzelmann U, Walle G, Ehlen A, Lugin S, Finckbohner M, Bessert S., NDT of railway components using induction thermography. AIP conference proceedings, 1706(150001), 2016, 1-8.
- [27] Non-destructive testing - Penetrant testing - Part 1: General principles, UNI EN ISO 3452-1, Milan, Unificazione Italiana, 2013.
- [28] Non-destructive testing - Qualification and certification of NDT personnel, UNI EN ISO 9712, Milan, Unificazione Italiana, 2012.
- [29] Non-destructive testing - Ultrasonic testing - General principles, UNI EN ISO 16810, Milan, Unificazione Italiana, 2014.
- [30] Non-destructive testing of welds - Radiographic testing - Part 1: X- and gamma-ray techniques with film, UNI EN ISO 17636-1, Milan, Unificazione Italiana, 2013.
- [31] Non-destructive testing of welds - Radiographic testing - Part 2: X- and gamma-ray techniques with digital detectors, UNI EN ISO 17636-2, Milan, Unificazione Italiana, 2013.
- [32] Non-destructive testing of welds - Ultrasonic testing - Characterization of discontinuities in welds, UNI EN ISO 23279, Milan, Unificazione Italiana, 2017.
- [33] Non-destructive testing of welds - Ultrasonic testing - Techniques, testing levels, and assessment, UNI EN ISO 17640, Milan, Unificazione Italiana, 2019.
- [34] Non-destructive testing of welds - Visual testing of fusion-welded joints, UNI EN ISO 17637, Milan, Unificazione Italiana, 2017.

- [35] Nordmark G. E., Herbein W. C., Dickerson P. B., Montemarano T. W., Effect of Weld Discontinuities on Fatigue of Aluminium Butt Joints, American Welding Society - Welding Research Supplement, Miami, 1986, 162-173.
- [36] Railway applications - Welding of railway vehicles and components - Part 3: Design requirements, UNI EN ISO 15085-3, Milan, Unificazione Italiana, 2008.
- [37] Reichelt W. R., Evanco J.W., Hoy M. G., Effects of Shielding Gas on Gas Metal Arc Welding Aluminum, 60th Annual Meeting in Detroit (USA), April 8-12, 1979, 147-155.
- [38] Roemer J., Pieczonka L., Uhl T., Laser Spot Thermography Of Welded Joints, Diagnostyka, 15(2), 2014, 43-49.
- [39] S.J. Maddox, Review of fatigue assessment procedures for welded aluminium structures, International Journal of Fatigue, 25(12), 2003, 1359-1378.
- [40] Sawczuk W., Identification of the hot spots phenomenon in brakes by using a thermal imaging camera, Quantitative Infrared Thermography Journal, 2016, 720-729.
- [41] Shen F., Zhao B., Li L., Chua C., Zhou K., Fatigue damage evolution and lifetime prediction of welded joints with the consideration of residual stresses and porosity, International Journal of Fatigue, 103, 2017, 272-279.
- [42] Shrestha R., Kisoo K., Wontae K., Investigation of Lock-in Infrared Thermography for Evaluation of Subsurface Defects Size and Depth, International Journal of precision engineering and manufacturing, 16(11), 2015, 2255-2264.
- [43] Specification and qualification of welding procedures for metallic materials - General rules, UNI EN ISO 15607, Milan, Unificazione Italiana, 2020.
- [44] Specification and qualification of welding procedures for metallic materials - Welding procedure specification - Part 1: Arc welding, UNI EN ISO 15609-1, Milan, Unificazione Italiana, 2020.
- [45] Specification and qualification of welding procedures for metallic materials - Welding procedure test - Part 2: Arc welding of aluminium and its alloys, UNI EN ISO 15614-2, Milan, Unificazione Italiana, 2006.

- [46] Szwed M., Pieczonka L., Uhl T., Application of Vibrothermography in Nondestructive Testing of Structures, 6th European Workshop on Structural Health Monitoring, Desdren, July 3-6, 2012, 1-17.
- [47] Welding - Arc-welded joints in aluminium and its alloys - Quality levels for imperfections, UNI EN ISO 10042, Milan, Unificazione Italiana, 2018.
- [48] Welding and allied processes - Classification of geometric imperfections in metallic materials - Part 1: Fusion welding, UNI EN ISO 6520-1, International Organization for Standardization, 2007.
- [49] Welding and allied processes — Nomenclature of processes and reference numbers, UNI EN ISO 4063, Milan, Unificazione Italiana, 2011.
- [50] Welding personnel - Qualification testing of welding operators and weld setters for mechanized and automatic welding of metallic materials, UNI EN ISO 14732, Milan, Unificazione Italiana, 2013.
- [51] Weman K, Welding Processes Handbook 2nd ED, Woodhead Publishing Limited, Philadelphia (USA), 2011, 75-97.
- [52] Wu., Zweschper T., Salerno A., Busse G., Lock-in thermography for non-destructive evaluation of aerospace structures, 7th European Conference on Non-destructive Testing, Copenhagen, 3(9), 26-29 May 1998.
- [53] Wysocka-Fotek O. , Maj M., Oliferuk W., Use of pulsed IR thermography for determination of size and depth of subsurface defect taking into account the shape of its cross-section area, Archives of metallurgy and materials, 60(2), 2015, 615-620.
- [54] Yoonjae C., Ranjit S., Seungju L., Wontae K., Thermographic Inspection of Internal Defects in Steel Structures: Analysis of Signal Processing Techniques in Pulsed Thermography, Sensors, 21(6015), 2020, 1-17